Obtaining Forest Description for Small-scale Forests Using an Integrated Remote Sensing Approach

---

A thesis submitted in partial fulfilment

of the requirements for the Degree of

Doctor of Philosophy in Forestry

by

Cong Xu

School of Forestry

University of Canterbury

2017

Table of Contents

List of Figures

List of Tables

Abstract

The estimated total forest plantation area in New Zealand is approximately 1.70 million ha. Approximately 70% of the plantations with area over 1000 ha are owned by large-scale owners, whose forests undergo regular monitoring and assessment. The remaining 30% of plantation forests are small-scale and are less likely to have regular area and yield assessments. Knowledge of these small-scale forests, especially those under 100 ha, remains very limited, yet they are expected to comprise over 40% of the total radiata pine (*Pinus radiata* D. Don) harvest volume by 2020. It is critical to better understand the small-scale forest resource in order to plan effectively for marketing, harvesting, logistics and transport capacity for this future resource. A remote sensing solution to small-scale forest description is necessary because conducting a comprehensive survey and field assessment on those patchy forests is impractical. The objective of this research is to apply multi-sensor remote sensing techniques-LiDAR and RapidEye to derive area, stand age and yield information for small-scale forests in New Zealand.

This research compared a factorial combination of two classification approaches (Nearest Neighbour and Classification and Regression Tree) and two remote sensing datasets (RapidEye and RapidEye plus LiDAR) for their ability to accurately classify land cover, specifically planted forest area. The research further determined the optimal modelling approach for deriving forest stand variables - mean top height, basal area, volume and stand age by comparing the performance of two parametric models (multiple linear regression and seemingly unrelated regression) and two non-parametric models (k-Nearest Neighbour and Random Forest) with RapidEye-derived metrics, LiDAR-derived metrics and a combination of both. The optimal mapping and modelling approaches developed on a training area, was then applied to the entire study area, the Wairarapa Region of New Zealand.

CART using a combination of RapidEye and LiDAR metrics outperformed the other three approaches producing the highest accuracy for mapping forest plantations. This method was further examined by comparing the mapped plantations with manually digitised plantations based on aerial photography. Across all sample grids, the mapping approach overestimated the plantation area by 3%. It was also found that forest patches exceeding 10 ha achieved higher conformance with the digitised areas.

LiDAR-derived metrics were found to be more useful in estimating all four forest stand variables relative to RapidEye metrics; combining LiDAR metrics with RapidEye metrics did not provide significant gains (on average 0.2% reduction in RMSE) in variable prediction. Non-parametric models and parametric models performed similarly, likely due to the narrow range of structural characteristics in the collected field data. Overall, multiple linear regression was deemed to be the best option for estimating forest variables for less well known forests as the approach has provided sound and consistent estimation of stand variables and it is relatively easy to understand and interpret.

The optimal area mapping and modelling approaches were applied to the Wairarapa region (594 000 ha), resulting in area and yield description for the region. Overall the mapped plantation area was 3.4% lower than the National Exotic Forest Description (NEFD) recorded plantation area. NEFD is an annual report that provides detailed area and yield description for New Zealand's plantation forests. The description of the large-scale forests from NEFD is reliable as it is captured directly from surveys collected from forest owners, whereas the description of small-scale forests is less reliable as the information from over half of these forests is imputed indirectly based on nursery studies. Forest stand variables mean top height, basal area, volume and age were modelled for the region using multiple linear regression with LiDAR-derived metrics. Based on the modelled stand variables, the recoverable volume at different ages (yield table) was generated. The yield tables developed using modelled information were within a realistic range and were slightly lower than NEFD yield tables.

Overall, the mapping and modelling approach developed in this research provided a proof of concept for deriving area and yield information using remote sensing data, and is especially relevant for small-scale forests where limited information is currently available. The wood availability from these small-scale forests could be more accurately addressed at a national level using this approach.

Acknowledgements

I would like to express my sincere gratitude to my primary supervisor Professor Bruce Manley for the continuous support of my PhD study - his patience, encouragement and knowledge. I am also in debt to my associate supervisor Dr. Justin Morgenroth for his insightful and professional advice, and for challenging me to push this research forward. The guidance from both supervisors helped me throughout this study and the writing of this thesis.

My sincere thanks go to Dr Luis Apiolaza, Dr Daniel Gerhard and Mr Jonathan Dash for providing valuable advice on the statistical analysis. Many thanks to Dr Michael Watt for reviewing the literature review chapter and providing useful feedback for publication. And Dr Pete Watt for providing useful suggestions at the early stage of this thesis.

I would also like to thank the Greater Wellington Region and Landcare Research for providing the LiDAR data; Indufor Asia Pacific and Blackbridge Ltd for providing the RapidEye images; and Land Information New Zealand for providing the aerial photography required for this research. Special thanks to Nelson Forests for providing additional LiDAR data. I am very grateful to the forest managers and consultants in the Wairarapa region for providing access to forest plots and associated data as well as providing valuable staff time to assist with the data collection: Alan Bell, Colin Bradley, Robin Britt, Malte Coulmann, Guy Farman, Sean McBride, Stuart Orme and Tom Ward. I also want to thank David Chandler for providing plot access and data for a pilot study prior to the main research. Special thanks to Huimin Lin for assisting with the field data collection, and to Tingdong Guo for conducting the independent classification accuracy assessment.

I would like to acknowledge the financial support in the form of a scholarship from the School of Forestry, University of Canterbury (PhD Scholarship 2013-2016, Owen Browning 2014, T W Adams Scholarship 2016-2017).

I am also very grateful to the support staff Jeanette Allen, Vicki Wilton and David Clark from the School of Forestry and Justin Harrison and John Thyne from the Geography department, for their assistance whenever needed.

I would like to thank my fellow postgraduate students for their support, cooperation and friendship at the School of Forestry. Special thanks to my friends Andy, Jimmy and Nancy for keeping me entertained and providing endless encouragement during my PhD.

Finally, my deepest appreciation goes to my family. Thanks to my parents for their unconditional love, support and sacrifices. Thanks to my husband Carl for his emotional support, understanding and encouragement at all times.

Chapter 1 - Thesis Introduction

1.1 Remote Sensing in Forestry

Decision making in commercial forest management relies on descriptive information of the forest resource for a range of temporal and spatial scales. Collection of such information is a fundamental task in forest management and monitoring. Up-to-date, high quality data is the key for good forest management. Traditionally these data have been collected from forest inventory practices; many medium to large scale forests have established routine area assessment techniques and inventories. However with substantial cost involved in inventory and rapid development of technology, data collection using remote sensing approaches have become pervasive, allowing a reduced scope of field work and cost, and the ability to capture additional forest variables (Benko & Balenovic, 2011; Boyd & Danson, 2005; Haywood & Stone, 2009).

Remote sensing techniques that are commonly applied in forestry include aerial photography, optical satellite imagery (mainly multi-spectral) and Light Detection and Ranging (LiDAR). Aerial photograph interpretation has been, and still is, the key remote technique for obtaining forest stand areas (Kadmon, 2001; Morgenroth & Visser, 2013). The analysis of aerial photographs for forest management is mainly based on manual interpretation using image characteristics such as shape, pattern and texture to delineate forest stand boundaries (Wang & Boesch, 2007). The delineation of forest classes still heavily relies on the capacity of operators and experience to qualitatively assess the spatial features in a scene (Kovats, 1997).

Satellite imagery, which covers a large extent and contains spectral and contextual attributes, has been increasingly applied in land cover mapping (Mallinis et al., 2008; Yu et al., 2006) and forest stand variable derivation (Wolter et al., 2009; Wulder & Seemann, 2003). Satellite imagery is considered as one of the most cost efficient sources for large scale analysis (Wulder & Seemann, 2003), yet use in operational forestry remains limited mainly due to insufficient resolution (Wang et al., 2010). Additionally, like aerial photography, satellite imagery cannot capture detail below the forest canopy, and hence cannot directly measure vegetation structure (Hyde et al., 2006).

In recent decades LiDAR, which is an active sensor, has been extensively used in forest practice for examining forest structure and underlying topography. As opposed to passive sensors like aerial photography and satellite imagery which provide horizontal

characterisation of vegetation cover, LiDAR derives vertical structure by actively emitting laser pulses, which reflect off a target object, thereby producing an accurate representation of the object as a 3D point cloud (Lim et al., 2003; Wehr & Lohr, 1999). LiDAR has demonstrated its superiority in assessing forest structural variables such as canopy height (Naesset & Bjerknes, 2001), basal area (Packalen & Maltamo, 2008), biomass (d'Oliveira et al., 2012) and volume (Hall et al., 2005). Despite these benefits, the high cost of LiDAR acquisition and lack of processing expertise generally precludes wall-to-wall LiDAR surveys for operational use (Lefsky et al., 2001b; Morgenroth & Visser, 2013).

In order to take advantage of different types of sensor and overcome the limitations of individual sensors, LiDAR and satellite sensors have been combined in a number of studies to provide more information on forest structure and dynamics (Hudak et al., 2009). Combined use of optical images and LiDAR in forestry utilises both the spectral information in optical imagery and the 3D information in LiDAR. For example, combined LiDAR-derived information and satellite imagery have been used in forest cover classification (Dupuy et al., 2013), estimation of forest height (Hudak et al., 2002), volume (Tonolli et al., 2011), biomass (Estornell et al., 2012; Mora et al., 2013) and site productivity (Watt et al., 2015).

1.2 Research Motivation

Forestry is a significant industry in New Zealand, being the third largest export earner contributing $5 billion annually (NZFOA, 2016). New Zealand's net stocked production forests, which are dominated by radiata pine, cover approximately 1.70 million hectares as at 1 April 2016 (MPI, 2016a). The New Zealand National Exotic Forest Description (NEFD) carries out annual surveys of forest owners and managers who own forest plantations, in order to compile summaries of the stocked forest areas, planting and harvesting information and the yield of plantation forests in every region.

There are approximately 100 large-scale forest owners who own plantations greater than 1000 ha who account for 70% of the national plantation estate (MPI, 2016a). Large-scale forests are generally managed professionally with regular assessment of forest areas and yield through aerial photography and inventory in order to support management decisions. The area and yield descriptions from large-scale forest owners are captured from annual surveys sent by MPI, hence the information from large-scale owners especially those with more than 10 000 ha of forests, is considered the most reliable source of the NEFD data (MPI, 2014). On the other hand, there are many small-scale forest owners (less than 1000 ha) who are reported to

own 30% of the total plantation area. The forest description of smaller-scale forests is less reliable due to inconsistent area definition and management practices. The data provided by small-scale forest owners is likely to be more variable in terms of reliability as 1) some of the areas reported may well be gross areas rather than net stocked areas, 2) data potentially contain higher non-sampling errors due to reporting inaccuracies and responses based on owners' estimates and 3) errors raised in transferring non-electronical data into the database (MPI, 2014).

In addition, the NEFD survey only directly captures 257 000 ha of the 537 000 ha of small-scale forests in New Zealand; the rest (52% of all small-scale forests) is imputed from annual nursery surveys (MPI, 2014). Nursery surveys of new plantings, which are based on the number of seedlings sold, have been used since 1992 by MPI to estimate new plantings in the NEFD, especially for small-scale forests. The approach was considered as a reasonable and efficient way of estimating, but also less accurate than alternative methods (Manley et al., 2003). However, since 2006 new plantings have not been added to the NEFD due to the low levels of new seedlings planted (MPI, 2016a). The limitations of this imputation process are that it does not provide direct measurement of the plantation area, nor describe where the plantations are located.

The yield information of New Zealand plantations is summarised in the wood availability forecasts which consists of a series of regional and national wood availability forecasts for New Zealand's plantation estate that used as a planning tool for forestry industry, government and infrastructure and service providers. The latest report was prepared by Indufor Asia Pacific for the period 2014-2050 (MPI, 2016b). The yield tables used in the wood availability forecast report were based on yield tables provided by several large-scale forest owners in each region, which were then averaged on an area-weighted basis and calibrated to derive the regional yield tables for different regimes. The area-weighted average regional yield tables developed for the large-scale forests were also applied to the small-scale forests. It was assumed that the yield tables from large-scale owners who undertake regular yield assessment and well-designed silvicultural operations in their estate were the same as the small-scales owners whose forests may not undergo these optimal management practices. Unfortunately, there is no existing yield information that is directly based on surveys from the small-scale forests.

Overall, the lack of reliability of forest description for small-scale forests has led to insufficient understanding of the wood supply from these forests. These small-scale forests, which were mostly planted as post-1989 forests, will play an important role in providing

wood supply in the next few decades. By 2020, the small-scale forests will have the capacity to provide around 15 million m^3 of radiata pine logs per annum, which will be over 40% of the total radiata pine supply (MPI, 2016b). Therefore, it is critical to understand the resources from these small-scale forests in order to effectively plan marketing, harvesting, logistics and transport capacity that are required for additional wood availability.

The spatial existence of 67 000 ha of small-scale forests was obtained using surveys developed by AgriQuality (MPI, 2014), which relied on the intersected spatial datasets of AgriBase™ 1, Land Cover Database (LCDB), and non-spatial surveys and field data. However, the satellite imagery used to derive the LCBD were SPOT and Landsat (MfE, 2004), which are medium resolution (10 to 30m) that could potentially overlook small patches of forests. Additionally, the spatial representation of small-scale forests has not been updated since the survey. The lack of certainty about the spatial extent, distribution and yield of small-scale forests suggests there is a need to develop a spatial database of small-scale forests with accurate forest description information, so that the potential wood supply from small-scale forests will be better understood. Geospatial and remote sensing information are likely the most efficient and consistent means to achieve this goal.

Geospatial data including both vector and raster layers in New Zealand are increasingly becoming available for public use and can be accessed through a number of source providers, which include Land Information New Zealand (LINZ)[2], Landcare Research Land Resource Information System (LRIS) Portal[3], Statistics New Zealand Digital Boundaries[4] and Koordinates[5]. Under the Creative commons attribution 3.0 New Zealand License, high resolution aerial photography covering almost the whole country has become available. Furthermore, a number of regional councils have acquired LiDAR for updating topography, which could potentially be used in forest mapping. RapidEye, which is 6.5 m resampled to 5 m spatial resolution multispectral satellite imagery, can be acquired cost-effectively.

With the advanced development of remote sensing technologies and free or low-cost availability of imagery and LiDAR datasets, the description of plantation forests especially

1 AgriBaseTM is developed by Assure Quality, which is a spatial layer of classification of farms by predominant farm use and breakdown of farm activities, livestock species and area of each land use.

2 http://data.linz.govt.nz/

3 http://lris.scinfo.org.nz

4 http://www.stats.govt.nz/browse_for_stats/people_and_communities/Geographic-areas/digital-boundary-files.aspx

5 http://koordinates.com

small-scale forests could be potentially enhanced. This research intends to evaluate the possibility of deriving a forest description for small-scale forests utilising remote sensing datasets, by applying an integrated approach with LiDAR and RapidEye imagery to provide estimation of net stocked area of plantations, height, basal area, age class and volume in order to improve the understanding of the potential wood supply from small-scale forests.

1.3 Research Objectives

The main objective of this research is to apply multi-sensor remote sensing techniques-LiDAR and RapidEye to derive area and yield information for small-scale forests in New Zealand through a case study in the Wairarapa region. Additionally, using combined LiDAR and satellite imagery together with field plot information, this research proposes to evaluate a range of parametric and non-parametric models to estimate forest structural characteristics (height, diameter and volume) as well as stand age using integrated LiDAR and satellite imagery, in order to determine the most appropriate approach for estimating each variable.

Specific research objectives include:

- To provide a review of the theories and applications of integrated LiDAR and other optical sensors in forestry, and determine whether sensor fusion has superior performance relative to individual sensors for delineating forest areas, identifying forest species, estimating forest age and productivity, height and volume.
- To evaluate different combinations of mapping algorithms and remote sensing datasets by comparing the stocked forest areas derived from RapidEye, LiDAR and combined sensors against manual interpretation from aerial photography, in order to determine the accuracy of each technique in area assessment and find the optimal approach with the highest mapping accuracy.
- To evaluate parametric and non-parametric models for deriving forest stand variables –height, basal area, volume and stand age from parameters derived from LiDAR, RapidEye or combined, in order to find the optimal modelling approach and remote sensing dataset for estimating these stand variables.
- To apply the optimal area mapping and modelling approaches developed from the previous two objectives to the Wairarapa region, and provide area and yield description for the region.

The proposed research aims to test the possibility of utilising the integrated LiDAR and multispectral imagery to extract an enhanced forest description of small-scale forests. The outcome of this research will enhance the understanding of small-scale forests in terms of the net stocked areas and the yield of the forests for the Wairarapa region. This information is extremely important to the government in reporting national forest information, and to the forestry sector for wood availability forecasting.

1.4 Thesis Structure

Since the first integrated study of LiDAR and satellite imagery Landsat TM in 2002 (Hudak et al., 2002), there has been substantial research using fusion of active LiDAR and passive optical sensors in deriving forest area (Machala & Zejdova, 2014; Nordkvist et al., 2012), classifying species mix (Dalponte et al., 2012; Sasaki et al., 2012), and extracting forest structural variables (Mora et al., 2013; Popescu et al., 2004). However, there has not been a comprehensive review on the studies of utilising integrated LiDAR and other remote sensing approaches conducted over the last decade. Therefore, the second chapter reports a comprehensive review on that subject, and uses the findings from the review to develop appropriate approaches for deriving forest area and yield information.

This research intends to use remote sensing datasets LiDAR and RapidEye, and these datasets generally require some pre-processing prior to conducting analysis. Therefore, the third chapter will detail the steps required for processing LiDAR raw point clouds and correcting RapidEye imagery, as well as deriving useful metrics and surfaces from the remote sensing datasets.

The fourth chapter will address the details of using LiDAR and RapidEye derived surfaces to map plantation area, specifically to examine four combinations of mapping approaches and input datasets on selected samples from study area: 1) Nearest-Neighbour (NN) approach with RapidEye, 2) Classification and Regression Tree (CART) with RapidEye, 3) NN with both RapidEye and LiDAR and 4) CART with both RapidEye and LiDAR, and determine the optimal approach for deriving plantation areas based on comparison of classification accuracy. The plantation areas derived using the automated mapping approach will be further compared with the area derived by manual digitisation from high resolution aerial photography to determine the mapping accuracy of the developed approach.

Chapter five of this thesis will focus on developing the optimal approach for estimating forest stand variables – mean top height, basal area, standing volume and stand age by comparing the performance of multiple linear regression, seemingly unrelated regression, k-nearest

neighbour and random forest models with RapidEye metrics, LiDAR metrics and combined metrics.

The optimal mapping approach developed from chapter four and the optimal modelling approach developed from chapter five will be applied to the Wairarapa region in chapter six, in order to develop knowledge of plantation area and yield for the total forest estate for the region. Finally chapter seven will summarise all key findings of this research and address limitations and directions for future research.

Chapter 2 - Literature Review: Integrating data from discrete return airborne LiDAR and optical sensors to enhance the accuracy of forest description

The contents of this chapter have been published as the following paper; the manuscript presented here is identical to the published article except for minor typesetting and copyediting changes.

Xu, C., Morgenroth, J., & Manley, B. (2015). Integrating Data from Discrete Return Airborne LiDAR and Optical Sensors to Enhance the Accuracy of Forest Description: A Review. Current Forestry Reports, 1(3), 206-219. doi: 10.1007/s40725-015-0019-3

1.1 Introduction

Forests provide timber and non-timber products, habitats for a diverse range of flora and fauna, as well as social benefits such as shelter, food and employment. Managing forests to optimize one or more of these benefits is challenging as they are dynamic and undergo continual change from both natural and human-induced afforestation and deforestation (Food and Agriculture Organization, 2014). Effective forest management requires comprehensive forest data for a range of temporal and spatial scales. However, obtaining full descriptive data from ground-based approaches is often infeasible (Boyd & Danson, 2005). Remote sensing, including aerial photography, satellite imagery, and LiDAR (light detection and ranging), has increasingly been used as a means of cost-effectively capturing forest data (Boyd & Danson, 2005; Roberts et al., 2007).

Aerial photography is the most widely used remote sensing technique in forest management (Morgenroth & Visser, 2013). Image characteristics such as shape, pattern and texture are used to delineate forest stand boundaries (Wang & Boesch, 2007), estimate tree height and crown diameter (Tuominen & Pekkarinen, 2005) and identify species (Haara & Haarala, 2002). Kovats (1997) demonstrated that tree height can be measured using high-resolution stereoscopic aerial photos with photogrammetric techniques to measure the lengths of shadows projected onto the ground. Likewise, Dandois and Ellis (2013) accurately measured tree height on aerial photos using a computer vision technique. However, these techniques have not been applied operationally as they are dependent on a number of factors including presence of open flat ground and specified sun elevation and angle. Furthermore, subjective interpretation often results in inconsistent degrees of precision and accuracy (Holmgren et al., 1997).

Apart from aerial photography, research has increasingly employed satellite imagery in forest assessment. Satellite multi- and hyper-spectral sensors capture the electromagnetic radiation emitted by the sun and reflected by the earth's surface (Campbell & Wynne 2011). Spectral and contextual attributes derived from satellite sensors can be modelled against empirically derived biophysical features of the forest, such as stand basal area, height and crown closure (Maselli et al., 2005; Wolter et al., 2009), stand density (Ingram et al., 2005), Leaf Area Index (LAI) (Cohen et al., 2003; Eklundh et al., 2001; Jensen & Binford, 2004) and forest volume and biomass (Franco-Lopez et al., 2001; Hall et al., 2006; Zheng et al., 2004). Development of textural analysis such as the grey-level co-occurrence matrix (GLCM) has also allowed the use of additional information from optical sensors to assess forest stand variables such as height, basal area and stand density (Kayitakire et al., 2006). Recently, high-resolution satellite imagery (sub-metre) has been used to measure forest structural variables at a finer scale, which makes possible automated detection of individual trees via crown delineation, and modelling individual tree crown size, height, diameter, volume, age class and species composition (Immitzer et al., 2012; Kayitakire et al., 2006; Roberts et al., 2007; Shamsoddini et al., 2013).

Advantages of optical sensors include large coverage of forest area, easy access and low cost (Hudak et al., 2002); consequently, data from optical sensors are useful for large-scale forest assessment and monitoring (Wulder & Seemann, 2003). The key limitation of passive optical sensors is that they cannot capture detail below the forest canopy, and hence cannot directly measure vegetation structure (Hyde et al., 2006).

LiDAR, an active sensor, has been increasingly used in forest assessment. LiDAR directly measures canopy height, which is a commonly used attribute to describe forest structure (Hudak et al., 2009). Allometric relationships between tree height and diameter at breast height (DBH) have been derived for various tree species (Bi et al., 2012; Gill et al., 2000; Peper et al., 2001) and these two variables are commonly used to derive volume (Zianis & Seura, 2005). LiDAR-measured heights, together with other LiDAR-derived metrics (e.g. penetration metrics), are important for modelling other structural attributes, such as canopy cover (McIntosh et al., 2012), stem density (Naesset & Bjerknes, 2001), basal area (Packalen & Maltamo, 2008), biomass (d'Oliveira et al., 2012; Naesset, 2007), volume (Hall et al., 2005) and LAI (Jensen et al., 2008).

LiDAR is demonstrably superior to passive optical sensors for assessing forest structural variables, especially canopy height (Donoghue & Watt, 2006; Eid et al., 2004). Discrete return airborne LiDAR systems now collect stand-level and regional wall-to-wall forest structure attributes (tree height, stand volume and basal area) in the national inventory

programs of Finland, Norway and Sweden (Naesset, 2007; Naesset et al., 2004). Despite these examples, the high cost of LiDAR acquisition and lack of processing expertise generally precludes wall-to-wall LiDAR surveys for operational use (Lefsky et al., 2001b; Morgenroth & Visser, 2013).

In order to overcome the limitations of individual sensors and optimize the advantages of different types of sensors, discrete return LiDAR and optical sensors have been integrated to provide more comprehensive and accurate characterisation of forest structure and dynamics (Hudak et al., 2009). The intention is to keep the acquisition cost low (McInerney et al., 2010) while using the relationship between LiDAR and optical data to better describe a larger extent of the forest resource (Pascual et al., 2010). Combined use of optical images and LiDAR in forestry utilises both the spectral information in optical imagery and the 3-D information in LiDAR. Therefore, when combining LiDAR and optical spectral sensors, information from both sensors is integrated and more accurate results are expected.

Since optical sensors and discrete return LiDAR have been extensively studied and applied in forestry, a number of reviews on their individual use have been conducted (Ackermann, 1999; Boyd & Danson, 2005; Dubayah & Drake, 2000; Gleason & Im, 2011; Lim et al., 2003; Roberts et al., 2007; Ustin & Gamon, 2010; Wehr & Lohr, 1999; Wulder et al., 2012). However, no comprehensive review of the fusion of discrete return LiDAR with optical sensors has been conducted despite more than a decade having passed since the first integrated study of discrete return LiDAR and Landsat ETM+ (Hudak et al., 2002). This chapter will address this gap in the literature by reviewing research on the combined use of discrete return LiDAR and optical sensors across a broad range of applications in forestry, specifically with respect to forest delineation and classification, and estimating forest age, species and forest structural variables. This review is limited to sensor fusion studies where multi-sensors are used simultaneously to assess forest attributes.

2.1 Fusion of LiDAR and Optical Sensors

2.1.1 Forest Delineation and Classification

Forest classification and forest boundary delineation are important in both natural and planted forest management in assessing forest types and areas, as understanding forest area and location is fundamental for a broad field of applications and users (Eysn et al., 2012). Aerial photography is most commonly used to determine forest area through manual interpretation. However, forest stand delineation based on manual interpretation of aerial photos can be highly subjective and time-consuming. Forest cover type classification can be achieved by automated image classification by assigning forest cover types and estimating forest variables

based on the spectral, textural and auxiliary information in the image. This produces a more objective delineation and reduces time and associated costs (Mustonen et al., 2008).

LiDAR data adds a new source of information for forest classification and delineation through direct estimation of forest canopy size and height. Incorporating LiDAR into optical sensor mapping utilises both spectral and structural information to achieve a more accurate forest classification. Nordkvist et al. (2012) integrated low density discrete return airborne LiDAR-derived height metrics with SPOT 5 HRG spectral information for vegetation classification in Sweden, and achieved 16.1% improvement in classification accuracy compared to using SPOT only. The study also compared maximum likelihood and object-based decision tree classification approaches and found the best accuracy was achieved by decision tree classification.

Sasaki et al. (2012) achieved a minor improvement in overall land cover classification accuracy (95% to 97.5%) by an object-based classification approach integrating inputs from high resolution spectral images captured by digital camera with LiDAR-derived metrics including height, ratio, pulse and intensity parameters. Additionally, Bork and Su (2007) used a maximum likelihood approach to classify eight vegetation classes. Using only airborne LiDAR inputs achieved lower accuracy than using only a digital multispectral image. The fusion of LiDAR and multispectral imagery increased classification accuracy by 15-20%. A more recent study explored the benefits of incorporating a Digital Elevation Model (DEM) and Digital Surface Model (DSM) derived from LiDAR into tropical forest mapping using SPOT 5 HRG imagery. This approach enhanced image segmentation and successfully differentiated six vegetation classes, producing an overall forest classification accuracy of 91% (Dupuy et al., 2013).

The combination of aerial photography and LiDAR has also commonly been used for forest delineation. Wang et al. (2008) developed an approach to automatically delineate forest boundaries using both aerial photography and a LiDAR-derived Canopy Height Model (CHM) for the National Forest Inventory of Switzerland. The approach involved two processes: 1) detecting forests using a moving window over the CHM and delineating forest boundaries by analysing the CHM-derived curvature value, vegetation index and 2) using textural values of segmented image objects. Although there are no statistical improvements calculated, the visual results relative to manual digitisation looked very promising. Haywood and Stone (2009) developed an automated approach that transforms aerial photos and LiDAR CHM into vectorised forest stand boundaries (65% overall accuracy). The study did not explicitly show an improvement using sensor fusion, but it demonstrated the possibility of operationalising the fusion of optical sensor and LiDAR in natural forests stand delineation.

A summary of recent studies using integrated LiDAR and optical sensors is shown in Table 2-1. All of these studies have either shown an improvement (up to 20%) in forest classification results compared to using a single sensor, or made it possible to discriminate further forest classes that otherwise could not be identified by single sensors. All studies reviewed in this section used discrete return LiDAR and other optical sensors. LiDAR data has been acquired at point densities ranging from 0.54 points m^{-2} to 11.3 points m^{-2}, with all but one study reporting point density lower than 2 points m^{-2}. It appears that low density LiDAR is sufficient to classify forest types and delineate forest boundaries when integrated with optical sensors, as only the interpolated LiDAR surfaces are used as inputs.

When a fusion approach is used, the common approach to classify forest types and delineate forest boundaries is image classification based on inputs derived from both LiDAR and optical sensors. Machala and Zejdova (2014) listed 26 customised arithmetic features derived from discrete return LiDAR and multispectral sensor data that are useful inputs for classifying forest covers. The inputs are commonly rasterised and applied with automated image classification analysis. There is a clear trend towards the use of Object-Based Image Analysis (OBIA) rather than pixel-based classification like the maximum likelihood approach. Pixel-based image classification that ignores spatial association among pixels, tends to be sensitive to spectral variations hence it is likely to result in a relatively high level of misclassification (Lu & Weng, 2007). OBIA overcomes the issues by carrying out classification on segmented objects that are similar to real land cover features in size and shape (Chubey et al., 2006). The approach allows consideration of multiple image elements and scales such as texture, shape and context, as opposed to pixel-based classification that solely relies on the pixel values.

Overall, OBIA has been proven to produce more accurate classification results compared to a pixel-based approach with single sensor analysis (Gao, 2009). This may explain why OBIA is favoured in forest classification and delineation with integrated sensors. The statistics to evaluate the performance of forest type classification include classification accuracy matrices or confusion matrices, which compare the classified classes against reference classification and generate a series of statistics such as overall classification accuracy, producer's and user's accuracy and kappa coefficient (Foody, 2002).

Table 2-1: Recent studies of forest classification and delineation using integrated LiDAR and optical sensors.

Forest Species/Type	Remote Sensing Data used	Metrics derived	Estimated Parameters	Approach	Accuracy/Error	Reference
Mixed tropical forest reserves	Discrete return airborne LiDAR (2 points m^{-2}), Aerial photo (AP) and SPOT5 HRG	LiDAR derived DEM and DSM, spectral bands from AP and SPOT	Forest type classification	Image segmentation and multi-level decision-tree classification	Overall classification accuracy: 91%	Dupuy et al. (2013)
Wetland forests including pine, spruce and birch	Discrete return airborne LiDAR (1.6 points m^{-2})and SPOT5 HRG	SPOT spectral bands; LiDAR-derived height, canopy returns	Vegetation classification	Supervised maximum likelihood and decision tree classification	Overall accuracy SPOT only: 55.8%; combined SPOT and LiDAR: 71.9%	Nordkvist et al. (2012)
Mixed forest dominated by oak	Discrete return small-footprint airborne LiDAR (11.3 points m^{-2}) and simultaneously collected NIR digital image (0.18 m)	Spectral bands and NDVI from digital image; LiDAR derived DEM, CHM and intensity	Land cover classification and species classification	Image segmentation and object-based decision tree classification	Overall accuracy digital image only: 95%, combined with LiDAR: 97.5%	Sasaki et al. (2012)
Natural eucalyptus forest	AP and discrete return airborne LiDAR (0.96 points m^{-2})	Textural and spectral information from aerial photo; LiDAR derived CHM	Forest stand delineation	Automated imagery segmentation	Overall accuracy of 65%	Haywood and Stone (2009)
All forests in Switzerland (National Forest Inventory)	AP and discrete return small-footprint airborne LiDAR	AP derived vegetation indices (VI), textural information and LiDAR derived CHM	Forest detection and delineation	Decision tree using CHM, curvature feature and VI	Visual results only	Wang et al. (2008)
Mixed vegetation in rangeland including aspen forest	Discrete return airborne LiDAR (0.54 points m^{-2})and simultaneously collected digital image (0.5 m)	LiDAR height and DEM; RGB, digital image intensity and hue	Vegetation type classified	Supervised maximum likelihood classification and decision tree	Overall classification accuracy for LiDAR and Image only is 64.8% and 74.6% respectively, integrated approach: 91%	Bork and Su (2007)

2.2 Forest Species

Accurate characterization of species is important in forest management, resource planning and monitoring. Remote sensing technologies have been widely used for forest species classification (Immitzer et al., 2012; Orka et al., 2013). The recent development of laser scanning also offers the possibility of automatically identifying individual trees and obtaining height and canopy measurements from them (Hirata et al., 2009; Li et al., 2012; Yu et al., 2011), hence providing the possibility of classifying individual tree species (Holmgren et al., 2008).

More accurate species classification is expected from the fusion of LiDAR and other sensors due to the synergy of both structural and spectral data. Holmgren et al. (2008) used airborne LiDAR-derived height, canopy and intensity parameters to delineate individual tree crowns and calculate tree crown heights and areas, then identified tree species for delineated tree crowns using a maximum likelihood approach by integrating LiDAR data with features from high resolution Digital Mapping Camera (DMC) digital images. The overall species classification accuracy was 96%, which was an improvement from using LiDAR (91%) and digital imagery individually (88%). Ke et al. (2010) evaluated the combined spectral and textural layers from Quickbird imagery and topography, canopy height and intensity from low density LiDAR (0.16 points m^{-2}) for forest species classification, using object-based segmentation and machine learning decision trees. The highest classification accuracy (Kappa = 91.6%) was achieved using both spectral and LiDAR-derived metrics with accuracies that were 20% greater than those that used individual sensors.

Sasaki et al. (2012) classified 16 tree species with high density (11.3 points m^{-2}) airborne discrete return LiDAR and multispectral imagery. Although the object-based decision tree classification produced low overall accuracy (31.5%), a 17% improvement was made with inputs from both sensors. Some species such as pine and poplar gained significant improvement (32% and 56% respectively) with sensor fusion compared with using digital images only. A more recent study used very high resolution WorldView-2 images and discrete return airborne LiDAR for object-based species classification in a temperate rainforest in Australia. It utilised the spectral features and GLCM textures from the images, and a LiDAR-derived CHM and associated statistics to conduct an object-based decision tree classification on a mixture of natural and plantation forest species. The accuracy for LiDAR-only and image-only species classification was 61% and 70% respectively, whereas combined sensors improved species classification to 82% (Zhang & Liu, 2013).

Hyperspectral sensors have also been integrated with LiDAR in forest species classification. Several studies have indicated fusion between hyperspectral and LiDAR data enhances forest species differentiation. Dalponte et al. (2008) tested Leave-one-out Covariance (LOOC), Support Vector Machines (SVM) and k-Nearest Neighbour (k-NN) classifiers for forest species classification using hyperspectral bands and a LiDAR-derived CHM. The best classification accuracy was found using SVM. In total 23 tree species classes were successfully identified with the technique, with some classes over 90% accurate. The overall kappa accuracy using combined sensors was 89.2%, which was slightly higher than using individual sensors (hyperspectral only: 87.9%, LiDAR only: 89%). Jones et al. (2010) applied similar datasets and techniques to classify more than ten forest species classes. They found most species classes gained accuracy improvement with fusion of hyperspectral and LiDAR inputs (ranging from 0.3% to 19%) although the overall accuracy improvement was only minor (1.2%).

The way that sensor fusion has been performed is that high resolution optical imagery defines forest stand boundaries and provides spectral separation between different forest species. The addition of LiDAR-derived topographic and height and intensity information further reduces within class spectral variations caused by topography, and enhances variations between species classes as different tree species tend to have different heights (Ke et al., 2010). Recent studies integrating LiDAR with other sensors to estimate forest species are shown in Table 2-2. These studies show that sensor fusion has improved the accuracy of species identification and classification by up to 21%. It is worth noting that species classification from sensor fusion approaches has yielded high variation in accuracies, ranging from 48.4% to 96% as a result of large variations in species composition in these studies. Discrete return airborne LiDAR was the most common sensor type and the range of point densities was large, spanning 0.16 points m^{-2} – 50 points m^{-2}. The point density of LiDAR acquisitions for species classification was generally higher than for forest area delineation. As with forest area classification, object-based decision tree classification is predominantly used in species classification with LiDAR and multispectral sensors.

Hyperspectral sensors capture finer details in the spectral signature (i.e. narrower spectral bands) than multispectral sensors, which allows more detailed differentiation between similar forest types (Dalponte et al., 2008). Generally, hyperspectral sensors alone have shown promising capability in species classification probably due to high spectral resolution. This explains why only minor improvements in species classification accuracy were observed when LiDAR was added (Table 2-2). Despite high species classification accuracy using only hyperspectral imagery (relative to multispectral imagery), there is no evidence to suggest that

fusion of LiDAR and hyperspectral sensors classifies species more accurately than fusion of LiDAR and multispectral sensors. The processing of hyperspectral data can add complexity as they contain a vast array of spectral bands, so a feature selection process is required to eliminate any redundant bands (Dalponte et al., 2008). Rather than conventional classification approaches, non-parametric classifiers, especially SVM has been used when classifying hyperspectral data. SVM is a linear binary classifier that assigns a given test sample from one of the possible labels (Mountrakis et al., 2011). The application of SVM has improved classification accuracy, analysis time and stability with hyperspectral data (Jones et al., 2010).

Table 2-2: Recent studies of forest species identification using integrated LiDAR and optical sensors

Forest Species/Type	Remote Sensing Data used	Metrics derived	Estimated Parameters	Approach	Accuracy/Error	Reference
Cool temperate rain forest	Discrete return airborne LiDAR and WorldView-2	Spectral and textural information from WorldView-2; LiDAR-derived CHM and DEM	Forest species classification	Object-based classification using decision trees	Overall accuracy WorldView-2: 70.4%; LiDAR: 61.39%; combined sensors: 82.35%	Zhang and Liu (2013)
Mixed forest dominated by oak	Discrete return airborne LiDAR (11.3 points m^{-2})and simultaneously collected digital image (0.18 m)	Spectral bands and NDVI from digital image; LiDAR derived DEM, CHM and intensity	Land cover classification and species classification	Image segmentation and object-based classification using decision trees	Overall accuracy digital image only: 31.5%; combined sensors: 48.4%	Sasaki et al. (2012)
Mixed deciduous forest: maple, beech, pine and spruce	Quickbird and discrete return airborne LiDAR (0.16 points m^{-2})	Quickbird spectral bands; DEM, terrain layers, CHM and intensity from LiDAR	Forest species classification	Object-based classification using machine learning decision trees	Overall accuracy from Quickbird only: 63%, combined sensors : 83%	Ke et al. (2010)
Mixed species forest dominated by Douglas-fir	Transect hyperspectral (2m resolution) and discrete return airborne LiDAR (0.4 points m^{-2})	LiDAR CHM and canopy volume; selected hyperspectral channels	Forest species classification	Support vector machine classification	Overall accuracy using only hyperspectral: 72.3%, combined sensors 73.5%	Jones et al. (2010)
Mixed spruce, pine and deciduous species	Discrete return airborne LiDAR (50 points m^{-2}) and DMC (0.6 m)	Height, canopy, pulse and intensity variables from LiDAR; spectral bands from DMC	Individual tree species identification	Maximum likelihood classification of derived individual tree crown	Overall classification accuracy for DMC only: 88%, LiDAR only: 91%, and combined sensors: 96%	Holmgren et al. (2008)
Mixed oak species (>20 species)	Hyperspectral (1m resolution) and discrete return airborne LiDAR (5.6 points m^{-2})	LiDAR DEM and intensity; selected hyperspectral channels	Area of species composition	SVM, LOOC and k-NN	Highest Kappa Accuracy from Hyperspectral only: 87.9%; LiDAR only: 89%, combined sensors 89.2%	Dalponte et al. (2008)

2.3 Tree Height

Canopy height is considered the key attribute for understanding the vertical structure of forests, and is a crucial parameter for modelling forest growth. LiDAR is the best remote sensing method available for tree height measurement (Lefsky et al., 2001a). It has been suggested that the use of LiDAR and other sensors can potentially be a substitute for field measured canopy heights (McInerney et al., 2010).

Spectral reflectance in the form of either raw band value or band ratios (e.g. NDVI) is the primary input from satellite imagery when integrated with LiDAR data to estimate height. Combining LiDAR-derived heights with Very High Resolution (VHR) imagery and aerial photos provides the means to more accurately segment individual trees, hence to estimate forest attributes at the individual tree level (Mora et al., 2013). McCombs et al. (2003) combined small-foot print LiDAR and high-resolution digital multispectral imagery captured by Spectral Visions to identify individual stems and estimate plot mean height in two planted pine forests. A focal search function was used to identify the location of individual trees based on LiDAR-derived tree height and NIR reflectance from an image. Tree identification accuracy increased by 7.6% for high density plots and 18.8% for low density plots using combined sensors. However, no improvement in height was reported using the combined approach.

Suárez et al. (2005) used high-resolution aerial photography and LiDAR-derived Tree Canopy Model (TCM) to segment individual Sitka spruce trees in order to derive individual tree height. The study found the method successfully estimated individual tree height, especially for larger trees (R^2= 0.86). The study only used the combined sensor approach, hence no comparison with a single sensor was reported. Popescu and Wynne (2004) utilised multispectral ATLAS imagery to stratify forest types using maximum likelihood classification, which facilitated the identification of single trees and the estimation of their heights with LiDAR. Single trees were identified using a variable window technique with local maximum focal filtering over both LiDAR and ATLAS features. Minor improvement on height estimation with sensor fusion was observed (R^2 increased by 1% for pines and up to 3% for deciduous). A canopy fuel study also observed a minor improvement in canopy height estimation using metrics derived from both LiDAR and DMC imagery compared to LiDAR alone (R^2 of 0.957 and 0.935 respectively). The study also examined the canopy base height which is the lowest green foliage and found a 6% improvement with the sensor fusion (Erdody & Moskal, 2010).

The fusion of LiDAR and optical sensors has been used in both identifying or delineating individual trees and estimating single tree height. There are a variety of statistical algorithms adopted to predict tree height based on metrics derived from LiDAR and optical sensors. All the height estimation studies we reviewed (Table 2-3) applied a linear or multiple regression equation solved using ordinary least squares (OLS). Model performances were evaluated by the coefficient of determination (R^2) and Root Mean Square Error (RMSE).

Table 2-3 shows that LiDAR has already proven very accurate in canopy height estimation. Fusion with other optical sensors added little improvement in height estimation accuracy (1-7%). One study even reported a slight negative influence on height estimation with sensor fusion compared to using LiDAR alone (McCombs et al., 2003). A benefit of sensor fusion for tree height estimation is that it supports tree delineation, which is difficult to achieve with small-footprint or lower point density LiDAR alone. All studies in Table 2-3 acquired low to medium density LiDAR, ranging from 1 point m^{-2} to 4 points m^{-2}. The point densities here are lower and have less variation than point densities reported in studies focused on area delineation and species classification. The high R^2 values are evidence that despite the lower point density, tree and canopy height can be estimated with high accuracy.

Table 2-3: Recent studies of forest height estimation using integrated LiDAR and optical sensors

Forest Species/Type	Remote Sensing Data used	Metrics derived	Estimated Parameters	Approach	Results	Reference
Conifer forest dominated by Ponderosa pine, Douglas-fir, grand fir and lodgepole pine	Discrete return airborne LiDAR (>4 points m^{-2}) and simultaneously collected digital image (0.6 m)	LiDAR height variables and intensity; Digital imagery spectral bands and NDVI	Canopy fuel attributes: canopy height (CH), canopy base height (CBH)	Multiple regression modelling	CH R^2 LiDAR only: 0.935, image only: 0.415 and combined sensors: 0.957 CBH R2 LiDAR only: 0.783, image only: 0.309 and combined sensors: 0.843	Erdody and Moskal (2010)
Sitka spruce forest	Discrete return airborne LiDAR (3-4 points m^{-2}) and aerial photo (0.25 m)	LiDAR CHM, aerial photo bands	Individual tree height	Segmentation of image to delineate individual trees	Combined sensors: R^2 = 0.69-0.86	Suárez et al. (2005)
Mixed deciduous and coniferous	Discrete return airborne LiDAR (2 points m^{-2}) and ATLAS image	LiDAR CHM, classified imagery derived crown form	Individual tree height	Forest type classification by ATLAS, variable window size filtering for tree identification, regression modelling	Pine: Height best LiDAR only R^2 = 0.96, combined sensor R^2 = 0.97 Deciduous: Height best LiDAR only R^2 = 0.76, combined sensor R^2 = 0.79	Popescu and Wynne (2004)
15-year-old loblolly pine plantation	Discrete return airborne LiDAR (1-1.5 points m^{-2}) and digital imagery (0.6 m)	CHM and intensity from LiDAR; NIR band from digital imagery	Individual tree identification and mean height	Identify and count trees with a focal window passing over, derive individual tree height based on LiDAR	Low density (3m spacing): Tree identification accuracy image only R^2: 0.924 LiDAR only: 0.873, combined sensors: 0.948. LiDAR underestimated mean height by 0.38m, combined underestimated men height by 0.50m High density (2.4m spacing): Tree identification accuracy image only R^2: 0.786, LiDAR only: 0.647, combined sensors: 0.835. LiDAR underestimated mean height by 0.15m, combined underestimated men height by 0.42m	McCombs et al. (2003)
Douglas fir , hemlock and other hardwood	Discrete airborne (~1 points m^{-2}) LiDAR and Landsat ETM+	Landsat spectral bands, LiDAR height- square root transformed	Canopy height	Empirical modelling, semi-variogram models	Combined sensors: R^2 = 0.73-0.96	Hudak et al. (2002)

2.4 Forest Volume and Biomass

Height and diameter measurements are highly correlated with forest volume and above-ground biomass in deciduous, coniferous and tropical forests (Dubayah & Drake, 2000). Volume provides an understanding of forest productivity and structure. Forest biomass allows the estimation of the carbon content in forests, which is important for understanding carbon stock changes associated with deforestation, forest degradation and afforestation. Carbon reporting is required to fulfil obligations to international agreements such as the United Nations Framework Convention on Climate Change (UNFCCC) (Rosenqvist et al., 2003). Additionally, accurate estimation of biomass in forested areas is essential for developing sustainable climate-friendly strategies (Jochem et al., 2010). Forest volume and biomass can be directly measured in the field through destructive sampling, but usually they are estimated based on measured variables such as diameter and height. Remote sensing has been widely applied to estimate forest volume and biomass due to extensive coverage and cost efficiency (Gleason & Im, 2011).

Fusion of LiDAR and optical sensors has been studied for estimating forest volume and biomass at the individual tree level (St-Onge et al., 2008) or plot level (Tonolli et al., 2011), and achieves more accurate estimation than single sensors. An early study used small-footprint airborne LiDAR and multispectral ATLAS imagery to explore the possibility of estimating forest volume and biomass in mixed-species forests. Popescu et al. (2004) used spectral information and a LiDAR-derived CHM to delineate individual tree crowns and estimated tree height, basal area, volume and biomass at the plot level using linear regression models. Promising results were achieved for coniferous forests, with R^2 of 0.83 for volume and 0.82 for biomass. Though it was not quantified, the authors commented that an improvement in estimation accuracy was achieved with sensor fusion compared to LiDAR alone.

Tonolli et al. (2011) estimated tree stem volume at plot level with integration of low density discrete return airborne LiDAR and multispectral IRS data. Height metrics and canopy variables extracted from LiDAR, together with spectral bands and band ratios extracted from IRS were correlated with the tree volume calculated from field inventory data. The combined sensor approach consistently produced higher R^2 and lower RMSE across all species compared to using either sensor alone. Wallerman and Holmgren (2007) predicted forest height, stem density and mean volume using a canonical correlation approach with inputs derived from both LiDAR and SPOT 5 HRG. Using the combined sensors achieved a more accurate mean stand volume estimation compared with using LiDAR only, resulting in a 2-4% lower RMSE. Estornell et al. (2012) used stepwise regression to find the best fit between

LiDAR and spectral data from digital images against field measurements, they observed a significant improvement in modelling vegetation volume and biomass when both LiDAR and digital images were used, with R^2 increasing by 12% for volume and 29% for biomass compared to LiDAR only models.

Most studies reviewed in this chapter related to volume and/or biomass estimation using linear or multiple regression models to correlate LiDAR and optical sensor derived metrics with field measurements. However, OLS regression assumes that the explanatory variables are free of measurement errors, which is not realistic in remote sensing data inputs (Berterretche et al., 2005). So, there has been increasing use of non-parametric modelling approaches to model forest volume with integrated LiDAR and spectral inputs. For example, Packalen and Maltamo (2007) applied k most similar neighbour (k-MSN) imputation to predict species-specific volume at the stand level from airborne LiDAR-derived height metrics and aerial photograph-derived spectral and textural features. They found that the basal area and volume estimation using inputs from both sensors were accurate (RMSE= 8.63% and 10.36% respectively), although deciduous species showed higher errors than coniferous species (up to 34% higher RMSE). Cartus et al. (2012) used a Random Forest (RF) regression tree algorithm to predict stand level canopy height and Growing Stock Volume (GSV) over a large plantation area, using metrics derived from low density discrete return LiDAR, RADAR sensor (ALOS PALSA) and Landsat ETM+. The fusion of RADAR and Landsat produced a minor improvement (6%) in GSV estimation compared with using LiDAR. Although the study did not combine LiDAR with Landsat, it demonstrated a well described methodology of using RF to model forests attributes with different sensor inputs.

Overall, optical sensors alone have not shown good performance in assessing forest volume and biomass; recent studies have demonstrated more significant improvement (up to 55%) in modelling forest volume and biomass with the addition of LiDAR (Table 2-4). In terms of the measuring model performance, R^2 and RMSE are commonly used. Some studies also measure the bias of models (Brosofske et al., 2014). A wide range of R^2 values was reported for data fusion approaches to estimating both biomass and volume. Biomass estimates ranged from R^2 = 0.33 to 0.82, while volume estimates ranged from R^2 = 0.39 to 0.87. In both cases, the lowest R^2 values were associated with estimates for deciduous forests. It appears that the biomass and volume for deciduous forests are more challenging to predict even with integration of LiDAR and optical sensors. This is an area where the development of species-specific techniques could significantly improve results. Furthermore, most studies reviewed in this section used low to medium density discrete return airborne LiDAR. Higher density LiDAR data or other forms of LiDAR acquisition, such as full waveform or terrestrial LiDAR,

could potentially enhance the volume and biomass estimation particularly for deciduous forests due to analysis at a finer scale.

Table 2-4: Recent studies of forest volume and biomass using integrated LiDAR and optical sensors

Forest Species/Type	Remote Sensing Data used	Metrics derived	Estimated Parameters	Approach	Results	Reference
Even aged *Pinus radiata* and *Eucalyptus globulus* plantations	Discrete return airborne LiDAR (1-3 points m^{-2}) , ALOS PALSAR Landsat ETM+	LiDAR-derived CHM, height and canopy metrics; ALOS-derived intensity and coherence, Landsat spectral bands	Stand-level canopy height (CH) and Growing stock volume (GSV)	Segmentation to delineate stand objects, Random Forest imputation of CH and GSV using field-collected variables and sensor variables	CH R^2 LiDAR only: 0.93, RMSE% =7.08; combined sensors: 0.86, RMSE% =9.7 GSV R^2 LiDAR only: 0.81, RMSE% =22; combined sensors: 0.87, RMSE% =15	Cartus et al. (2012)
Mixed forest dominated by oak, with ground vegetation	Discrete return airborne LiDAR (8 points m^{-2}) and digital image	LiDAR-derived height metrics; image bands and NDVI	Volume and biomass of shrub vegetation	Stepwise regression analysis	Biomass R^2 LiDAR only: 0.67; image only: 0.34; combined sensors: 0.79 Volume R^2 LiDAR only: 0.55; image only: 0.29; combined sensors: 0.84	Estornell et al. (2012)
Mixed conifers including fir, spruce, larch and pine	Discrete return airborne LiDAR (0.48 points m^{-2}) and IRS	Height and coverage metrics from LiDAR, spectral bands, band ratios and vegetation indices from IRS	Stem volume	Linear regression of field-collected variables and sensor variables	All species LiDAR only: R^2=0.7, RMSE%= 19.2; IRS only: R^2=0.42, RMSE%= 26.6; Combined sensors: R^2=0.72, RMSE%= 18.5 Same pattern for individual species	Tonolli et al. (2011)
Mixed Balsam fir, spruce, birch, aspen, pine	Discrete return airborne LiDAR(3 points m^{-2}), IKONOS	LiDAR CHM, IKONOS DSM	Height and AGB	Co-registration of LiDAR and IKONOS to get IKONOS-LiDAR CHM	Height R^2 LiDAR only: 0.75, combined sensors: 0.87 Biomass R^2 LiDAR only = 0.87, combined sensors: 0.79	St-Onge et al. (2008)
Boreal forest dominated by coniferous species and some deciduous	Discrete return airborne LiDAR (0.7 points m^{-2}) and AP with NIR (0.5 m)	LiDAR-derived height metrics, AP spectral and textural metrics	Basal area (BA) and volume (V) at plot level and stand level	k-MSN imputation of field-collected variables and sensor variables	All species: BA RMSE=8.63%, V RMSE = 10.36% Deciduous: BA RMSE=52.53%, V RMSE= 62.33% Pine: BA RMSE=27.05 %, V RMSE = 28.08% Spruce: BA RMSE=31.3 %, V RMSE = 32.64%	Packalen and Maltamo (2007)
Scots pine, Norway spruce and birch	Discrete return airborne LiDAR (1.5-2 points m^{-2}) and SPOT 5 HRG	LiDAR CHM, SPOT spectral bands	Stand mean volume and stem density	Canonical correlation approach and cross validation	Stand mean volume: LiDAR only RMSE up to 23%, combined sensors RMSE =20 %. Stem density: LiDAR only RMSE up to 30% , combined sensors RMSE = 22%	Wallerman and Holmgren (2007)
Mixed deciduous and coniferous	Discrete return airborne LiDAR (2 points m^{-2}) and ATLAS	LiDAR CHM, crown diameter and number of trees; Image spectral bands and classified forest types	Plot-level volume and biomass	Forest type classification by ATLAS, variable window size filtering for tree identification, regression modelling	Volume estimation: R^2=0.83 for pine and 0.39 for deciduous Biomass estimation: R^2=0.82 for pine and 0.33 for deciduous	Popescu et al. (2004)

2.5 Forest Age and Productivity

Too few studies prevent firm conclusions from being drawn about the utility of sensor fusion for forest age and productivity estimation. Nevertheless, a summary of existing studies is presented. Forest age is highly correlated with growth and is a key attribute in forest information systems (Clark et al., 2006). Stand age is an important variable but it may not always be available, such as for extensive national forest inventories (Tomé et al., 2006) and uneven-aged natural forests (Weber & Boss, 2009). Stand age data could be collected by field inventory and ring count analysis, but this is labour intensive and lacks consistency among different cruising crews (Avery & Berlin, 1992; Avery & Burkhart, 1983). Therefore, alternative approaches are desirable and remote sensing techniques have been useful in estimating forest age. Research has shown that forest age is correlated with spectral reflectance of satellite imagery (Cohen et al., 1995), especially the near infrared band and its derived vegetation indices (Jensen et al., 1999). Remote sensing data is also capable of estimating age or age classes based on the differences in tree size, density, understory and canopy developments (Gemmell, 1995).

Because tree height is a strong predictor of forest age and active sensors directly measure height, studies have incorporated active sensors into forest age estimation to improve accuracy. Vega and St-Onge (2009) developed a method of classifying unknown forest age based on existing age-height correlations and a time-series of CHMs derived from both aerial photography and LiDAR. CHMs were reconstructed for a period of 58 years based on historic AP-derived CHMs and a recent LiDAR-derived CHM. The RMSE of the estimated forest age was 7 years.

Forest site productivity refers to the potential tree height or aboveground wood volume for a particular forest site (Skovsgaard & Vanclay, 2008). Understanding patterns in forest productivity is critical to forest resource management and influences tree species selection, design of optimal silvicultural regimes and forecasting timber yields (Bontemps & Bouriaud, 2014). Site productivity is often 0dominant trees at a reference age (Sharma et al., 2012; Skovsgaard & Vanclay, 2008). SI is a widely accepted quantification of productivity, as stand height or current height growth seems to correlate well with stand volume growth (Skovsgaard & Vanclay, 2008). Also, compared to comprehensive assessments of forest site condition, SI is a simple variable that is relatively easy and inexpensive to measure and is generally not affected by management practices (Chen & Zhu, 2012). However in order to estimate SI, stand age must be known.

The information on tree height at various ages used for building SI is normally derived from measurements of trees from sample plots (Raulier et al., 2003). However, field measurements sometimes cannot capture the spatial variation of forest productivity due to limited scale (Vega & St-Onge, 2009). Improvements in availability of remotely sensed data such as LiDAR have yielded

opportunities for estimating site productivity at increasingly finer scales. Studies have successfully utilised LiDAR to estimate dominant tree height and evaluate SI and site type for boreal forest in Finland (Holopainen et al., 2010), radiata pine in Australia (Rombouts et al., 2010) and eucalyptus plantations in Brazil (Packalén et al., 2011) with given forest age. Alternatively, it is also possible to determine SI from single-tree-based LiDAR to extract tree height at the individual tree level so that site index can be predicted at stand level. For example, Gatziolis (2007) overlaid field-delineated individual tree crowns on a LiDAR point cloud to estimate dominant tree height; together with stand age information collected from the field, the SI at plot level was estimated. Chen and Zhu (2012) used LiDAR-derived heights for individual trees in combination with stand age to predict stand level SI for radiata pine plantations in Australia.

Although LiDAR can accurately estimate tree heights and hence SI, the use of a LiDAR sensor alone to estimate productivity can be limiting, especially if forests lack stand age information. So far, very few studies have used integrated sensors to evaluate site productivity. Lefsky et al. (2005) derived stand age by classifying a multi-temporal sequence of Landsat MSS and TM images, and extracted stand height and aboveground net primary production of wood (NPP AW) from field measurements and LiDAR transects. In this study NPP AW, which is calculated as the average increment in biomass over a time period, was used as the indicator for forest productivity. A study mentioned earlier by Vega and St-Onge (2009) used aerial photos obtained between 1945 - 2003 and recent LiDAR data to reconstruct CHMs over 58 years to estimate SI for jack pine over an extended region; stand SI was estimated with an average RMSE of 2.41 m. The approach developed produced continuous SI and age maps in a spatially explicit way.

To date, too few integrated sensory studies have estimated forest age and/or productivity to prove or disprove the utility of the approach. Most age estimation research today is focussed on using a single sensor or using time-series analysis of remote sensing data (Cohen et al., 1995; Jensen et al., 1999; Lefsky et al., 2005; Weber & Boss, 2009). Both productivity studies (Lefsky et al., 2005; Vega & St-Onge, 2009) used optical sensors to gain stand age information in order to evaluate forest productivity, yet neither was considered a sensor fusion approach as the inputs from both LiDAR and optical sensors were not used simultaneously. As a consequence of the lack of previous studies, it is not possible to draw conclusions about whether sensor fusion can improve forest age or productivity estimation, but promise has been shown.

2.6 Conclusion

The studies reviewed in this paper confirmed that fusion of primarily airborne LiDAR and optical sensors can improve many aspects of forest description. In particular, sensor fusion significantly improved delineatation of forest areas (by up to 20%), identification of species (by up to 21%), and estimation of forest volume and biomass (by up to 55%). As LiDAR alone has proven very effective in measuring canopy height, improvements in height estimation due to sensor fusion have been relatively small (between 1 to 7%). The improvement of integrating LiDAR and optical sensors for forest age and productivity assessment cannot be fully evaluated due to the limited number of studies, yet they provide future research directions for sensor fusion application. Some studies also showed estimating forest height (Popescu & Wynne, 2004) and volume (Packalen & Maltamo, 2007) of deciduous forests can be more challenging than coniferous forests possibly due to more complex forest structure and seasonal changes.

The approaches applied for classifying forest types and species, and estimating forest structural varibles with inputs from LiDAR and spectral data are relatively standardised. However, forest delineation appears to lack a common approach to evaluate performance. It was noted that some studies tend to compare the automated stand delineation results with manual interpretation (Haywood & Stone, 2009; Wang et al., 2008), yet in reality manual results are not always available. Mustonen et al. (2008) assessed the variation in mean height, diameter and volume within delineated stands as a basis for evaluating results, which may be an appropriate approach for future studies. Moreover, modelling approaches for predicting forest height and volume commonly used linear or multiple regression analysis, or non-parametric approaches such as kNN and Random Forest. None of these works for all situations, therefore consideration should be given to selecting the most appropriate modelling approach. Brosofske et al. (2014) provided a thorough review on modelling approaches for estimating forest variables, which serves as a reference for selecting regression models.

While fusion appears to be effective in a research environment, a challenge will be to operationalise the research such that forestry companies and governments can implement data fusion for improved forest management. Research on implementation will have to consider how to include data fusion into a standard forest mapping environment and also how to fully utilise the advantages of sensor fusion without incurring substantial extra costs. Additionally, the studies reviewed are primarily discrete return airborne LiDAR, which has been well developed and widely studied. Fusion of optical sensors with other forms of LiDAR such as fullwave form and terrestrial scanners is worth exploring in deriving an enhanced forest description.

Chapter 3 - Remote Sensing Data Processing

3.1 Introduction

This research involves three sets of remote sensing data: aerial photography, airborne LiDAR and Rapid Eye (Table 3-1). This chapter details the pre-processing steps undertaken to render the remote sensing datasets ready for area and yield analysis.

Table 3-1: General description of remote sensing datasets

Dataset	Resolution	Description	Supplier
Aerial Photography	0.3 m	Othorectified aerial photography acquired by regional councils in 2013	LINZ
Airborne LiDAR	1.3 points m^{-2}	Acquired for Wellington Region in 2013	Greater Wellington Region Council
RapidEye	5 m	Resampled 5 m resolution multispectral imagery	RapidEye Oceania distributor - AAM Group

3.2 Study Area

The study area for this research is Wairarapa region, which is located at the south-eastern corner of the North Island (Figure 3-1). The region consists of three districts: Masterton, Carterton and South Wairarapa. The NEFD indicates there are 51 871 ha of forest plantations in Wairarapa Region (MPI, 2014), approximately 50% of the plantations are owned by small-scale forest owners (i.e. <1000ha) (Figure 3-2). This region is selected due to its large area of small-scale plantations and the availability of recent LiDAR coverage.

Figure 3-1: Study Area: The red shaded area shows the research area

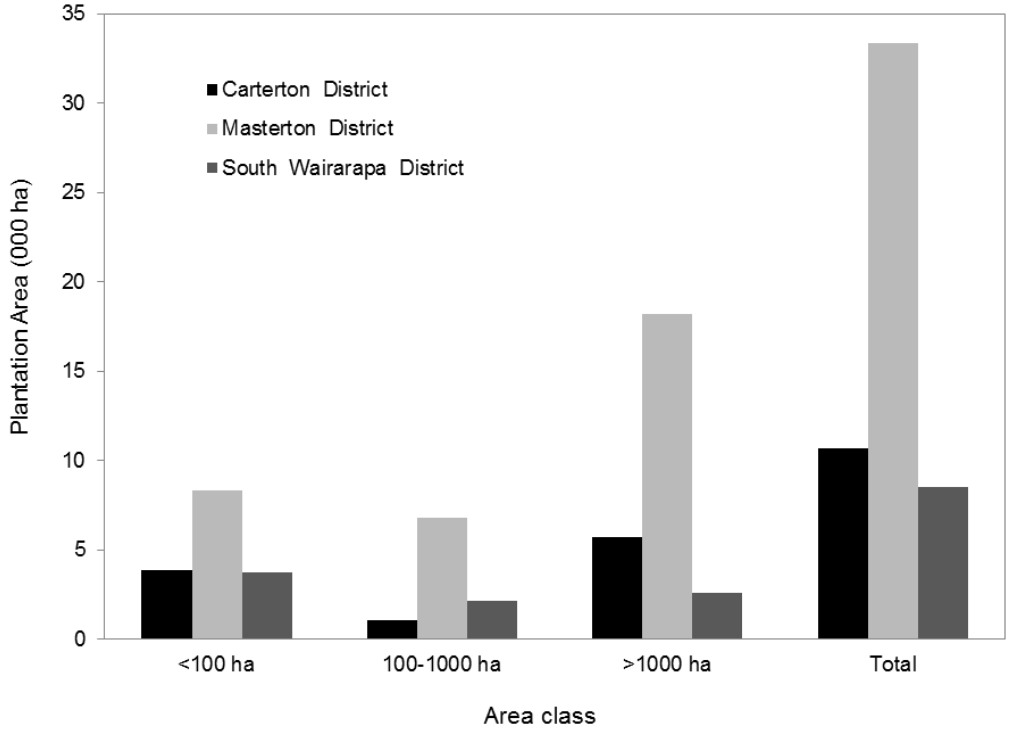

Figure 3-2: Plantation area summary by area class and district, data provided by MPI

3.3 Datasets Description

3.3.1 Aerial Photography

The Wellington Regional Council (WRC) acquired orthorectified aerial photography on six dates between 10 December 2012 and 30 January 2013. In total 764 aerial photos covered the Wairarapa region. The aerial photos were distributed freely by Land Information New Zealand (LINZ) under the Common Creative Licence 3.0. The specifications for the aerial photography campaign are shown in Table 3-2. The delivered aerial photographs were used as the basis for manual interpretation and land class digitisation to serve as the ground truth dataset, against which classified datasets would be compared.

Table 3-2: Specifications for the Wairarapa region aerial photography campaign

Aerial Photograph Attributes	Details
Product	NZTM RGBI Orthophotos
File Format	TIF/TFW
File Naming	LINZ Topo50 - 1:5000 tiles
Bands	Red, Green, Blue and Intensity
Resolution	0.3m
Map Projection	NZTM
Photography	SN51023D
Date of photography	10 December 2012, 16 December 2012, 05 January 2013, 25 January 2013, 29 January 2013, 30 January 2013.

3.3.2 Airborne LiDAR

Wellington Regional Council and Landcare Research provided wall-to-wall LiDAR coverage over the Wairarapa Region. Airborne LiDAR survey data were collected by Aerial Surveys Ltd. from 4 January to 23 December 2013, the flight specifications are listed in Table 3-3. Due to extensive acquisition area, the region was divided into five sub-regions for LiDAR acquisition (Figure 3-3).

Table 3-3: LiDAR Survey Specification

LiDAR Attributes	Details
Scanner	Optech ALTM 3100EA
Flying Height	1000 m AMGL
Scan Angle	±18.8 °
Scan Frequency	53 Hz
Pulse Rate	100 kHz
Swath Overlap	50%
Swath Width	680 m
Planned point density	1.3 points m^{-2}
Cross Track Resolution	0.72 m
Down Track Resolution	0.80 m

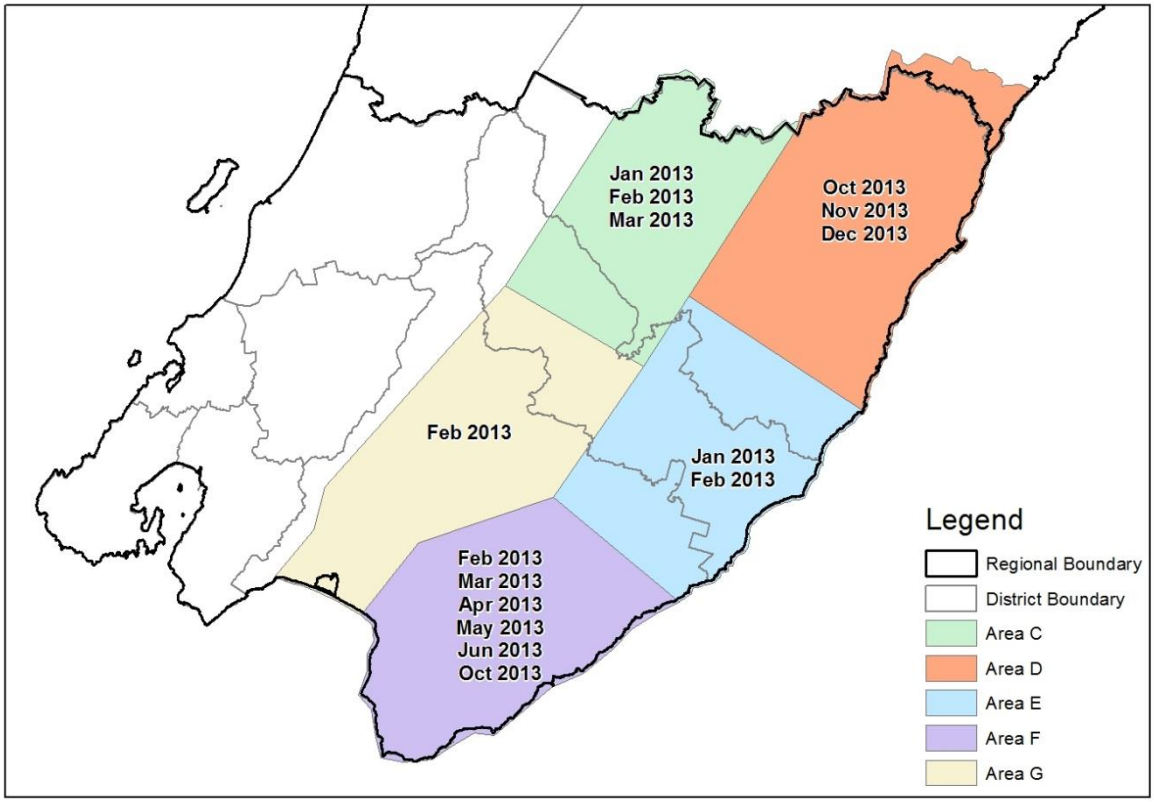

Figure 3-3: Aerial LiDAR Acquisition Dates by Areas

Landcare Research, as the agent for the WRC, delivered geo-referenced but unclassified raw LiDAR points, in LAS format, in 1km x 1km tiles. The planned point density was 1.3 points m^{-2}, the actual point density delivered was much higher due to high swath overlap. The delivered point density differs for each sub-region, but averages 3.76 points m^{-2} (Table 3-4).

Table 3-4: LiDAR Point Density for Each Acquisition Area

Area	No. of Tiles	Average Pt Density (points m^{-2})
C	1129	3.59
D	1701	3.65
E	1246	4.04
F	1385	4.4
G	1345	3.1
Total	**6806**	**3.76**

3.3.3 RapidEye

The RapidEye scenes are 3A products with radiometric, sensor and geometric corrections applied to the data. Imagery specifications are shown in Table 3-5. A total of 21 cloud-free images were acquired between 13 November 2013 and 20 February 2014 (Figure 3-4).

Table 3-5: RapidEye Satellite Specifications (BlackBridge, 2013)

RapidEye Attributes	Details
Number of Satellites	5
Spacecraft Lifetime	Over 7 years
Orbit Altitude	630 km in Sun-synchronous orbit
Equator Crossing Time	11:00 am local time (approximately)
Sensor Type	Multi-spectral push broom imager
Spectral Bands	Blue: 440-510 nm Green: 520-590 nm Red: 630-685 nm Red Edge: 690-730 nm NIR: 760-850 nm
Ground sampling distance (nadir)	6.5 m
Pixel size (orthorectified)	5 m
Swath Width	77 km
Revisit Time	Daily (Off-nadir)/ 5.5 days (at nadir)
Product Attribute	Details
Format	GeoTIFF
Bit Depth	16-bit unsigned integers
Individual image extent	25 x 25 km
Horizontal Datum	WGS84
Map Projection	Universal Transverse Mercator (UTM)

Figure 3-4: RapidEye Acquisition Date and Coverage

3.4 Dataset Processing

3.4.1 LiDAR Pre-processing

LiDAR data used for forestry applications are conventionally delivered as classified points (ground and non-ground points). However, LiDAR for this study came as unclassified raw data, thus some data filtering and classification steps were required in pre-processing LiDAR data. These steps were undertaken using Fusion (Pacific Northwest Research Station, USDA). A selection of ten las tiles covering representative land covers were tested before application to the entire LiDAR dataset.

1. Filtering points

Points that clearly did not represent ground or on-ground objects (e.g. vegetation) were classified as outliers and removed so that only relevant points were included in the analysis. In Fusion, the "FilterData" function was used to eliminate outliers by identifying and removing returns based on the range of observed elevation values in a comparison window. It works by computing the mean elevation and standard deviation of elevations for each comparison window. As suggested by the user guide and tested on a number of las tiles, any points that exceeded three times the standard deviation elevation of all surrounding points within a 100 x 100 m window were classified as outliers and

removed. The filtered las files were checked based on average elevation. Overall 0.3% of points were classified as outliers and removed. The average elevation of each region was within a normal range after point filtering (Table 3-6).

Table 3-6: The impact of point filtering by each acquisition area

Area	Average Elevation (m)		Proportion of Pts Filtered
	Raw Data	After Filtering	
C	1 062	352	0.50%
D	1 066	307	0.20%
E	1 013	328	0.20%
F	950	349	0.10%
G	964	185	0.60%
Average	1 011	304	0.30%

2. Classifying LiDAR points

Classifying LiDAR points is usually done using the industry standard package- TerraScan. However, this study did not have sufficient funding to use TerraScan. Instead, the function "GroundFilter" function in Fusion was used to classify the LiDAR point cloud into ground and non-ground points. The function is designed to filter LiDAR returns to identify returns that are possible ground points using an algorithm adapted from Kraus and Pfeifer (1998). The algorithm can be used with low-medium density point clouds (< 4 points m^{-2}) but some experimentation with the function's parameters was required to achieve an optimal classification (Appendix A). Although GroundFilter does not completely remove returns from large, relatively flat and elevated surfaces such as building tops, it manages to remove most vegetation returns with an appropriate weight coefficient and sufficient iterations. The weight parameter setting was g = -1.5 and w = 2 with 10 iterations. The developer claims the tool is sufficient in differentiating ground and non-ground points for calculating vegetation heights (McGaughey, 2016b).

To test the suitability of Fusion for classifying LiDAR points, a sample digital elevation model (DEM) generated from classified ground points using Terrascan was compared with the DEM generated using Fusion (Figure 3-5). The sample DEM was from a different study area where LiDAR data were delivered as classified ground and non-ground points.

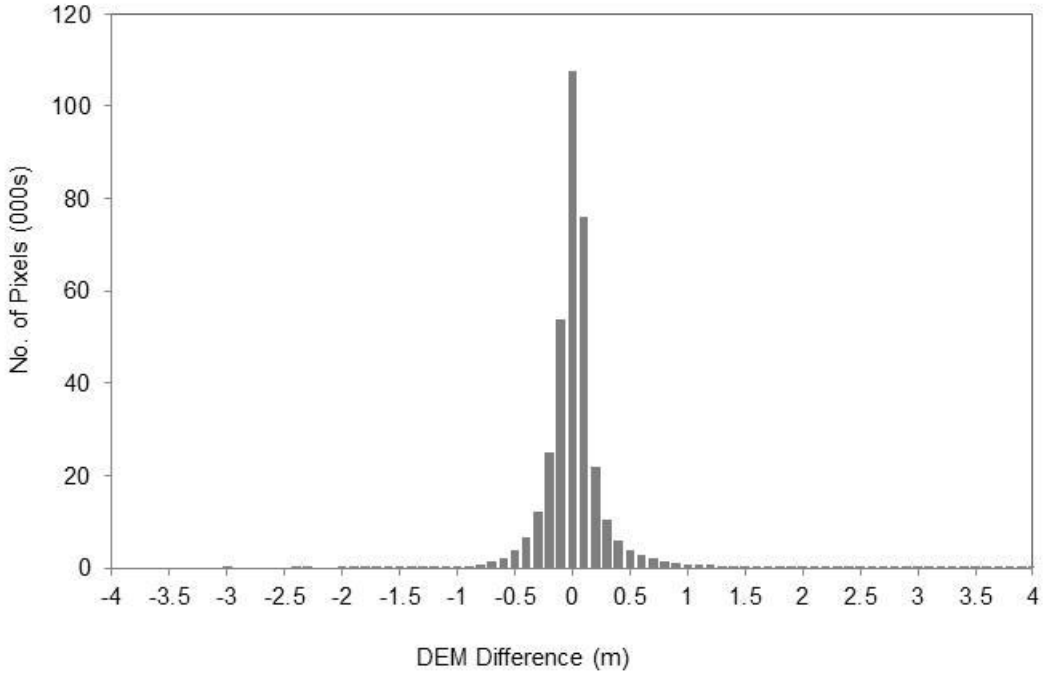

Figure 3-5: DEM comparison between TerraScan and Fusion

The sample DEM covered a typical range of elevation in forested areas (400-750m). The comparison (Figure 3-5) between two sets of DEM showed that nearly one third of pixels have the same elevation values (31%), and majority of pixels (68%) are within 0.1 m difference. Almost all pixels (98%) are within one-metre difference. For the whole comparison area, the mean DEM difference is 0.3 m, whereby the DEM derived using points from Fusion's "GroundFilter" function, slightly overestimated elevation in comparison to the TerreScan-derived elevation. The analysis confirmed that Fusion's 'GroundFilter" function was an adequate alternative to TerraScan, and as such, was used to classify ground and non-ground points for the entire area of interest.

3. Generate DEM Surfaces

Once all the points were classified, ground points were interpolated to produce a ground surface, or digital elevation model. The function "GridSurfaceCreate" in Fusion generates a gridded surface model from points. This function was used to generate a 1 m DEM from ground points. The DEM contains floating point elevation values.

4. Digital Surface Model

A 1 m DSM was generated using the Fusion function “CanopyModel”. This function creates a gridded surface, whereby the value in each cell corresponds to the elevation of the highest return within each cell.

5. Canopy Height Model

A 1 m canopy height model (CHM) was derived as the difference between the CSM and DEM. It is generated by using the same model used for generating DSM – “CanopyModel” with specification of DEMs. The algorithm calculates CHM by subtracting DEM from DSM.

A summary of the pre-processing steps is illustrated in Figure 3-6.

Step	Description	Output
Raw LiDAR point data	Raw LiDAR delivered, including outliers.	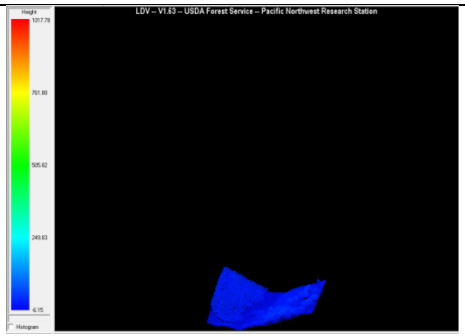
Filter LiDAR point data for outliers	Filter out outlier points: eliminate points beyond 3 standard deviations of the mean elevation within 100x100m window	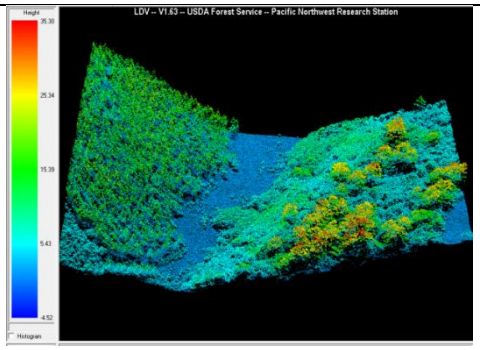
Classify ground point data	Use GroundFilter to filter ground points, with weight setting g=-1.5, w=2, iterations = 10	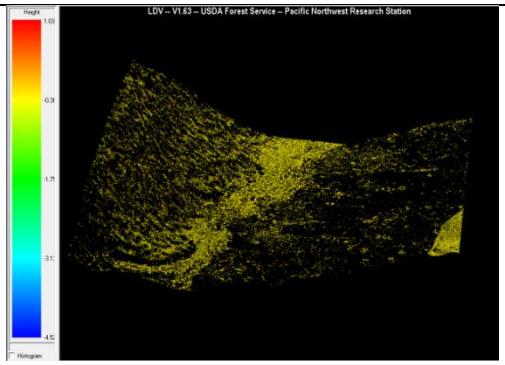
Generate ground surface-DTM	Interpolate the ground points into a raster, no filter used	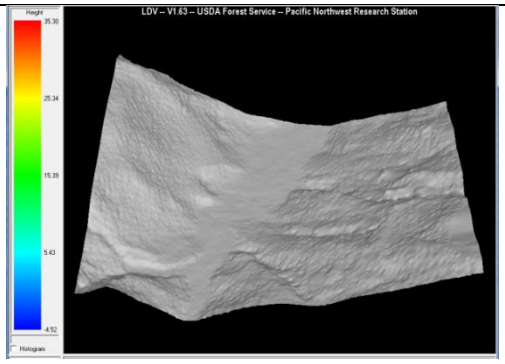

Step	Description	Output
Create Canopy Surface Model (CSM)	Use CanopyModel to generate a surface with the highest return within each grid cell, no filter used	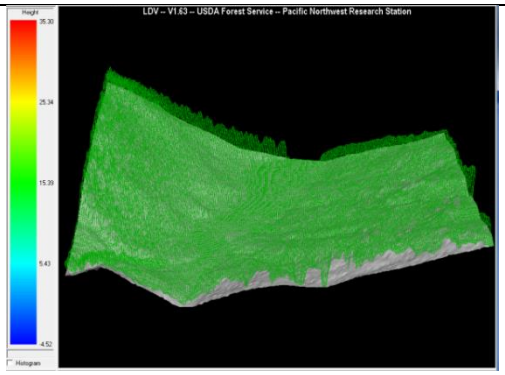
Canopy Height Model (CHM)	Subtract DTM from CSM to get the CHM	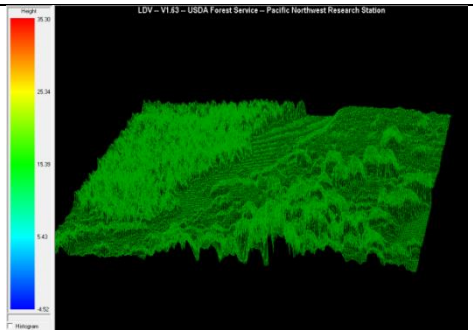

Figure 3-6: The individual steps of pre-processing LiDAR and some visual results

While height-related surfaces are primary LiDAR products used in classification, some studies showed that LiDAR-derived intensity images are also useful in supporting forest type classification along with height surfaces (Bork & Su, 2007; Sasaki et al., 2012). Generation of intensity images was attempted using "IntensityImage" in Fusion but the images showed inconsistent values (an example is shown in Figure 3-7) even after image colour balancing and point density thinning.

Generating high quality intensity images that can be used for classification requires appropriate geometric calibration and radiometric correction (Kaasalainen et al., 2011; Yan et al., 2012), as biases in LiDAR system parameters or measurements can lead to systematic errors that potentially cause classification errors (Yan et al., 2012). Intensity corrections and calibrations for all las files would consume substantial amount of time and resources, and is beyond the scope of this research. Additionally, using height-related surfaces such as DEM and CHM in classification have been very successful in many studies (Dupuy et al., 2013; Hellesen & Matikainen, 2013; Machala & Zejdova, 2014; Nordkvist et al., 2012). Therefore, it was decided that LiDAR intensity images would not be used in this study.

Figure 3-7: Intensity image example showing inconsistent spectral signature

3.4.2 Batch Derivation of LiDAR Surfaces

In total 6806 LiDAR tiles were delivered. Each tile was processed automatically using Windows Commander according to the procedures described above. However, edge effects were noticed when multiple LiDAR surfaces were mosaicked together (Figure 3-8). To address this issue, individual las tiles were merged into a LAS Dataset in ArcMap 10.2 (ESRI, Redlands, CA) prior to extracting surfaces, including a DEM, DSM, and CHM.

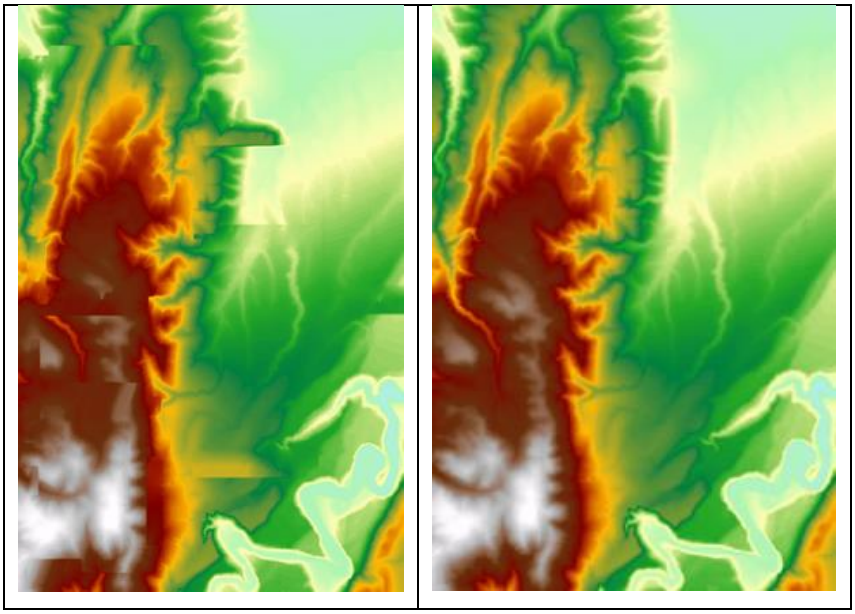

Figure 3-8: Mosaicing individual LiDAR-derived DEMs resulted in anomalies where pairs of tiles met (left). Merging all .las files into a LAS Dataset prior to generating a DEM solved this problem (right).

3.4.3 RapidEye Pre-processing

In order to extract surface parameters such as reflectance from RapidEye images, the influence of the atmosphere, solar illumination and terrain information need to be taken into account (Richter & Schläpfer, 2014). Atmospheric correction is an important step in image analysis, aiming to eliminate or greatly reduce the influence of atmosphere and solar illumination on spectral reflectance. It is especially critical for multi-temporal or multi-sensor scenes (Song et al., 2001).

Additionally, the effect of topography can severely bias the signals recorded in spectral sensors. The surface reflectance in forested areas with rugged terrain varies greatly with changes in solar elevation and azimuth, slope and aspect of the terrain, and the relative position of trees (Huang et al., 2008). As a result, the sunlit surface appears brighter than the surface under shadow, which can lead to different surface reflectance for the same land cover type (Hantson & Chuvieco, 2011). In this study, the forested areas are mainly located in the rolling hill area; therefore, the imagery required topographic correction.

Atmospheric corrections and topographic corrections were applied to all scenes using ATCOR3 for IMAGINE with ERDAS Imagine 2014 (Geosystems GmbH, Germering, Germany). ATCOR3 is developed by Richter and Schläpfer (2014) utilising MODTRAN atmospheric simulation code (Berk et al., 2008; Berk et al., 1998). ATCOR3 is an add-on package in ERDAS IMAGINE (Hexagon Geospatial, Łódź, Poland). The algorithm is reported to perform well for a wide range of sensors, terrains and land covers (Balthazar et al., 2012; Hantson & Chuvieco, 2011; Richter et al., 2009).

The key workflow of pre-processing RapidEye scenes are shown in Figure 3-9, full details of applying atmospheric and topographic corrections are in Appendix B. The DEM layers used for topographic correction are National 15m DEM developed by New Zealand School of Surveying. The DEM was resampled to 5 m to match the 5 m resolution RapidEye imagery. In spite of resampling to 5m resolution, the topographic correction process will not correct any micorelief finer than the original resolution. Overall undulation of the terrain at larger scale can be generally corrected (Figure 3-10).

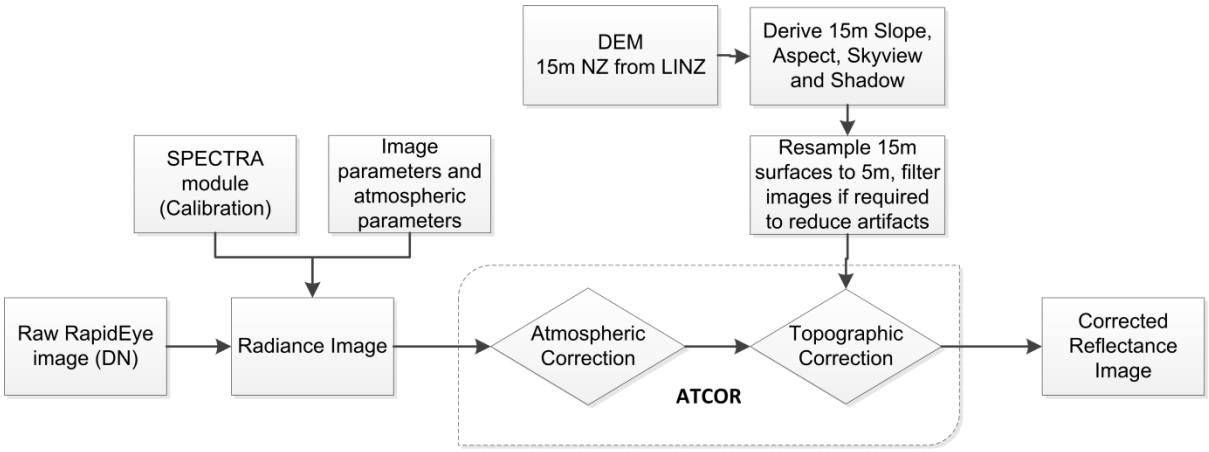

Figure 3-9: RapidEye Pre-processing Workflow

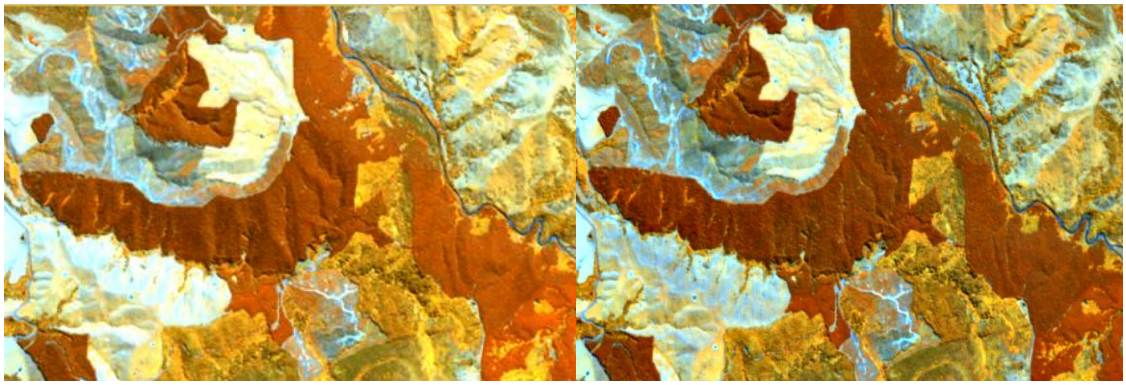

Figure 3-10: Raw RapidEye (left) and ATCOR3 processed RapidEye (right), the latter of which shows more consistent reflectance from comparable land cover types.

Chapter 4 - Developing an automated mapping approach to delineate plantation areas

4.1 Introduction

Forest classification and delineation is important in assessing forest types and areas, as understanding forest area and location is fundamental for plantation forest management, natural resource assessment, biodiversity and risk and hazard management (Eysn et al., 2012). Remote sensing plays an important role in forest detection and delineation. Aerial photography has traditionally been the most commonly used approach to determine forest area through manual interpretation in spite of being potentially subjective and time consuming (Mustonen et al., 2008). Optical sensors such as satellite imagery can also be used in forest type classification and delineation, by automatically assigning forest cover types and estimate forest variables with algorithms based on the spectral, textural and auxiliary information in the images. This produces a more objective delineation and reduces time and associated costs (Bork & Su, 2007; Nordkvist et al., 2012). LiDAR as an active sensor adds additional structural information for forest classification and delineation through direct estimation of forest canopy size and height. Combining LiDAR with optical sensors has been used in a number of studies and more accurate forest classification and delineation results were achieved relative to using an optical sensors alone (Bork & Su, 2007; Nordkvist et al., 2012; Sasaki et al., 2012; Wang et al., 2008).

This part of the research evaluates the performance of forest classification and delineation using RapidEye multispectral imagery alone and combined with LiDAR data. The aim is to develop an automated approach to detect and provide accurate estimation of the stocked areas for forests using an objected-based image analysis (OBIA) approach. The key objective is to compare the net stocked plantation areas derived by different combinations of remote sensing datasets and mapping approaches with the plantation areas manually digitised from high-resolution aerial photography in order to determine which approach provides the best potential for accurate automated plantation mapping. Specifically, this chapter will address the following research questions:

1. Which combination of remote sensing dataset and mapping approach produces the highest classification accuracy?

2. How different is the mapped plantation area compared with the manually digitised plantation area?

3. Is the performance of the classification approach affected by plantation patch size?

4.2 Methodology

4.2.1 Sample Selection

Due to the extensive study area, a stratified random sampling approach was applied to select representative samples for developing the mapping approach. The orthophoto survey grids (3.6 km x 2.4 km) were used as sampling grids, in total there were 764 grids covering Wairarapa with each had an area of 874 ha (Figure 4-1).

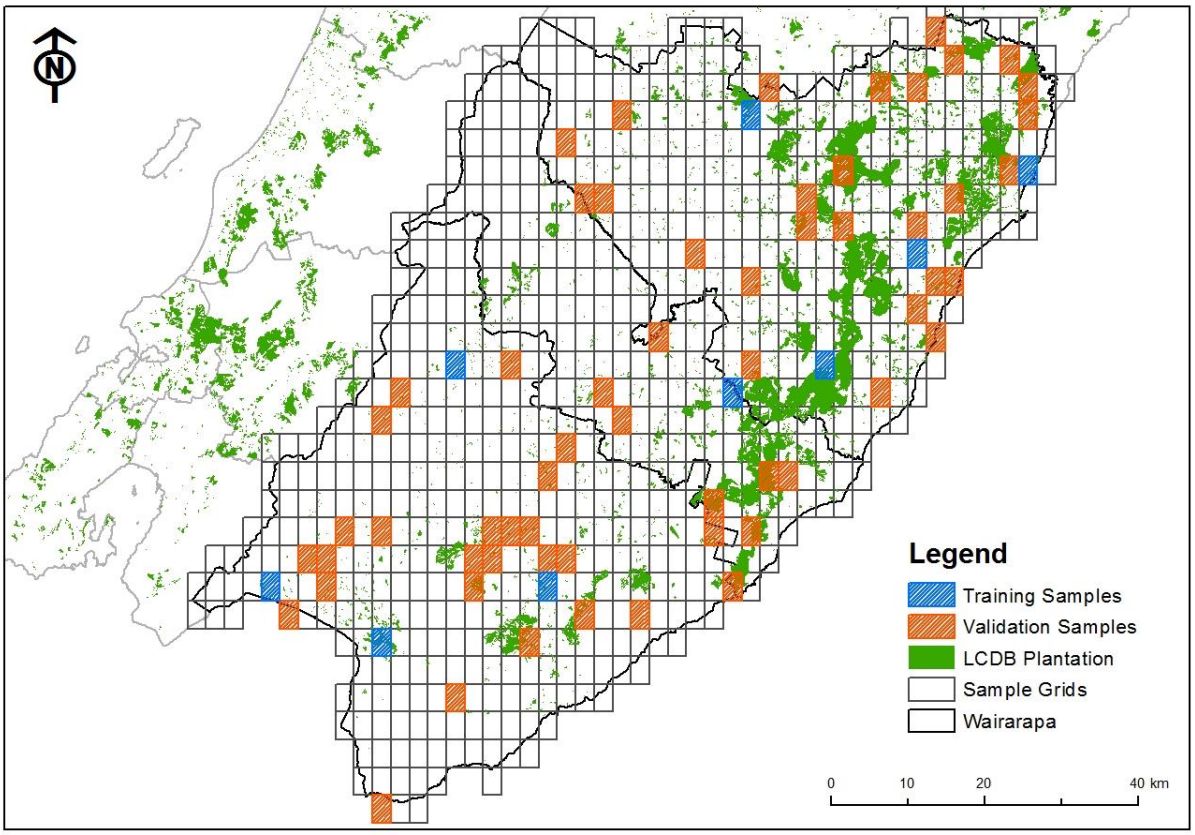

Figure 4-1: Sample grids selection and distribution for forest mapping

The most recent Landcover Database (LCDB) plantation areas which were mapped by New Zealand Landcare Research based on 2012 satellite imagery, were overlaid on sampling grids to allow calculation of total plantation area within each grid. Individual grids were then classified into three forest area classes based on plantation area:

- Forest Class 1: < 10 ha
- Forest Class 2: 10-100 ha
- Forest Class 3: > 100 ha

The binomial proportion power calculator developed based on Rosner (2011) suggested a minimum of 32 grids be selected as a representative sample of the study area. In total 69 sample grids were

selected to represent the Wairarapa region for plantation derivation. These included nine grids (three randomly selected from each forest area class), which served as the training grids for developing an OBIA forest mapping workflow, and 60 grids (20 randomly selected from each forest area class), which served as the validation grids. The total area of all 69 sample grids is 59 616ha, which accounts for 10% of the whole Wairarapa area.

4.2.2 Forest Mapping

The purpose is to develop an automated mapping process for delineating forest plantations using object based image analysis. The segmentation and classification steps for the OBIA are described in detail below; however, a brief overview of the mapping process is described here. The first step was to perform a land cover classification on the nine test grids using only RapidEye imagery and then a fusion of RapidEye and LiDAR-derived surfaces. Two classification algorithms, Nearest Neighbour (NN) and Classification and Regression Tree (CART), were undertaken on each test grid. Therefore, each test grid was subjected to four classifications:

- NN with RapidEye only,
- NN with RapidEye and LiDAR
- CART with RapidEye only
- CART with RapidEye and LiDAR

The classification accuracies from different sensor and algorithm combinations across the 9 training grids were compared to determine the approach with the highest accuracy. This approach was selected and applied to the 60 validation grids. The plantation areas in all 69 grids (9 test grids and 60 validation grids) were mapped using the selected approach and were compared with manual digitisation of plantation area from aerial photography. Figure 4-2 shows an overview of the plantation mapping process.

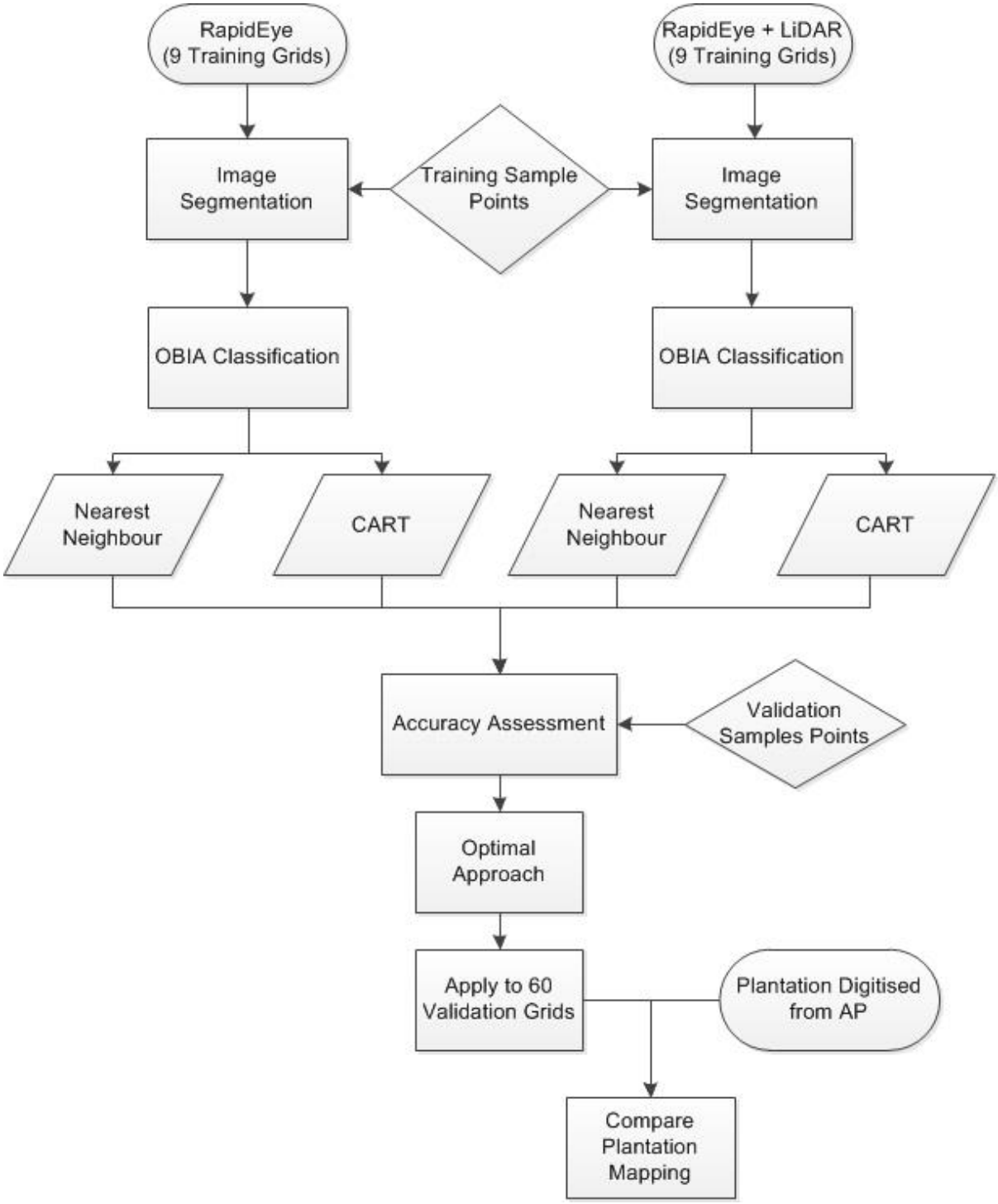

Figure 4-2: Overview of Mapping Workflow

RapidEye images were clipped to the grid extent to create image subsets for analysis. The analysis involved using OBIA to classify forest plantation area. OBIA is an image analysis approach that classifies groups of similar pixels (i.e. image objects) rather than individual pixels (Blaschke, 2010). Pixel-based image classification tends to be sensitive to spectral variations hence it is likely to result

in a high level of misclassification and reduce the accuracy of classification (Lu & Weng, 2007). OBIA segmentation processes create image objects that are similar to real land cover features in size and shape (Chubey et al., 2006). The approach allows the use of multiple image elements and scales such as texture, shape and context, as opposed to pixel-based classification that solely relies on the pixel value. Overall, OBIA has been proven to produce more accurate classification results compared to pixel-based approaches, producing improvement in classification accuracy ranging from 9% to 23% (Myint et al., 2011; Tehrany et al., 2014; Whiteside et al., 2011).

4.2.3 Segmentation

eCognition Developer 8.8 (Trimble Germany GmbH, München, Germany) is a popular OBIA software package and is used in this study. The software has a powerful development environment for object-based image segmentation and classification with the flexibility to design specific rule sets. An important prerequisite for OBIA classification is quality image segmentation. Segmentation that extracts meaningful objects by taking account of the scale of objects is used in eCognition's multi-resolution segmentation algorithm. Segmentation results are usually evaluated by qualitative and quantitative criteria. A qualitative criterion is visual evaluation by human eye. It is done by comparing multiple segmentations at different parameter settings, or comparing against the manually digitised segments if applicable (Baatz & Schäpe, 2000). Visual assessment is by far the most commonly used method to evaluate segmentation results (Zhang et al., 2008). However, visual assessment can be highly subjective and the process can be time and labour intensive (Johnson & Xie, 2011). On the other hand, quantitative criteria for segmentation evaluation examine the average heterogeneity of image objects and determine the most appropriate segmentation by finding the minimum heterogeneity result (Baatz & Schäpe, 2000). To this end, an ESP (estimation of scale parameter) tool was used to find the optimal scale parameter for multi-resolution segmentation. It was implemented as a customised rule set in eCognition that runs multiple segmentations with a defined fixed increment for the scale parameter, and calculates the local variance (LV, the mean standard deviation for all objects) and the rate of change (ROC) to assess the change of LV from one scale level to another (Drăguţ et al., 2014; Drăguţ et al., 2010).

$$ROC = \frac{LV-(LV-1)}{LV-1} \times 100 \qquad (1)$$

Based on results from the nine training grids, a graph was generated showing the LV and ROC for each scale level. ROC generally decreased as the scale increased, and the peaks of the curve indicated an appropriate scale level for segmentation (Appendix C).

It was also noticed that sample grids with low forest cover (i.e. small and patchy forests) generally required a finer scale factor, whereas grids that contained large and continuous forest cover did not require as fine scale parameter. Based on both EPS results and visual observation, scale parameters ranging from 100 – 140 were chosen for grids depending on their forest cover class (Table 4-1):

Table 4-1: Parameters used in multi-resolution segmentation

	Forest Class	Scale	Shape	Compactness	Image Weight
RapidEye only	1	100	0.2	0.5	Red, Green, Blue, RedEdge: 1, NIR: 2
	2	120	0.2	0.5	Red, Green, Blue, RedEdge: 1, NIR: 2
	3	140	0.2	0.5	Red, Green, Blue, RedEdge: 1, NIR: 2
RapidEye + LiDAR	1	100	0.2	0.5	Red, Green, Blue, RedEdge: 1, NIR, CHM: 2
	2	120	0.2	0.5	Red, Green, Blue, RedEdge: 1, NIR, CHM: 2
	3	140	0.2	0.5	Red, Green, Blue, RedEdge: 1, NIR, CHM: 2

4.2.4 Classification

Although the key purpose is to derive forest plantation area, it is important to include other representative land cover classes in classification so that sources of errors can be traced. Prior to classification, the land cover classes of the study area were determined. The New Zealand Land Cover Database (LCDB) is a digital map layer representing the land cover of New Zealand. It was developed using satellite imagery acquired at different times. The land cover classes used in this study were inspired by the LCDB first order classes, together with the features in the specific study area. Six land cover classes were determined and shown in Table 4-2.

Table 4-2: Description of land covers classes

Land Class	Description
Bare ground	Land that is exposed with bare soil. e.g. Roads, harvested area
Grassland	Natural high and low tussock grassland
Natural Forest	Closed naturally generated forests. e.g. Kauri, rimu, totara, native beech forests
Planted Forest	Closed planted forests, including both deciduous and conifers
Shrubland and scrub	Open forest (low density), riparian vegetation, both indigenous and exotic scrub
Water	River and lake, including shores

Two commonly used supervised OBIA classification approaches, NN and CART, were evaluated for their utility in land cover classification. Both are classification algorithms built into eCognition. For both approaches, sample points that are representative of each land cover class were manually selected in ArcGIS (ESRI, California, USA) based on high resolution aerial photography, and were then used as the training sample points for supervised OBIA classification. There was no target for the

required number of points prior to selection. A total of 702 sample points representing six land cover classes were selected for the nine training grids Table 4-3.

Table 4-3: Training sample points for supervised classification

Training Grid ID	Land Cover Classes						Total
	Bareground	Grassland	Natural Forest	Planted Forest	Shrubland and Scrub	Water	
BN35_1004	5	13	3	16		2	39
BP33_0908	12	17	10	11	4	4	58
BP35_0908	8	12	16	18	9		63
BP35_1003	7	12	18	15	27	13	92
BP36_0209	3	13	17	35	31	7	106
BP36_0503	10	18	18	15	15	8	84
BQ32_0708	9	13	23	13	15	14	87
BQ33_0904	6	9	38	20	20	6	99
BQ34_0703	9	17	24	15	4	5	74
Total	**69**	**124**	**167**	**158**	**125**	**59**	**702**

4.2.4.1 Nearest Neighbour Classification

Nearest Neighbour classification is a non-parametric classifier, and assumes there is no Gaussian distribution of input data (Hubert-Moy et al., 2001). The classification algorithm computes the Euclidean distance (also called feature space distance) iteratively from image objects to be classified to the nearest training sample points and assigns them into that class (Mallinis et al., 2008). The process consists of two steps: 1. training the classification algorithm by assigning sampled land cover classes to image objects; 2. classifying unclassified image objects in the image based on their nearest sample neighbours. Based on the image object's feature space distance to its nearest neighbouring sample, the Nearest Neighbour classifier calculates a membership value between zero and one. For an image object to be classified, only the nearest sample is used to evaluate its membership value. The membership value is one when an image object is identical to a sample. If the image object differs from the sample, the membership is assigned based on a fuzzy analysis on the feature space distance to the nearest sample of a class (Trimble, 2013). NN has been applied in delineating forest polygons with OBIA analysis (Mallinis et al., 2008), classifying forested land covers (Machala & Zejdova, 2014), delineating forested and non-forested areas (Haapanen et al., 2004) and describing vegetation species composition and structure (Ohmann & Gregory, 2002).

There were 87 input features used for RapidEye classification and 99 features used to classify RapidEye combined with LiDAR; these features include both customised and built-in features in eCognition. All LiDAR-derived surfaces were re-sampled to 5 metre resolution to be consistent with RapidEye imagery. A summary of the features are listed in Table 4-4. Customised features refer to band ratios or vegetation indices calculated from RapidEye spectral bands, to provide additional and more standardised spectral description of images. In total 17 customised features were derived based

on research from Machala and Zejdova (2014) and Rana et al. (2014) (shown in Table 4-5). The CHM is the key input layer for vegetation classification. Some additional layers have proven to be useful in differentiating vegetation types, including the CSM, DEM, standard deviation and skewness of elevation and slope (Blanchard et al., 2011).

Table 4-4: Summary of selected features used in NN and CART classification

Feature Type	Features	Description
Customised Features	Customised attributes calculated based on band ratios	Band ratios or Vegetation Indices calculated from RapidEye bands, listed in Table 5
Layer Values	Mean values	The mean value of image objects, including the mean of each band; mean of DEM, DSM, CHM and slope for LiDAR
	Standard Deviation	The standard deviation of each band, including the standard deviation of each band; Standard deviation of DEM, DSM, CHM and slope for LiDAR
	Skewness	The distribution of all intensity values within an image object, including the skewness of each band; skewness of DEM, DSM, CHM and slope for LiDAR
	Brightness	Sum of the mean for all bands divided by the number of bands
Texture	Texture after Haralick	GLCM (Grey Level Co-occurrence Matrix): measures how often different combinations of pixel gray levels occur in an image. Features used: GLCM Homogeneity, GLCM Contrast, GLCM Dissimilarity, GLCM Entropy, GLCM Mean and GLCM Standard Deviation at all four directions
Geometry	Extent	Area, Border length, Length, Length/Thickness, Length/Width, No. of pixels, Rel. Border to Image Border, Thickness, Volume and Width
	Shape	Asymmetry, Border Index, Compactness, Density, Elliptic Fit, Main direction, Radius of largest enclosed ellipse, Radius of smallest enclosing ellipse, Rectangular Fit, Roundness, Shape Index

Table 4-5: Details of customised features used in classification (Machala & Zejdova, 2014; Rana et al., 2014)

Features	Description
BlueRatio	blue/(blue+green+red+re+nir)
EVI	2.5((nir-red)/(nir+6red-7.5blue+1))
Green/Blue	green/blue
Green/Red	green/red
GreenRatio	green/(blue+green+red+re+nir)
GreenXRE/Red	green*re/red
NDVI	(nir-red)/(nir+red)
NIR/Blue	nir/blue
NIR/Green	nir/green
NIR/Red	nir/red
NIR/RedSDRatio	(nir*StDev nir)/(red* StDev nir)
NIRRatio	nir/(blue+green+red+re+nir)
RedRatio	red/(blue+green+red+re+nir)
REGNDVI	(re-green)/(re+green)
RENDVI	(re-red)/(re+red)
RERatio	re/(blue+green+red+re+nir)
3bandratio	nir/red/green

Prior to classification, all input features were evaluated using Feature Space Optimisation in eCognition to calculate the best combination of features in the feature space. The Feature Space Optimisation tool calculates the separation Euclidian distance between all samples of all classes with all possible combinations of input features, and finds the feature combination that produces the largest separation distance (which is the largest average minimum distance) between samples of different land cover classes. The combination of features that produces the largest separation distance was selected to use for classification. Feature Space Optimisation was applied to all nine training grids to define the optimal features to be used in classification.

Figure 4-3 plots the separation distance against the number of features evaluated, together with the change of distance when adding one extra feature to classification for one of the nine training grids. Theoretically, the best feature combination should be at 37 features where the separation distance is the largest. For all nine training grids, the optimal number of features ranged from 37 to 56. However, the change curve suggests that at 19 features, there was no obvious further improvement in the separation distance when adding additional features to the analysis. That means the advantage of adding one extra feature is diminishing after 19 features. Furthermore, there was no obvious difference in classification based on visual assessment using 19 features and 37 features. Therefore, 19 features were selected as the optimal number of features for the training grid. Similarly, the analysis was carried out for the other eight training grids, with the optimal number of features ranging

from 17 to 26. Together with training sample points and selected features, NN classification was performed automatically on the nine grids using eCognition.

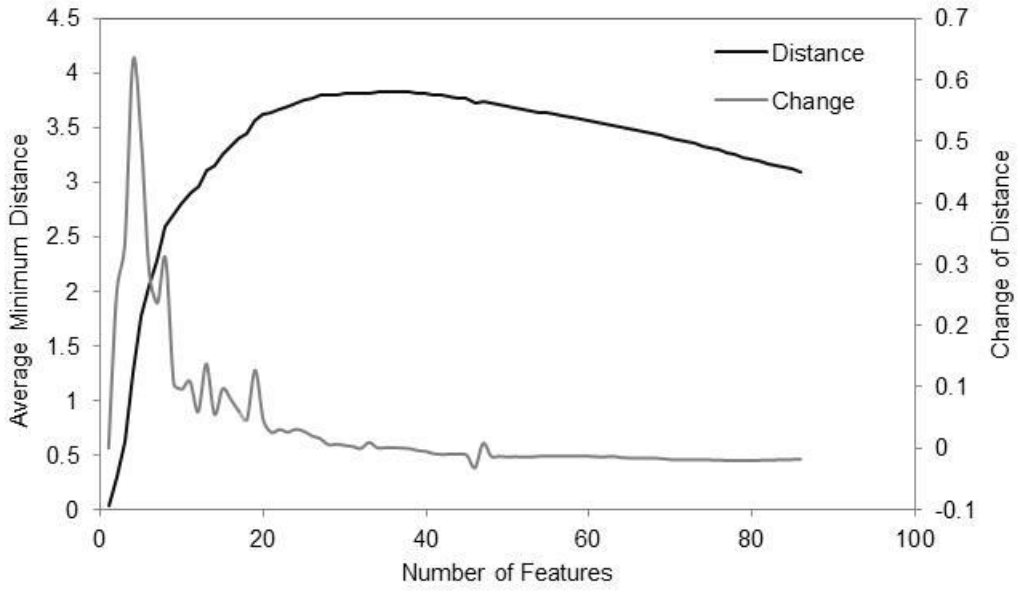

Figure 4-3: Feature Space Optimisation produced distance between object features

4.2.4.2 Decision Tree (aka CART - classification and regression tree)

Decision tree is a non-parametric statistical technique that allows selection of the most appropriate explanatory variables through tree form learning, which can be used in data mining (Breiman et al., 1984). The algorithm allows the classes from representative training samples to be split in an optimal manner. The purpose is to create a model that predicts the land cover of a target object based on attributes attached to training samples. A tree can be "learned" by splitting the source set into subsets based on an attribute value test. This process is repeated on each derived subset in a recursive manner called recursive partitioning. The subsequent subsets are separated further until no further division is possible or the tree reaches a defined maximum depth (Breiman et al., 1984; Trimble, 2013). CART has been used in a number of studies for land cover classification (Hellesen & Matikainen, 2013), delineating forest boundaries (Mallinis et al., 2008) and extracting forest variables (Chubey et al., 2006).

The features used in CART were the same as those used in NN classification (shown in Table 4-4 and Table 4-5). The CART process in eCognition involves defining CART parameters (maximum tree depth, minimum sample per node and cross validation folds) and applying these to the training samples. Different parameter values were tested, but in the end all three parameters were given a

value of 10 based on visual assessment of classification. Additionally, the same settings were used in a similar forest classification study (Hellesen & Matikainen, 2013).

4.2.5 Aerial Photo Interpretation

The stocked plantation areas were manually digitised in ArcGIS. Plantation assessment from orthophotos was used as the ground truthing data since aerial photography has higher resolution than other sensors used in this study. In general, the stocked plantation forests showed distinct characteristics on orthophotos, so they were easily differentiated from surrounding land cover classes. Occasionally, image stretching was applied to enhance orthophotos to allow clearer interpretation.

The guide to mapping forest land for the Emissions Trading Scheme (Ministry of Agriculture and Forestry, 2009) was used as a reference for manual digitisation of planted forests. Using the guide's definition, a forest has a minimum area of 1.0 hectare with tree cover greater than 30%. Furthermore, trees must have the potential to reach a minimum height of 5 metres at maturity and forest areas less than 30 metres wide are excluded.

Stricter mapping rules were adopted for the manual digitisation process in this study. For example:

- Maximum mapping scale: 1:1000
- All features were digitised at the maximum scale of 1:1000; some smaller features were digitised at 1:500
- Minimum mapping unit: 0.1 ha
- All isolated forest blocks over 0.1 ha were digitised. Any gaps within forests over 0.05 ha were digitised.
- Forest areas less than 15 metres wide were excluded, i.e. some narrow shelterbelts were not mapped as forest
- The minimum distance between forest patches was 50 metres, if the distance between two mapped forest patches was less than 50 m, they could be mapped as one patch. Otherwise, they needed to be digitised as separate forest patches.

4.2.6 Initial Accuracy Assessment

Quantitative assessment of classification results was obtained through a standard confusion matrix, which compares the classification results against corresponding ground truthing data or known reference points (Congalton, 1991). The purpose of the classification accuracy assessment was to determine how well the mapping approach detected plantation forests and differentiated plantation forests from other land cover classes. In this study, a stratified random sample of points was used for accuracy assessment. The number of points required was calculated based on multinomial probability theory (Congalton & Green, 2008; Plourde & Congalton, 2003). According to this theory, a minimum

of 636 points were required for accuracy assessment. The area proportion of each aggregated land cover class from New Zealand Land Cover Database (LCDB) was used as a basis to assign the number of points to each land cover class. In total 1200 points were randomly selected for all land cover classes. A trained aerial photography interpreter was provided with the points and asked to determine the true land cover class for each point. These reference points were then compared with the classified results to establish the confusion matrix. Based on the confusion matrix, the overall accuracy, producer's accuracy and user's accuracy were reported for each land cover class.

The overall accuracy is calculated as the proportion of the number of corrected classified points over the total number of points. The producer's accuracy (corresponding to the omission error) is the number of correctly classified points of each land cover class divided by the total number of reference points in each corresponding land cover class, which indicates the probability of a reference point being correctly classified. On the other hand, the user's accuracy (corresponding to commission error) is the number of correctly classified points of each land cover class divided by the total number of points that were classified in that land cover class, it is indicative of the probability that a point classified actually represents that class on ground (Congalton, 1991).

The accuracy of the two different automated classification approaches was determined by comparing the classification accuracies in the confusion matrices developed based on the nine training grids. The approach and remote sensing data combination that produced the highest overall accuracy was then further iteratively refined until the mapping accuracy reached a minimum classification accuracy of 85%. This threshold was set based on a review of comparable forest mapping studies using remote sensing technique, which have produced classification accuracy ranging from 65% to 98% (Bork & Su, 2007; Dupuy et al., 2013; Haywood & Stone, 2009; Hellesen & Matikainen, 2013; Machala & Zejdova, 2014; Nordkvist et al., 2012; Sasaki et al., 2012). Therefore, a mid-range value of 85% was set as the minimum acceptable classification accuracy.

The refinements were implemented in a decision tree to adjust the thresholds of object features for each misclassified land cover based on the automated classification results. For example, natural forests and planted forests tend to be mixed up, a customised feature RE Ratio (Red Edge Ratio) was useful in separating natural and planted forests. The RE Ratio values generally ranged between 0.19 and 0.22 for planted forests and over 0.23 for natural forests, hence it was used as a criterion to separate planted forest or natural forest. Moreover, REGNDVI which is a vegetation index incorporating Red Edge and Green band was found very useful in differentiating vegetation and non-vegetation classes. Together with LiDAR derived canopy height information (Mean CHM), they were used often to separate between vegetated land cover classes. Furthermore, the spectral and textural values between natural forests and shrubland were similar. Therefore, after reviewing many "truthing" points on aerial photos, it was decided that a cut-off canopy height of 8 metres was used to

differentiate natural forest and shrubland. A full description of the classification refinement can be found in Figure 4-4. The chart provides a basic structure of the steps undertaken to reduce the classification errors, the threshold values can be varied when classifying different sample grids.

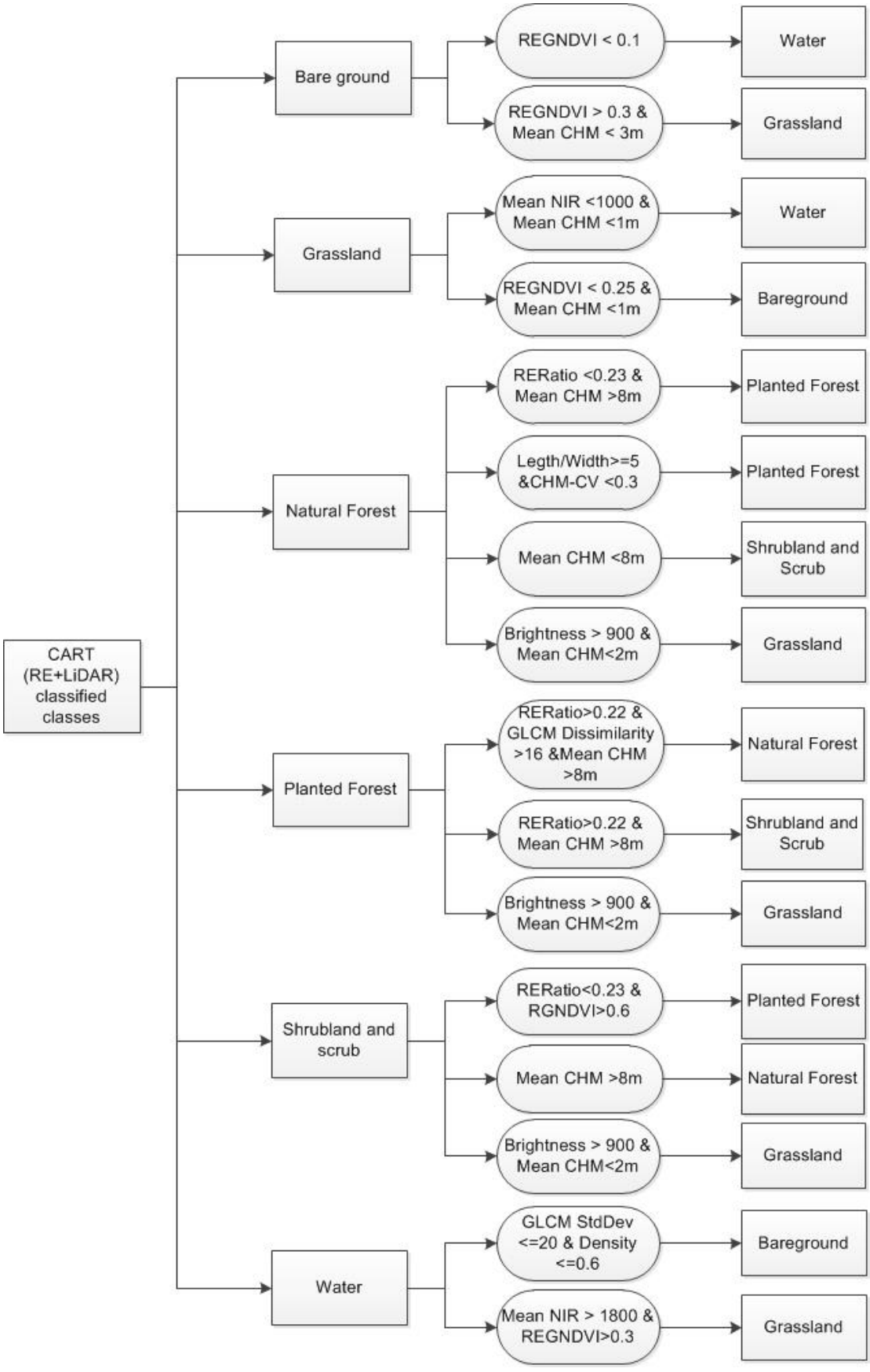

Figure 4-4: Example showing further refinements of each land cover class

4.2.7 Overall Classification Accuracy Assessment

Once the classification approach reached the target accuracy, the approach was validated using a larger subset of 60 validation grids. The accuracy assessment involved the same approach used for the nine training grids- establishing a confusion matrix that compared the mapped land cover class with the reference land cover class. A new set of 1200 validation points covering the larger extent were generated and used in classification accuracy assessment.

4.2.8 Assessing the accuracy of automatically classified plantation areas

The purpose of the analysis is to evaluate how well the mapping approach delineated forest plantation boundaries. The total plantation area mapped by the mapping approach was compared with the manual interpretation grid by grid for all nine training and 60 validation grids. Additionally, since LCDB contains the spatial representation of plantation area, the mapped plantation area for all 69 grids was compared to the latest LCDB plantation area. The comparison only included areas with standing trees so that any harvested areas and areas waiting to be replanted were not included.

To better understand the effect of forest patch size on mapping success, mapped and digitised forest patches were compared. Where a single mapped forest patch corresponded to a single digitised forest patch, it is straight forward to compare the areas. However, where a single mapped forest patch corresponded to two or more digitised patches, or vice-versa, a different approach was required. In such cases, the combined area of the two or more smaller patches was compared to the area of the corresponding single larger patch. For two or more forest patches to be considered as a block, they all would have to have some overlap with the single larger polygon or be separated by no more than 50 metres. In total 889 polygons were manually digitised and 584 sets of valid patch-to-patch comparisons were established. This excluded area that did not follow the mapping standards (such as area less than minimum mapping unit of 0.1 ha or shelterbelts that are less than 15m in width), harvested areas and new plantings. A paired t-test was used to determine whether the mapped and digitised plantation patch areas were statistically different.

4.3 Results and Discussion

4.3.1 Initial Land Cover Classification

The initial land cover classification was carried out on the nine training grids in order to determine which classification approach was the best, such that it could be applied to the remaining 60 validation grids. The classification accuracies for each land cover class achieved by the four combinations of classification approaches are shown in Table 4-6. The overall classification accuracy was the lowest (60%) when using NN-RE only approach; whereas the classification accuracy was the

highest (75%) using CART-RE+LiDAR approach. Using only RapidEye imagery has produced overall classification of 60% and 67% for NN and CART respectively. Incorporating LiDAR data has improved the classification accuracy slightly – 3% and 8% respectively for NN and CART. Overall, CART outperformed the NN algorithm in overall classification and most of the individual land cover classifications. However, there was no obvious difference observed in the classification accuracy for bare ground when using different classification approaches, and NN appeared to perform slightly better in classifying the water class. In general, when only RapidEye imagery was used, CART improved the overall classification accuracy by 7%. When incorporating LiDAR data, there was a 12% improvement relative to NN. The superiority of CART was also observed by Mallinis et al. (2008) who found that CART improved classification accuracy by over 20% compared to NN approach in classifying natural forest in Northern Greece.

The improvement of sensor fusion shown here is consistent with what other studies have found although the amount of improvement in this study appeared lower compared to Bork and Su (2007) and Nordkvist et al. (2012), who had 15-20% improvement when combining LiDAR surfaces with optical sensors. Using only RapidEye enables the capture of plantations reasonably well; giving a minimum producer's accuracy of 80% and a minimum user's accuracy of 83% both achieved by NN-RE only. There was a small improvement in the producer's accuracy when incorporating LiDAR surfaces; reaching 82% accuracy with a NN approach and 88% with a CART approach. Using both RapidEye and LiDAR benefited the classification of natural forest and shrubland the most compared to using RapidEye alone. Table 4-6 indicates that the producer's accuracy of natural forest has increased by 13% using a NN approach; and the producer's accuracy of shrubland and scrub has increased by 31% using a CART approach.

It can be noticed that the classification accuracies in the initial classification assessment were not very high compared to some other land cover classification studies. This is because the classifications were by completely automated (i.e. without any user's refinement); as such the comparison between approaches is unbiased and independent. The classification accuracy comparison serves as an interim analysis and provided the basis for selecting the best classification approach. The selected approach will be further refined to achieve a higher classification accuracy that is comparable to other studies. Both the overall and plantation classification accuracy were highest using the CART approach with both RapidEye and LiDAR data as inputs. Therefore, it is clear that using CART with both RapidEye and LiDAR data as inputs is the optimal mapping approach.

Table 4-6: Classification accuracy comparison among classification approach and datasets for nine training grids. NN-RE: Nearest Neighbour classification with RapidEye only, NN-RE+LiDAR: Nearest Neighbour classification with RapidEye and LiDAR, CART-RE: Classification and Regression Tree with RapidEye only, Classification and Regression Tree with RapidEye and LiDAR

	NN - RE		NN - RE+LiDAR		CART - RE		CART - RE+LiDAR	
Land Cover	Producer's accuracy	User's Accuracy	Producer's accuracy	User's Accuracy	Producer's accuracy	User's Accuracy	Producer's accuracy	User's Accuracy
Bare ground	40%	20%	40%	23%	43%	20%	38%	26%
Grassland	59%	90%	60%	89%	69%	91%	76%	90%
Natural Forest	52%	39%	65%	46%	68%	50%	67%	71%
Planted Forest	80%	83%	82%	86%	81%	94%	88%	90%
Shrubland and scrub	55%	34%	58%	40%	46%	41%	77%	55%
Water	80%	21%	80%	21%	70%	16%	90%	26%
Overall Accuracy	**60%**		**63%**		**67%**		**75%**	

The error matrix of the CART-RE+LiDAR approach (Table 4-7) indicates that the approach produces classification errors; in particular, the classification accuracy was very low for bare ground. Most of the bare ground was misclassified into water or grassland, which all contain no tall vegetation and could have similar spectral signatures. Most of the grassland and water were misclassified as bare ground. Natural forest was confused with shrubland and planted forests, 70% of the omission error of natural forests was due to misclassification into shrubland and planted forests. The omission error of classifying shrubland and scrub was 22% lower than the commission error, suggesting that this land cover was under-classified. The other classes that were misclassified into shrubland were mainly natural forest and grassland. Planted forest was the most accurately classified land cover giving relatively high producer's and user's accuracy. Both omission (12%) and commission errors (10%) were mostly the result of confusion between planted forest and natural forest.

Table 4-7: Initial classification accuracy results based on nine training grids for the selected approach: CART-RE+LiDAR

	Reference data							
Classes	**Bareground**	**Grassland**	**Natural Forest**	**Planted Forest**	**Shrubland and scrub**	**Water**	**Total**	**User's accuracy**
Bareground	23	63	1	0	2	1	90	26%
Grassland	19	471	14	9	11	0	524	90%
Natural Forest	3	12	107	13	15	0	150	71%
Planted Forest	0	2	13	174	4	0	193	90%
Shrubland and scrub	3	66	24	0	115	0	208	55%
Water	12	9	1	1	3	9	35	26%
Total	60	623	160	197	150	10	1200	
Producer's Accuracy	**38%**	**76%**	**67%**	**88%**	**77%**	**90%**		**75%**

Understanding where the classification errors come from is helpful in refining the classification algorithm to minimise those errors. The land cover classes that were mistaken for other land cover classes were noted and incorporated into the classification refinement. Following refinement of the classification approach, the overall accuracy for all land cover classes increased by 10%, from 75% to 85% (Table 4-8), which met the target classification accuracy. For individual land cover classes, the producer's accuracy of bareground, grassland and natural forests increased by at least 7%. However, the refined classification approach did not provide much improvement for plantation forest and increased the producer's accuracy by 1%. The user's accuracy for all classes except natural forests was improved at various degrees. At 85%, the overall classification accuracy is not very high, but is comparable with some recent forest classification studies. Haywood and Stone (2009) developed an automated approach that applied aerial photos and LiDAR CHM to delineate Eucalyptus forest boundaries and achieved 65% overall accuracy. Pham et al. (2016) used Quickbird and LiDAR to classify forest species in a New Zealand urban environment and achieved an overall accuracy of 85%. Another OBIA classification by Dupuy et al. (2013) used SPOT 5 and LiDAR surfaces to classify tropical vegetation type and gained 92% overall accuracy.

Table 4-8: Classification accuracy matrix for nine training grids using the refined mapping approach

	Reference data							
Classes	**Bareground**	**Grassland**	**Natural Forest**	**Planted Forest**	**Shrubs and scrub**	**Water**	**Total**	**User's Accuracy**
Bareground	27	16	1	2	1	1	48	56%
Grassland	24	571	7	6	13	0	621	92%
Natural Forest	5	15	127	14	19	0	180	71%
Planted Forest	0	4	8	175	4	0	191	92%
Shrubland and scrub	1	17	17	0	113	0	148	76%
Water	3	0	0	0	0	9	12	75%
Total	60	623	160	197	150	10	1200	
Producer's Accuracy	**45%**	**92%**	**79%**	**89%**	**75%**	**90%**		**85%**

Despite general improvements in classification, errors for some classes, especially bareground, still remain. Almost half of the bareground was misclassified into grassland and in many cases grassland was misclassified as bareground. The omission errors for planted forests mainly came from natural forests and some from grassland. It was understandable that planted forests tended to have similar spectral signature and height to natural forests, yet the misclassification to grassland raised concerns. Apart from planted forest, natural forests and shrubland also appeared to be misclassified as grassland. In order to further examine these errors, all classification errors were manually reviewed to identify whether the errors were due to the classification approach or some other reasons.

It was noticed that some of the remaining misclassifications were due to changes that occurred over time; this is a consequence of the RapidEye images being collected approximately one year later than the reference aerial photos. For example, in Figure 4-5, the aerial photo shows planted forest, but the RapidEye image shows the same area as bareground which has been harvested. Another factor that affected the classification accuracy was the resolution of RapidEye imagery, which is coarser than aerial photography used for ground truthing. The difference in pixel size could affect the classification accuracy (see example in Figure 4-6). The classification errors caused by temporal change and resolution difference were quantified after reviewing all classification errors. In total there were 178 classification errors within all 1200 reference points. It was found that 22 errors, which accounted for 12% of all errors, were due to temporal difference in RapidEye and aerial photograph; and 65 errors, which accounted for 37% of all errors, were due to difference in resolution of RapidEye. If those errors were excluded the overall classification accuracy would reach 91%. Therefore, it is important to obtain remote sensing data and truthing information at the same time to reduce the errors caused by temporal difference. The difference in the data resolution in this study remains as a limitation of using remote sensing for classification.

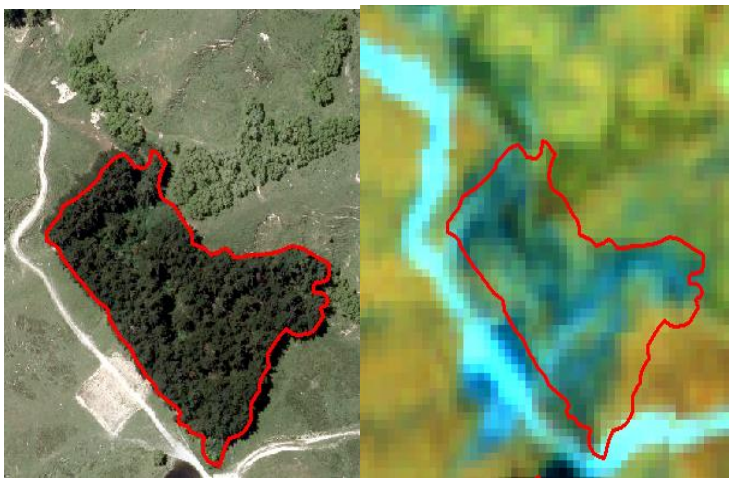

Figure 4-5: Example showing the different classification caused by change. The image on the left shows a plantation patch on an aerial photo, on the right the same area was shown to be harvested on RapidEye imagery, which would be classified as bare ground.

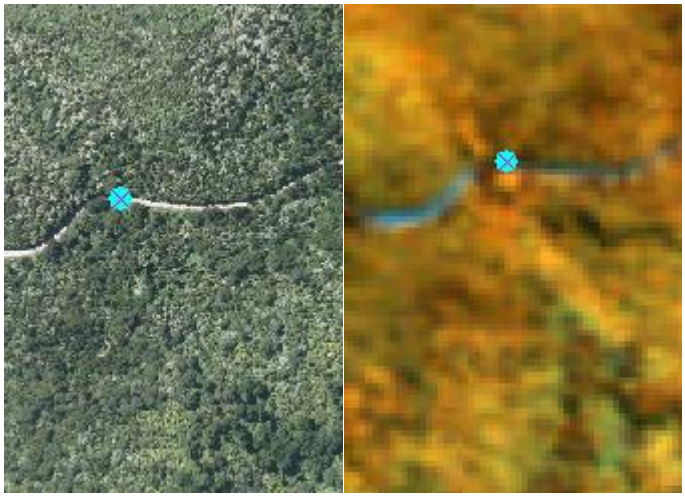

Figure 4-6: Example showing the different classification caused by image pixel size. The point on the left image shows a road within a natural forest on aerial photo, and was classed as "bare ground" by the operator manually. The image on the right shows the same area on RapidEye, which was classified as natural forest as the coarser pixel size resulted in the road not being classified by the classification approach on RapidEye.

4.3.2 Land Cover Classification of all Validation Grids

Having refined the classification approach to achieve an acceptable accuracy assessment for the nine training grids, the approach was then applied to all 60 validation grids. The overall classification accuracy of 60 validation grids was 89% (Table 4-9). Based on producer's accuracy, grassland, natural forest and water were more accurately classified than bareground, planted forest and shrubland. This indicates that bareground, planted forests and shrubland tend to be misclassified into other land cover classes. Based on user's accuracy, other classes were more likely to be misclassified into bareground, natural forests and shrubland. The producer's accuracy for plantation was 79% and user's accuracy for plantation was 94%, which means that the classification approach tends to under-classify planted forests. The omission error for planted forests was 21% and most of these were contributed by natural forest and Shrubland. Similarly, commission occurred when natural forests or shrubland were misclassified as plantations. The commission error for planted forests was much lower at 6%, which suggests the classification approach does not tend to misclassify other classes as planted forests.

The overall accuracy (89%) achieved for all validation grids was also within the range of other studies, but did not reach the top accuracies like Hellesen and Matikainen (2013) and Sasaki et al. (2012) who produced classification accuracy over 95%. It is worth noting that almost all comparable classification studies were applied on a single study area with limited spatial coverage, ranging from 100 ha to 1500 ha (Hellesen & Matikainen, 2013; Machala & Zejdova, 2014; Räsänen et al., 2014; Sasaki et al., 2012). This study area contains 69 sample grids that are geographically separated from each other, with a total area of 59 616 ha. The largest study area reviewed was by Bork and Su (2007), who

classified vegetation classes in a rangeland covering 2400 ha and obtained an overall accuracy of 83.9%. Designing a mapping approach that works for a larger study area can be more challenging as more variations need to be taken account, such as topographic variation, spectral variation from satellite imagery and land cover variation.

Since plantations are being actively managed, many misclassifications of plantation are caused by temporal changes such as harvesting and new plantings. By reviewing all 135 classification errors it was found that 33 errors (accounted for 24% of all errors) were caused by temporal change of land cover classes. By excluding the reference points where changes occurred, the producer's accuracy of plantation increases to 89%, the user's accuracy remained unchanged, and the overall accuracy increased by 2% (Table 4-10). Because the classification approach did not appear to differentiate new plantings and grassland, it tended to misclassify new plantings to grassland and shrubland if the new plantings are taller. Likewise, the misclassification of bareground to grassland was also mainly caused by temporal differences in an actively managed agricultural environment. If there was no temporal difference in the image source used, the classification would have been improved especially for dynamic land cover classes such as bareground and planted forest.

Table 4-9: Classification accuracy matrix for 60 validation grids (all points)

	Reference							
Classification	**Bareground**	**Grassland**	**Natural Forest**	**Planted Forest**	**Shrubland and scrub**	**Water**	**Total**	**User's Accuracy**
Bareground	23	6	0	4	1	3	37	62%
Grassland	7	641	8	6	14	1	677	95%
Natural Forest	0	8	141	11	17	0	177	80%
Planted Forest	0	0	6	131	2	0	139	94%
Shrubland and scrub	1	16	11	13	111	0	152	73%
Water	0	0	0	0	0	18	18	100%
Total	31	671	166	165	145	22	1200	
Producer's Accuracy	**74%**	**96%**	**85%**	**79%**	**77%**	**82%**		**89%**

Table 4-10: Classification accuracy matrix for 60 validation grids (excluding errors resulted from temporal change)

	Reference							
Classification	**Bareground**	**Grassland**	**Natural Forest**	**Planted Forest**	**Shrubland and scrub**	**Water**	**Total**	**User's Accuracy**
Bareground	23	1	0	1	1	2	28	82%
Grassland	0	641	8	0	14	1	664	97%
Natural Forest	0	8	141	11	17	0	177	80%
Planted Forest	0	0	6	131	2	0	139	94%
Shrubland and scrub	1	14	11	4	111	0	141	79%
Water	0	0	0	0	0	18	18	100%
Total	24	664	166	147	145	21	1167	
Producer's Accuracy	**96%**	**97%**	**85%**	**89%**	**77%**	**86%**		**91%**

4.3.3 Study Area (Grid-Level) Plantation Area Comparison

All plantations mapped from nine training grids and 60 validation grids were compared with manually digitised plantations from aerial photography. This was done to gain a better understanding of the limits of automatically mapping forest plantations. Overall, the area of plantation digitised from aerial photography was 485 ha greater than the area mapped from RapidEye and LiDAR (Table 4-11). In other words, the mapping approach underestimated plantation area by 7.8%. This is likely because aerial photography has 0.3 m resolution, which is much finer than RapidEye and LiDAR (5 m). The finer spatial resolution of the aerial photography allowed detection of additional features such as new plantings during manual digitisation. Such features are less likely to be detected by automated classification of coarser resolution RapidEye. It is possible to derive young plantation areas using finer resolution imagery, as a study by Zhou et al. (2013) using 0.5 m resolution Worldview imagery successfully mapped the growth density of young plantations that were less than two years old.

After excluding all the new plantings detected during manual digitisation of aerial photography, the mapping approach overestimated the plantation area by 168 ha, which was 3% of the total area digitised. This is understandable as RapidEye and LiDAR have coarser resolution and are more likely to misclassify small forest patches, gaps or roads within forests. The Mean Absolute Error (MAE) and Root-Mean-Square-Error (RMSE) were much lower when new plantings were excluded (Table 4-11). The plantation area comparison at each grid level is summarised in Appendix D.

Table 4-11: Overall area comparison between planted forests mapped by mapping approach and digitised from aerial photography, based on both nine test grids and 60 validation grids.

	Total Digitised (ha)	Total Mapped (ha)	Difference (ha)	Difference (%)	MAE (ha)	RMSE (ha)
All standing trees	6244. 4	5759. 2	-485.2	-7.8%	13.6	42.5
Exclude new plantings	5590. 8	5759. 2	168. 5	3.0%	5.7	9.6

4.3.4 Comparison to LCDB

The latest LCDB indicates that the planted forest area (Class "Exotic Forest" in LCDB) for the nine training grids and validation grids was 6941.6 ha, which is 11% more than the digitised plantation area including new plantings, and 24% more than the digitised plantation area excluding new plantings. This suggests that the current LCDB plantation tends to overestimate the plantation area. Since LCDB is a well-developed mapping system led by Landcare Research with decades of peer-reviewed research (Landcare Research, 2016), this overestimation could be largely due to the use of a coarser sensor SPOT 5, which is 10 m resolution as opposed to 5 m RapidEye. The imagery used for developing LCDB was last acquired in 2012, which is one year older than the aerial photography, and two years older than RapidEye imagery. The temporal difference between LCDB and this study is difficult to assess due to lack of satellite imagery for developing LCDB.

Figure 4-7 provides a visual comparison of the plantation area mapped by manual digitisation, the automated mapping approach, and the LCDB mapped plantation area for reference. Using the mapping approach with RapidEye and LiDAR data, plantations and forest gaps were able to be mapped with a high degree of certainty, relative to LCDB. LCDB provides reasonable means for detecting and summarising plantation area, but with the limitation in resolution, LCDB may not be suitable for providing accurate estimation of plantation area at small-scales.

Comparison Scenario	Digitised Plantation	Mapped Plantation	LCDB Plantation
Quality of forest boundary delineation			
Exclusion of forests gaps and roads			
Miscassilfication of small natural forest patch into plantation			

Figure 4-7: Visual examples of plantation mapped in comparison to digitised plantation and LCDB plantation.

4.3.5 Patch-Level Plantation Area Comparison

Patch-level comparison was conducted to examine whether the accuracy of the classification approach varies with the size of plantation patch. For all patch-level comparisons, with an average digitised patch size of 9.5 ha, the mapping approach tends to overestimate plantation area by 2.1% with a mean absolute error of 0.8 ha (Table 4-12). For forest patches under one hectare, with an average digitised patch size of 0.3 ha, mapping appears to be less accurate, overestimating plantation area by 8.2%, with a mean absolute error of 0.3 ha. However, the total area of these patches is small, so the relatively large error in small plantation patch estimation only caused 8.9 ha over estimation for all grids (Table 4-12). On the other hand, although forest patches exceeding one hectare were only overestimated by 1.9% (MAE = 1.46 ha), the errors associated with these patches were the main

contributor to the overall error. The above comparisons include forest patches not mapped or digitised, which means that if a forest patch was digitised but not mapped, the mapped area is recorded as zero.

Table 4-12: Patch-level comparison summary

	Digitised plantation area (ha)	Average digitised patch size (ha)	Mapped plantation Area (ha)	Difference between mapped and digitised (ha)	Difference between mapped and digitised (%)	MAE (ha)	RMSE (ha)
All	5 557.1	9.5	5 671.3	114.2	2.1%	0.8	2.3
< 1 ha	109.2	0.3	118.1	8.9	8.2%	0.3	0.4
> 1 ha	5 447.9	20.3	5 553.2	105.3	1.9%	1.5	3.4

A paired two-tail t-test was used to determine whether the difference between the mean area of digitised forest patches and mapped forest patches is significant (Table 4-13). The absolute value of t statistics for all patches and > 1 ha patches were marginally larger than the critical two-tail t value and the p-value is just under 0.05, which suggests that the average patch size mapped and digitised are statistically different. However, t-tests on < 1 ha patches were not significant, with the p-value greater than 0.05. This suggests that there was no obvious difference in the average patch size digitised and mapped for less than 1ha patches.

Table 4-13: Results of Paired t-test for comparison of digitised and mapped plantation patches

Statistics	All patches	<1 ha patches	>1 ha patches
Observations	584	317	267
t Statistics	-2.066	-0.959	-2.011
P(T<=t) two-tail	0.039	0.338	0.045
t critical two-tail	1.964	1.967	1.969

In order to further visualise the digitised and mapped plantations, only non-zero comparisons were used in the plot of the mapped and digitised plantation. That excludes 142 polygons missed by mapping and 22 polygons missed by digitisation, leaving 423 sets of non-zero comparisons. The digitised and mapped plantation areas at patch-level are plotted in Figure 4-8. Both charts show that digitised and mapped patch areas closely correlate, especially for larger forest patches. Smaller patches appear more difficult to map accurately as there are more discrepancies in areas for smaller areas.

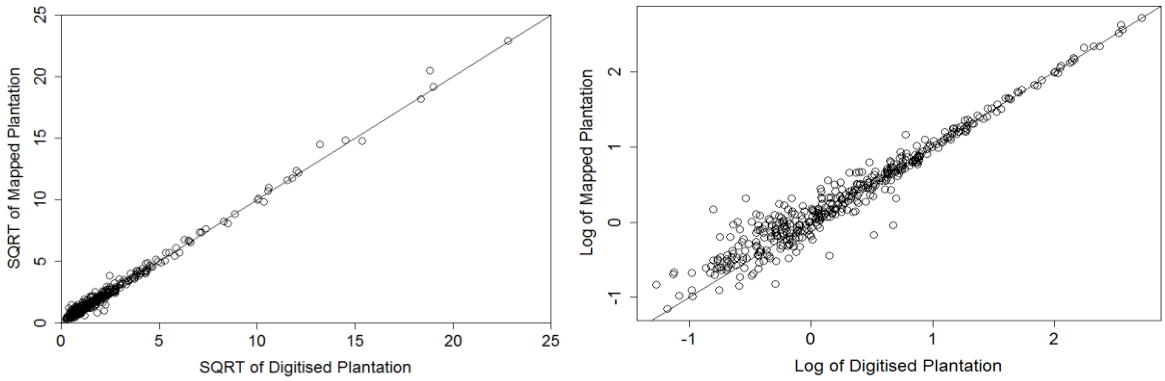

Figure 4-8: Plot of digitised mapped plantation areas, left chart applied a square root (SQRT) transformation, right chart applied logarithm transformation with base of 10. Both trend lines are 1:1 lines.

Figure 4-9 confirms previous observations by plotting the absolute error with patch size, which shows that errors tend to decrease with increasing patch size. The mapping errors appear to be greater and have more variability for smaller forest patches, whereas forest patches that exceed 10 ha the errors become much smaller and less variable (within 20% error).

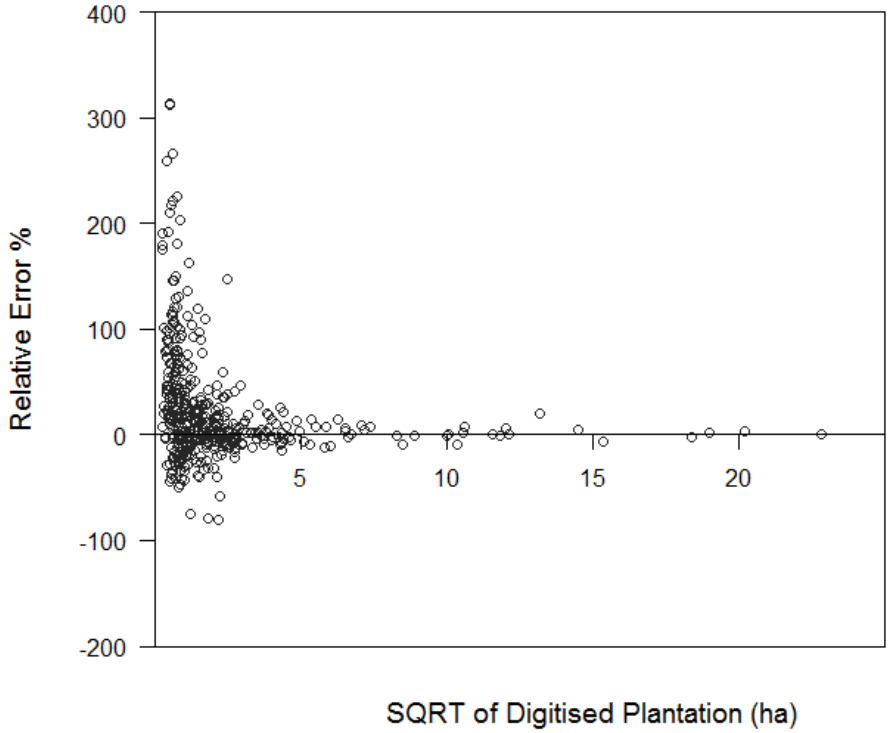

Figure 4-9: Plot of forest patch size against mapping error, forest patch size is expressed as square root of digitised plantation area, error is expressed as the relative error percentage which was calculated as the difference of mapped and digitised area divided by the digitised area.

4.4 Conclusion

In this study, a factorial combination of two classification approaches and two remote sensing datasets were compared for their ability to accurately classify land cover, specifically plantation forest area. The approaches included nearest neighbour with RapidEye only, nearest neighbour with RapidEye and LiDAR, CART with RapidEye and CART with RapidEye and LiDAR. In an initial classification of nine training grids, CART with RapidEye and LiDAR outperformed the other three approaches producing the highest overall accuracy and plantation accuracy. The addition of LiDAR data to RapidEye has improved the overall classification accuracy by 8% using CART approach, and the producer's accuracy of planted forest improved by 7% compared to using RapidEye images alone. Therefore, CART approach with both RapidEye and LiDAR was chosen for land cover mapping in the remaining 60 validation grids.

Overall the selected mapping approach gave good classification results, producing 89% overall accuracy; the producer's accuracy for plantation was 79% and user's accuracy was 91%. After excluding the harvested area and new plantings due to temporal differences between the aerial photography and satellite imagery, the producer's accuracy of plantation increased to 89%. The mapping approach used here has produced classification results comparable to previous studies (Haywood & Stone, 2009; Hellesen & Matikainen, 2013; Machala & Zejdova, 2014; Nordkvist et al., 2012; Sasaki et al., 2012). The efficiency of the method was further examined by comparing the mapped plantation area with manually digitised plantation area. For all sample grids, the mapping approach overestimated the plantation area by 3%, which is a significant improvement on the 24% overestimation by the LCDB. Patch size proved to have an impact on mapping accuracy. Mapping of smaller patches (less than 10 ha) appears more variable and less accurate compared to "true" representation, whereas larger patches (over 10 ha) are generally more accurately mapped (less than 20% error).

The combination of multispectral RapidEye features and relatively low point density LiDAR-derived surfaces proved to be sufficient to detect land cover features, though the mapping accuracy decreased in small plantation patches, the results of classification tree analysis can be easily interpreted and implemented (Hellesen & Matikainen, 2013). The CART approach with both RapidEye and LiDAR has proven to be an effective way in detecting and delineating planted forests, especially for forest patches larger than 10 ha. Given the fact that the approach is automated and easy to apply, it is potentially applicable for larger area plantation assessment and monitoring of changes. This will be further tested on the whole Wairarapa region in a subsequent chapter (Chapter 6). Furthermore, two non-parametric classifiers NN and CART were examined in this study, other non-parametric classifiers such as Random Forest (RF) and Support Vector Machine (SVM) have not been evaluated due to limited processing resources. These machine learning algorithms could be tested in the future

with CART to see which classifier produces the most accurate forest mapping accuracy for the New Zealand small-scale plantation estate. Recent studies have found alternative classification algorithms SVM and RF have also worked successfully in deriving forest areas (Müller et al., 2015; Pham et al., 2016).

Chapter 5 - Evaluation of modelling approaches to estimate forest stand variables

5.1 Introduction

Collecting detailed forest inventory data across a large and continuous area is not practical, so a variety of statistical methods have been used to predict forest attributes at unsampled locations. Regression, imputation and machine learning algorithms can be adopted to predict forest variables typically based on ancillary data that are available for the forest. The ancillary data act as explanatory variables and include ground samples from inventory or data extracted from remote sensors (such as satellite data or LiDAR) for model development and validation (Brosofske et al., 2014).

A number of modelling approaches have proven to be useful in estimating forest stand variables such as height, basal area and standing volume from remotely sensed data (Breidenbach et al., 2010; Brosofske et al., 2014; Hyyppa et al., 2008). They include both parametric and non-parametric approaches. Parametric approaches define linear or non-linear regression relationships between forest stand variables and remote sensor-derived variables (Chen & Hay, 2011; Shataee, 2013). The most common form of parametric regression for modelling forest attributes applies a simple or multiple linear regression equation solved using ordinary least squares (OLS), which aims to minimise the sum of squares of the differences between observed and predicted values (Tonolli et al., 2011). For example, it is common to predict forest height from LiDAR height percentile metrics using linear regression (Naesset, 2002; Suárez et al., 2005).

Chen and Hay (2011) claimed that parametric regression models fail to fully characterise forest complexity at finer scale, as a result of high structural variability within forest clusters especially with high resolution data. Furthermore, OLS regression assumes that the explanatory variables are free of measurement errors, which is not realistic in remote sensing data inputs (Berterretche et al., 2005). Overall parametric regression models may fail to simultaneously estimate more than one response variable as multiple response variables can restrict model validity and reduce model degrees of freedom (Breidenbach et al., 2010). Alternatively, non-parametric machine learning models have been increasingly used in predicting forest variables. The key advantage of non-parametric models over parametric models is that they do not rely on any probability distribution (Shataee, 2013). Commonly used models for estimating forest attributes include k-Nearest Neighbour (k-NN), Random Forest (RF) and Support Vector Machine (SVM).

Several authors have compared different modelling methods for assessing forest structure variables. Most studies show that non-parametric models tend to perform slightly better in estimating forest structural variables than parametric regression approaches. For example, Aertsen et al. (2010) compared five modelling approaches including parametric multiple linear regression (MLR) and four

non-parametric models which include classification and regression tree (CART), generalised additive model (GAM), artificial neural networks (ANN) and boosted regression tree (BRT), in predicting Site Index of mixed pine and cedar Mediterranean mountain forests. They found all non-parametric models except CART outperformed MLR (by up to 0.26 m root-mean-square-error (RMSE)). Chirici et al. (2008) tested different configurations of k-NN models in estimating forest growing stock volume in mixed alpine forests in Italy, and then compared the results with multiple linear regression. The estimation achieved marginally lower prediction error (by 5-7%) using the best k-NN model than the MLR model. Fehrmann et al. (2008) evaluated model performance for estimating single-tree biomass using k-NN and linear mixed-effect models, they found that in comparison to MLR models, the relative RMSE obtained using the k-NN model was 1% lower for spruce species and 0.5% lower for pine species.

However, it is not clear which non-parametric approach should be adopted as a number of comparisons among the models used in estimating forest variables have shown various results. k-NN was found to produce lower RMSE than Random Forest (RF) in imputing basal area and standing volume in the Irish National Forest Inventory, by up to 16 m^3 ha^{-1} and 1.8 m^2 ha^{-1} respectively (McInerney & Nieuwenhuis, 2009). However, RF was the overall best performing model in estimating basal area and tree density compared to other models including k-most similar neighbours (k-MSN) and gradient nearest neighbour (GNN) in a coniferous forest located in north-central Idaho, USA (Hudak et al., 2008). Furthermore, Breidenbach et al. (2010) compared k-MSN, RF and conditional inference trees (CF) approaches for predicting species-specific timber volume in a European mixed species forests. They found that all three approaches produced similar RMSE, whereas RF produced larger bias (1% more than the other two approaches). Shataee (2013) compared four types of non-parametric modelling approaches (k-NN, SVM, RF and ANN) in modelling forest volume and basal area with integrated LiDAR and Landsat TM, SVM showed better estimation results in both volume and basal area than the other approaches, followed by k-NN, with RF prediction accuracy being the lowest.

The outcomes of these studies suggest there is no single method that proves superior for all cases. According to Brosofske et al. (2014), selection of the best model is determined by the purpose of analysis, available data and the nature of the data, underlying biophysical conditions of the forest, and the type of response variables to be estimated. In order to best model forest variables, more than one modelling approach can be used to describe a forest by selecting the best model for each forest variable. For example, Mora et al. (2013) found that k-NN provided the best accuracy for forest canopy height estimation, while linear regression better modelled forest volume and above-ground biomass.

Besides forest stand variables, understanding forest stand age for plantations is critical for forest management. Stand age is a fundamental variable but it is not always available, especially for scattered small-scale forests as such information is held privately by individual forest owners. Alternatively, forest age can be assessed using other correlated factors that can be derived remotely. Research has shown that forest stand age is correlated with spectral reflectance of satellite imagery (Cohen et al., 1995), especially the near infrared band and its derived vegetation indices (Jensen et al., 1999). Additionally LiDAR-derived metrics have also proven to be useful in estimating forest age. Weber and Boss (2009) used LiDAR-derived height metrics and site condition variables such as slope and distance to streams to classify three stages of forest maturity in a mixed species forest using a CART approach. Falkowski et al. (2009) identified LiDAR-derived metrics (maximum, minimum height, and proportions of returns in different strata) and used a RF classifier to identify seven stages of forest succession in a mixed forest. Maltamo et al. (2009) used k-NN and k-MSN approaches to predict plot-level stand age in a mixed boreal forest using combined LiDAR-derived height, intensity and density metrics and aerial photography-derived spectral and textural information. For the forest, stand age ranged from 1 to 150 years old, the RMSE of age estimation ranged from 18 to 23 years.

More recently, Racine et al. (2014) used combined LiDAR-derived metrics and site attributes (such as elevation, slope and aspect) to predict forest stand age in a regenerated boreal forest using k-NN imputation. It was found that the prediction worked well with $R^2 = 0.83$ and RMSE of less than 10 years (19% of mean estimated age). Although these studies confirmed that LiDAR and remote sensing data can be used to predict forest stand age, there is an absence of research that compares different modelling approaches in estimating stand age from remote sensing data.

This chapter evaluates the performance of different parametric and non-parametric models in estimating forest stand variables. The main objective of this chapter is to find the optimal combination of remote sensing data and modelling approach that most accurately estimates mean top height (MTH), basal area (BA), standing volume (VOL) and stand age (Age) for planted forests especially small-scale plantations in the Wairarapa region of New Zealand. In particular, this chapter will answer the following research questions:

1. Can a combination of LiDAR and RapidEye data improve the estimation of forest stand variables compared with using either single sensor in isolation?
2. Which modelling approach (multiple linear regression, seemingly unrelated regression, k Nearest Neighbours and Random Forest) produces the highest accuracy and lowest error and bias for estimating forest stand variables?

5.2 Methodology

5.2.1 Plot Data

There are limited forest inventory data for small-scale forests in New Zealand's Wairarapa region. The only existing forest inventory available is the Field Measurement Approach (FMA) plot data, which has been set up as a basis for monitoring carbon changes for forests that are over 100 ha and entered in the Emissions Trading Scheme (ETS) (MPI, 2012a). Most of the FMA plot centres were established in 2012 using a consumer-grade GPS receiver. Since plot location offsets between field data and LiDAR can lead to errors in modelling (Gobakken & Naesset, 2009), it was unclear whether the consumer-grade GPS measurements of plot centres were sufficiently accurate.

A pilot study carried out in late 2013 at ten FMA plots in Oxford, Canterbury suggested that the discrepancy between a consumer-grade GPS receiver (Garmin 60CSx) and a survey grade GPS (Trimble GeoXH 6000) was up to 7.4 m in a horizontal direction. On this basis, it was deemed critical to re-measure FMA plot centres with a high-grade GPS receiver. Since the FMA plots only target post-1989 forests, an additional 16 pre-harvest inventory (PHI) plots aged between 26 and 28, and seven Forest Research Institute (FRI) trial plots aged 30 were also included. The FRI trial plots were established to evaluate the impact of different pruning height and stocking on forest growth, the plots selected for re-measurements only included those were pruned at standard heights: four plots were pruned at 7.6 m, one was pruned at 6 m and two unpruned plots and all seven plots were at a final stocking between 200 and 350 stems per hectare.

In May 2014, a total of 112 plots (including FMA, PHI and FRI plots) were re-measured and relocated using a Trimble GeoXH 6000. All plots visited were radiata pine plantations. The rationale of selecting these plots was to capture a range of age classes (age 9-30) and silvicultural regimes that are typically applied in the region. As the main purpose of field data collection was to provide validation data for remote sensing data, the plot selection was not based on statistical distribution, hence multiple plots within the same forest stand were included to maximise plot numbers. Twenty-one plots were unpruned and four were unthinned. Most plots have final stocking around 300-400 stems per hectare (Table 5-1). The plot centres were located with both Trimble GeoXH 6000 and Garmin 60CSx. The locations of Trimble GPS were then differentially corrected based on information from local field stations. Plot sizes varied from 0.01 ha to 0.1 ha depending on the intensity of stocking. Forest inventory measurements including over bark diameter at breast height (DBH) and tree height measurements were taken. DBH of all trees within a plot were measured. On average, 14 trees from each plot were measured for height using a vertex. The plot locations are shown in Figure 5-1. Plot slope ranged from 4° to 38°, and averaged 20°.

Table 5-1: Plot summary

Stand Variables	Mean	Range
Plot Area (ha)	0.06	0.01 - 0.1
Age (years)	20	9 - 30
Stocking (stems ha^{-2})	390	159 - 1212
Diameter at Breast Height (mm)	403	19 - 880
Individual Tree Height (m)	26.40	4.9 - 54.5
Mean Top Height (m)	25.13	9.10 - 42.30
Basal Area (m^2 ha^{-1})	49.69	16.32 - 99.99
Volume (m^3 ha^{-1})	436.70	67.75 - 1134.05

Using the plot data, several stand variables were calculated according to inventory data processing procedures widely applied operationally in New Zealand. Firstly, individual height and diameter relationships were derived using the Petterson equation (Petterson, 1955) from field measurements for each plot. The relationship was then used to estimate the height for trees that did not have field height measurement in the same plot.

$$H = 1.4 + (b + a/D)^{-2.5} \quad (2)$$

Where H is the tree height, D is the DBH, a and b are parameters.

The standing tree volume was calculated using all New Zealand volume equation No. 182 for pruned and thinned stands (Katz et al., 1984):

$$V = D^{1.79068} \times (H^2/(H - 1.4))^{1.07473} \times e^{-10.03201} \quad (3)$$

Where V stands for the volume and e is the natural logarithm constant at 2.71828.

Stand BA was calculated by summing the basal area of each tree in a plot and divided by the plot area. The Mean Top Diameter (MTD) is the DBH of the tree with basal area equal to the average basal area of the 100 largest (by DBH) trees per hectare. The Mean Top Height (MTH) is the height predicted from the height/diameter relationship (equation 2) for a tree with DBH equal to the MTD.

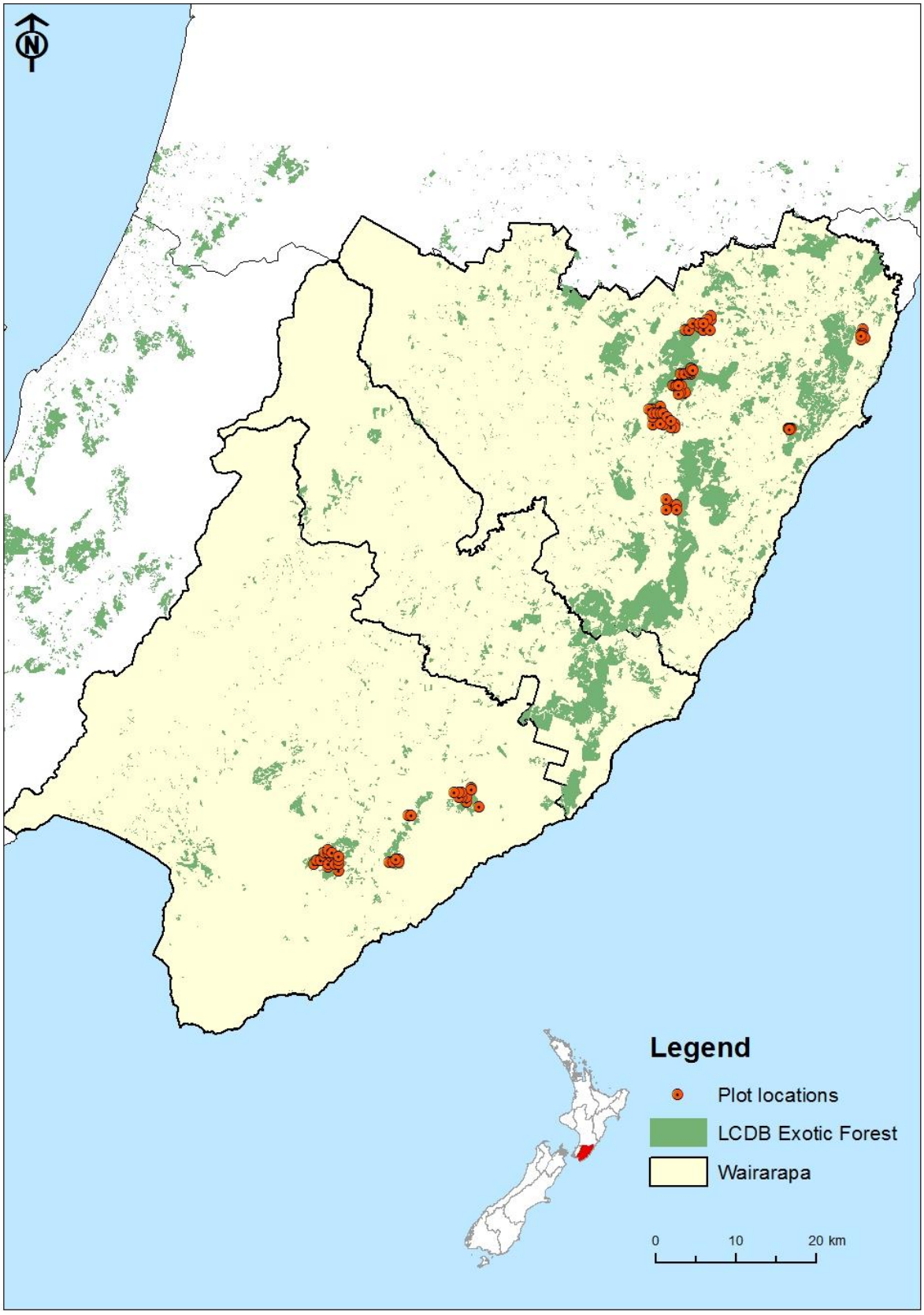

Figure 5-1: Plot locations over LCDB exotic forests. LCDBv4.1 (Landcare Research, 2016) is a spatial representation of land cover classes for New Zealand developed by Landcare Research.

5.3 Candidate predictors

5.3.1 Remote sensing data

LiDAR metrics have been extensively correlated with forest stand variables. Commonly used LiDAR metrics for deriving forest stand variables can be extracted easily using existing LiDAR processing packages. In total 111 LiDAR metrics, which belong to four categories - height, canopy cover, intensity and compound variables were extracted within each plot boundary (Table 5-2). Height metrics describe the height distribution statistically, and provide information on the vertical structure at different height levels. A minimum height threshold was set as 0.5 m so that only non-ground returns that are above 0.5 m were considered in the analysis. Canopy cover metrics were derived based on pulse returns, which provide a measure of canopy structure. For deriving canopy metrics, a height threshold of 3 m was set to compute ratio metrics describing forest canopy features. Intensity refers to the strength of each pulse that provides concentrated measurement of an object's reflectance, and intensity metrics provide a number of statistical descriptions of intensity distribution. Compound metrics were not directly derived but calculated from other metrics. The two compound metrics used here were differences between height percentiles that proved useful in estimating volume by Marshall et al. (2012).

For subsequent regression against field measured forest variables, the rationale for selecting these metrics is that firstly they have proven to be useful in other studies to estimate forest structural variables (Hall et al., 2005; Stephens et al., 2012; Stephens et al., 2007), and secondly they are relatively easy to compute using existing LiDAR processing software such as Fusion (McGaughey, 2016a) and LAStools (Rapidlasso GmbH, 2016).

RapidEye metrics were derived using eCognition (Trimble, 2016) within each defined plot boundary. Each plot boundary served as an image object, where the mean value of each metric was extracted for each individual plot. In total 76 metrics were derived including mean, standard deviation, skewness, texture, vegetation indices and customised band ratios. The details of the derivation of these metrics can be found in Chapter 4, Table 4-4 and Table 4-5. The geometry metrics which include the shape and extent details were not used in this chapter as these details are irrelevant within a defined plot boundary.

Table 5-2: Commonly use LiDAR metrics to derive stand attributes

Category	LiDAR Metrics	Metric Details	Source
Height variables	H_min	Minimum height	Fusion
	H_max	Maximum height	Fusion
	H_mean	Mean height	Fusion
	H_mode	Mode of height	Fusion
	H_sd	Standard deviation of height	Fusion
	H_qav	Average square height	LAStools
	H_var	Variance of height	Fusion
	H_cv	coefficient of variation of height	Fusion
	H_iq	Interquartile distance of height	Fusion
	H_Skewness	Skewness of height	Fusion
	H_Kurtosis	Kurtosis of height	Fusion
	H_AAD	Average Absolute Deviation of height	Fusion
	H_MAD_median	Median of the absolute deviations from the overall median height	Fusion
	H_MAD_mode	Median of the absolute deviations from the overall mode height	Fusion
	H_L1, H_L2, H_L3 and H_L4	Height L-moments	Fusion
	H_L_cv	Height L-moments coefficient of variation	Fusion
	H_L_skewness	Height L-moments skewness	Fusion
	H_L_kurtosis	Height L-moments kurtosis	Fusion
	H percentiles: H(01, 05, 10, 20, … 95, 99)	Quantiles of height	Fusion
	H_SQRTmeanSQ	Elev SQRT mean SQ	Fusion
	H_CURTmeanCUBE	Generalised means for the 2nd and 3rd power (Elev quadratic mean and Elev cubic mean)	Fusion
	KDE_H_modes	No. of modes in height kernel density estimation	Fusion
	KDE_H_min_mode	Minimum mode in height kernel density estimation	Fusion
	KDE_H_max_mode	Maximum mode in height kernel density estimation	Fusion
	KDE_H_mode_range	Range between the minimum and maximum mode values in height kernel density estimation	Fusion

Category	LiDAR Metrics	Metric Details	Source
	Total return count	Total return count	Fusion
	Total return count above 0.50	Total return count above 0.50	Fusion
	1st_return_above_0.5	Return 1 count above 0.50	Fusion
	2nd_return_above_0.5	Return 2 count above 0.50	Fusion
	3rd_return_above_0.5	Return 3 count above 0.50	Fusion
	4th_return_above_0.5	Return 4 count above 0.50	Fusion
	1st_returns	Total first returns	Fusion
	all_returns	Total all returns	Fusion
	1st_returns_above_mean	First returns above mean	Fusion
	1st_returns_above_mode	First returns above mode	Fusion
	all_returns_above_mean	All returns above mean	Fusion
	all_returns_above_mode	All returns above mode	Fusion
Canopy Cover	Canopy relief ratio	((mean - min) / (max – min)) of all returns	Fusion
	%1st_return_above_3m	Percentage first returns above 3.00	Fusion
	%all_return_above_3m	Percentage all returns above 3.00	Fusion
	(all_return_above_3m) / (total_1st_returns) * 100	Number of returns above 3m / total first returns * 100	Fusion
	1st_return_above_3m	First returns above 3.00	Fusion
	all_return_above_3m	All returns above 3.00	Fusion
	%1st_return_above_mean	Percentage first returns above mean	Fusion
	%1st_return_above_mode	Percentage first returns above mode	Fusion
	%all_return_above_mean	Percentage all returns above mean	Fusion
	%all_return_above_mode	Percentage all returns above mode	Fusion
	(All returns above mean) / (Total first returns) * 100	(All returns above mean) / (Total first returns) * 100	Fusion
	(All returns above mode) / (Total first returns) * 100	(All returns above mode) / (Total first returns) * 100	Fusion
	Canopy densities b(10, 20, 30, … 80, 90)	Canopy densities (bencentiles)	LAStools
Intensity variables	I_max	Minimum intenisty	Fusion
	I_min	Maximum intensity	Fusion
	I_mean	Mean intensity	Fusion

Category	LiDAR Metrics	Metric Details	Source
	I_mode	Mode of intensity	Fusion
	I_sd	Standard deviation of intensity	Fusion
	I_qav	Average square intensity	Fusion
	I_var	Variance of intensity	Fusion
	I_cv	Coefficient of variation of intenisty	Fusion
	I_iq	Interquartile distance of intensity	Fusion
	I_skewness	Skewness of intensity	Fusion
	I_kurtosis	Kurtosis of intensity	Fusion
	I_AAD	Average Absolute Deviation of intensity	Fusion
	I_L1, I_l2, I_L3 and L4	Intensity L-moments	Fusion
	I_L_cv	Intensity L-moments coefficient of variation	Fusion
	I_L_skewness	Intensity L-moments skewness	Fusion
	I_L_kurtosis	Intensity L-moments kurtosis	Fusion
	I(01, 05, 10 …, 95, 99)	Intensity percentiles	Fusion
Compound variables	p95-p30	95th height percentile - 30th height percentile	Calculated from Fusion metrics
	p70-p20	70th height percentile - 20th height percentile	Calculated from Fusion metrics

5.4 Modelling approaches

Four modelling approaches: parametric multiple linear regression and seemingly unrelated regression, together with non-parametric k-NN and Random Forest were evaluated to predict MTH, BA, VOL and age with three sets of explanatory variables: 1) LiDAR –derived metrics (111 variables), 2) RapidEye-derived metrics (76 variables), 3) Combined LiDAR and RapidEye metrics (187 variables). All 112 sets of plot data were used as the calibration data to develop the models predicting or imputing MTH, BA, VOL and age. The developed models were then validated using a 10-fold cross validation approach.

5.4.1 Multiple linear regression

Multiple linear regression solved using OLS has been the most common analytical approach for estimating multiple forest stand attributes from data collected from optical and LiDAR sensors. For example, multiple linear correlation has been established to estimate forest stand variables such as canopy height (Donoghue & Watt, 2006), basal area (Naesset, 2007), volume (Naesset, 2002) and leaf area index (Jensen et al., 2008).

Multiple linear regression was carried out in the base package in R (R Development Core Team, 2016). Due to the large number of candidate explanatory variables, a variable subsetting process was carried out to select the optimal combination of variables that produced the lowest Mallow's C_P (Mallows, 1973). Mallows' C_P is an indication of the fit of a regression model that takes into account the number of predictors. A small value means a model is relatively precise. The "leaps" package in R (Lumley & Miller, 2009) was used to perform an exhaustive search for the best subsets of explanatory variables in linear regression where all the possible combinations of the explanatory variables were being tested.

Since the remote sensing metrics were derived from the same data source, it is likely to contain closely correlated explanatory variables for both LiDAR and RapidEye derived metrics. For example, LiDAR –derived H90 and H80 and RapidEye-derived green band and green ratio are highly correlated variables. This is defined as multicollinearity in linear regression, which refers to two or more predictors in a multiple regression model being highly correlated. Although the R^2 of a model with correlated variables may not be affected (sometimes it is even higher with correlated variables), the performance of individual predictor may be overlooked (Graham, 2003) which potentially affects the decision on which predictors are useful for predicting forest stand variables. Since multicollinearity among explanatory variables can hamper the identification of a set of optimal explanatory variables, the collinearity among the selected variables needed to be identified following the exhaustive search with "leaps". A common approach is to calculate the variance inflation

factorsVIF) of the regression model, which measures the increase of variance of an estimated regression coefficient because of collinearity (O'Brien, 2007).

$$VIF = \frac{1}{(1-R_i^2)} \quad (4)$$

Where R_i^2 is the coefficient of determination of the regression with *i*th predictor that is associated with other predictors in the model. Variables were only retained if they are significant at p = 0.05 and the VIF among other variables was under ten. When there is a correlation among multiple predictors, the predictor with the highest VIF was removed first and if collinearity still occurred; the predictor with second largest VIF was removed. The process was repeated until the VIFs of all predictors were under ten.

5.4.2 Seemingly unrelated regression

Regression models involve developing statistical relationships from input independent variables to predict parameters under an assumed distribution. However, the OLS approach often assumes the response variables for each stand attribute are estimated independently of other stand variables, which may not be the case for forest stand variables as they are usually estimated from the same observations (Næsset et al., 2005). Therefore, OLS-based regressions can be statistically inefficient if there are strong correlations between the error terms of the respective regression models (Dash et al., 2016). Seemingly unrelated regression, which has been proven to improve parameter estimation efficiency when the error terms of models are correlated (Zellner, 1962), was used as an alternative to OLS multiple linear regression to simultaneously estimate forest stand variables. This has previously been used to estimate tree height, basal area, stem number and volume (Dash et al., 2016; Næsset et al., 2005). SUR was performed using the "systemfit" in R (Henningsen & Hamann, 2007), with the optimal variables selected from MLR.

5.4.3 K Nearest Neighbour

The k-Nearest Neighbour approach predicts unsampled response variables by calculating a statistical distance between the target and reference samples (also referred to as neighbours) then assigns values of the nearest neighbours to the target unit. The value k defines the number of neighbours included in the analysis (Brosofske et al., 2014). The k-NN approach considers one or more neighbours that are close to the target in order to improve prediction accuracy (Breidenbach et al., 2010). k-NN has been applied widely for predicting forest stand attributes and has achieved satisfactory results (McInerney & Nieuwenhuis, 2009; McInerney et al., 2010; McRoberts, 2012; McRoberts et al., 2015). k-NN was also used operationally to impute forest inventory variables for the National Inventories in Finland and Sweden (Tomppo et al., 2008).

There are large numbers of explanatory variables derived from remote sensing data. Including unrelated explanatory variables for predicting response variables can cause detrimental effects for many distance metrics and hence can affect k-NN model accuracy (McRoberts, 2012). Unlike the stepwise search or exhaustive search used for MLR models, k-NN imputation is fundamentally different due to the complexity of the model definition. As such, the model accuracy does not automatically improve as more predictors are used (Packalén et al., 2012). Therefore, a different variable selection approach is required for k-NN imputation. Packalén et al. (2012) compared three approaches (canonical analysis, random forest and simulated annealing) for selecting explanatory variables for k-NN imputation in remote sensing based forest inventory and found that a k-NN model using variables selected by simulated annealing (SA) produced the lowest RMSE. SA is a randomised local search method that selects variables by seeking the minimised RMSE by repeatedly imputing the response variables for the reference datasets using various sets of explanatory variables (Kirkpatrick et al., 1983). This approach provides an optimal approximation of variables within a large global search that can avoid local optima by controlling moves to worse solutions (Dash et al., 2015; Packalén et al., 2012). SA was performed for variable selection prior to k-NN modelling using the "caret" package in R (Kuhn, 2015),

All k-NN models were developed using the "yaImpute" package in R (Crookston & Finley, 2008). Generally there are three inputs required for the configuration of k-NN models: a distance metric that defines the statistical distance between reference and target; the number of neighbours (i.e. the value of k) and a weighting scheme for neighbours (Eskelson et al., 2009; McRoberts et al., 2015).

Several distance metrics have been used with k-NN models to describe the statistical distance between the reference and target observations, such as simple metrics that are independent of the response variables: Euclidean, Mahalanobis distance, and more complex metrics that are based on observations of the response variables – the Most Similar Neighbour (MSN), the Gradient Nearest Neighbour (GNN) and Random Forest (RF) distance (Brosofske et al., 2014). Despite the popularity of using k-

NN in forestry applications, there are very few studies that compare different distance metrics for k-NN. Both Hudak et al. (2008) and Dash et al. (2015) concluded that using the Random Forest (RF) proximity matrix defined distance outperformed other approaches (Euclidean, Mahalanobis, MSN and GNN) in k-NN modelling. Therefore, the model was developed using Random Forest to define the statistical distance between the target and reference observations in a covariate space. This distance metric was defined in the "yaImpute" package.

The neighbours were weighted inversely proportionally to the distance, a weight factor of 1/(1+d) was applied using settings in the "yaImpute" package. As described by McRoberts et al. (2015) and Dash et al. (2015) the most common approach to select a k value is to run a selection of k values in cross validation datasets, and choose the k value that results in the minimum RMSE.

5.4.4 Random Forest

The machine-learning algorithm Random Forest, which is also non-parametric, has been applied in forest modelling recently due to its robustness and improved accuracy. RF uses bootstrapping to randomly and iteratively sample data and variables to generate a large group of classification and regression trees, producing output that represents a statistical model of many decision trees (Breiman, 2001). Only a small number of predictor variables are used to find the best split at each tree node, hence RF tends to decrease the correlation between trees and reduce bias (Brosofske et al., 2014). RF represents the statistical mode of many decision trees so that it can produce more robust results (Hudak et al., 2008). RF is also comparatively simple to apply without sophisticated fine-tuning of parameters (Immitzer et al., 2012). The application of RF in a forestry context is recent, yet there are many studies using RF as an approach to estimate various forest attributes such as height (Cartus et al., 2012; Kellndorfer et al., 2010), volume and biomass (Latifi et al., 2012) with integrated optical and LiDAR sensors.

The application of Random Forest is straightforward in R using the "randomForest" package (Liaw & Wiener, 2002), with the algorithms originally developed by Breiman (2001) embedded in the package. The number of decision trees built was set at 500. Since RF automatically selects and evaluates explanatory variables used to develop decision trees, there is no need to do any variable selection prior to modelling.

5.5 Model Validation

All models developed were based on all the plot data; the model development process identifies appropriate predictors and parameters. Results from model development can only suggest the performance of the models for this particular dataset. However, it is unclear whether these models

would perform equally well for other datasets. Therefore, it is also necessary to find the out-of-sample accuracy for both parametric and non-parametric models by testing on different datasets. This process is generally referred as validation of models, which informs the performance of a model over a wide application perspective and provides information required to refine the initially developed model (Brosofske et al., 2014).

Ideally model validation is carried out with an independent dataset drawn from the population which the model will be applied. However, due to the limited field data collected, a cross validation approach using existing datasets was required. Kohavi (1995) suggested using a k-fold approach as it appeared to be less biased compared to leave-one-out validation and it is simple to apply. Therefore, a 10-fold analysis approach was used for cross validation of the models. All the plot data were randomly split into ten subsets, each set contains approximately 11 plots. A model was fit using nine out of the ten subsets (also referred as the training dataset) and then was used to predict the remaining set (also referred as the validation dataset). The process repeats until all subsets have been used once as the validation dataset. The overall model prediction error was the mean error from each of the repeated tests. Using this method, all of the operations are used to train and validate the model, which maximises the knowledge that can be obtained from the dataset (Kozak & Kozak, 2003).

Since a wide range of modelling approaches and predictors are available, choosing the best model can be challenging and needs careful attention. In terms of the measure of model performance, the Root Mean Square Error (RMSE) has been commonly used as a measure of model quality in predicting continuous variables (Katila & Tomppo, 2001). The prediction error of the developed model is interpreted as the RMSE of the model from cross-validation. However, the measure is not standardised (Brosofske et al., 2014), as many studies also tend to measure the mean deviation (MD) of models. MD is defined as the mean difference between the observed value and the predicted values of all population units. It is often referred to as the bias of prediction (McInerney & Nieuwenhuis, 2009).

In this study, the adjusted coefficient of determination (Adj. R^2) which takes account of the effect of multiple predictors was used to determine the goodness of fit during the model development stage. Furthermore, model performance among all four models was assessed based on the estimation errors using RMSE and MD in both absolute and relative terms. These measurements of errors were found to be the most commonly used in assessing model performance according to a number of recent k-NN imputation studies with remote sensing input data (Chirici et al., 2016). The relative terms were expressed as RMSE and MD percentage of the predicted mean.

$$\mathrm{RMSE} = \sqrt{\frac{\Sigma\left(y_i - \hat{y}_i\right)^2}{\mathrm{n}}} \tag{5}$$

$$MD = \frac{\Sigma(y_i - \hat{y}_i)}{n} \quad (6)$$

Where y_i is the measured value of response y in the validation dataset, $\hat{y}_i$ is the estimated response y and n is the number of the plots assessed.

5.6 Results

5.6.1 Comparison of GPS accuracy

The error reading shown on the Garmin 60CSx, which actually measures the estimate of position error (EPE) was manually recorded since the receiver does not automatically save the information. The EPE of Garmin GPS ranged from 1.6 to 8 m. The longer the GPS receiver was left at plot centre the more stable the reading became. When the EPE reading did not change for one minute, it was considered a stable value. It was observed during field data collection that at least 10 minutes was required for the error reading to stabilise.

The Trimble receiver automatically stores the accuracy every few seconds. The differentially corrected positional error ranged from 0.1 to 5.1 m. Similar to the Garmin receiver, longer waiting time appeared to stabilise the error reading. In order to achieve accurately positioned plot locations, both receivers were left at the plot location longer while tree measurements were being undertaken.

Based on the relationship between waiting time and Trimble GPS EPE (Figure 5-2), the positional error decreased below 2 m after leaving the receiver for over 40 minutes. The Trimble receiver achieved higher accuracy and precision than the Garmin receiver (Figure 5-3).

Eighty five out of 112 plots measured by the Trimble receiver achieved sub-metre accuracy, while another 24 achieved EPE below 2 m; only 3 plots had EPE above 2 m. On the other hand, Garmin GPS errors ranged from 1.6 to 8m, with majority of plots obtaining two to four metres of error and none achieved sub-metre accuracy.

The plot location offsets between field data and LiDAR can lead to errors in modelling when the plot data and remote sensing data are not lined up (Gobakken & Naesset, 2009). In this study where all the forests are radiata pine plantations, the offset between remote sensing data and field data may not be as significant an issue as in heterogeneous and complex natural forests. Nevertheless, obtaining the most accurate plot centres with the Trimble GPS receiver minimises this issue.

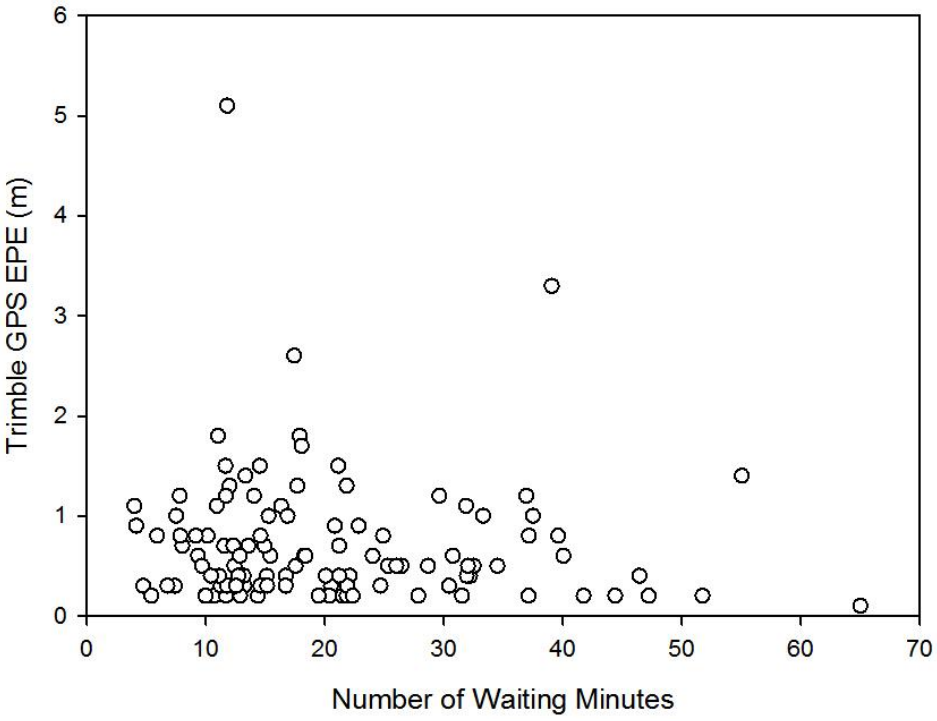

Figure 5-2: Trimble GPS EPE against waiting time (minutes), each open circle represents measured plot centre accuracy at its waiting time. There were larger GPS errors at low waiting time, whereas the GPS errors reduced at longer waiting time.

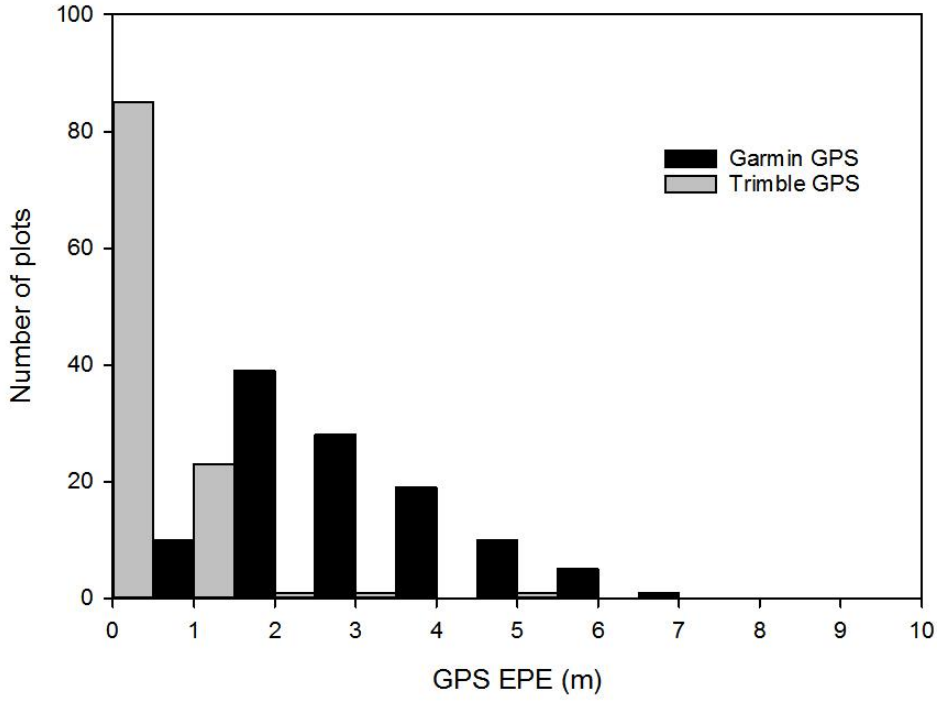

Figure 5-3: GPS errors from Garmin GPS receiver and Trimble GPS receiver.

5.7 Estimate of Stand Variables

5.7.1 Multiple Linear Regession

After evaluation of different models with various combinations of predictors and input parameter settings, a total of 48 models (for estimating four variables using four approaches and three input datasets) were finalised as the best models based on highest R^2 and lowest RMSE values, using all 112 sets of plot data and corresponding remote sensing data. These include modelling of mean top height, basal area, volume and age using LiDAR only, RapidEye only and combined LiDAR and RapidEye inputs with multiple linear regression, seemingly unrelated regression, k-Nearest-Neighbour and random forest models.

Figure 5-4 shows the correlation between predicted and observed MTH, BA, VOL and age using multiple linear regression models. Several important predictors, primarily LiDAR metrics, were identified for multiple linear regression models. MTH was predicted most accurately using a single LiDAR height metric (90^{th} height percentile), which explained 97% of the variability in MTH estimation (RMSE = 1.31 m, $RMSE_{\%}$ = 5%). LiDAR metrics also predicted BA reasonably accurate, explaining 73% of the variability in BA (RMSE = 9.47 m^2 ha^{-1}, $RMSE_{\%}$ = 19%). LiDAR metrics that contributed most to the prediction of BA included the quadratic mean height, 99^{th} percentile of intensity, 4^{th} returns above 0.5 m and percentage of first returns above 3 m. VOL was also modelled accurately with return, height and intensity metrics used for estimating BA as well as the percentage of all returns above 3 m over total first returns. Using these selected LiDAR metrics in a MLR model explained 88% of the variability in VOL (RMSE = 84.2 m^3 ha^{-1}, $RMSE_{\%}$ = 19%). LiDAR metrics including intensity skewness, 10^{th} percentile of intensity and 95^{th} percentile of height were selected as best predictors to estimate stand age, giving R^2 of 0.85 (RMSE 2.11 years, $RMSE_{\%}$ = 10%).

Multiple linear regression models developed using RapidEye metrics as explanatory variables performed significantly poorer than using only LiDAR metrics. The correlations between predicted and observed stand variables derived by RapidEye metrics were relatively weak, and the RMSEs produced increased by 4.36m for MTH , 2.23 m^2 ha^{-1} for BA, 94.70 m^3 ha^{-1} for VOL and 2.11 years for age, in comparison to using only LiDAR metrics. However, using RapidEye metrics especially textural values (CLCM correlation, mean and entropy) performed slightly better in estimating BA than other response variables, potentially due to correlation between the size of trees and image textural information. It was also worth noting that the removal of predictors due to collinearity affected the performance of models with RapidEye metrics. Overall, the R^2 of MTH, BA, VOL and age estimation using non-correlated RapidEye metrics reduced by 0.07, 0.04, 0.10 and 0.15 respectively compared to using all identified important RapidEye predictors. Nevertheless, due to the conditions of linear regression, these correlated variables are required to be excluded from selected

models. A full list of the RapidEye metrics used in modelling all stand variables is shown in Appendix E.

When combining both LiDAR and RapidEye metrics, the estimation of MTH and VOL improved only marginally, with R^2 improving by 1% compared with using LiDAR metrics only (R^2 = 0.98 for MTH, R^2 = 0.89 for VOL using combined sensors). The R^2 of BA and age improved slightly by 3% and 2.3% respectively (R^2 = 0.76 for BA, R^2 = 0.87 for age using combined sensors), and the RMSE decreased by 1% for both BA and age (RMSE = 8.95for BA and 1.94 for age). Overall, the benefits of combining LiDAR metrics with RapidEye metrics for MTH, BA, VOL and age estimation were not large. Visually (Figure 5-4) the most noticeable difference in comparing combined LiDAR and RapidEye metrics with LiDAR metrics is for basal area where a curvilinear relationship becomes more linear.

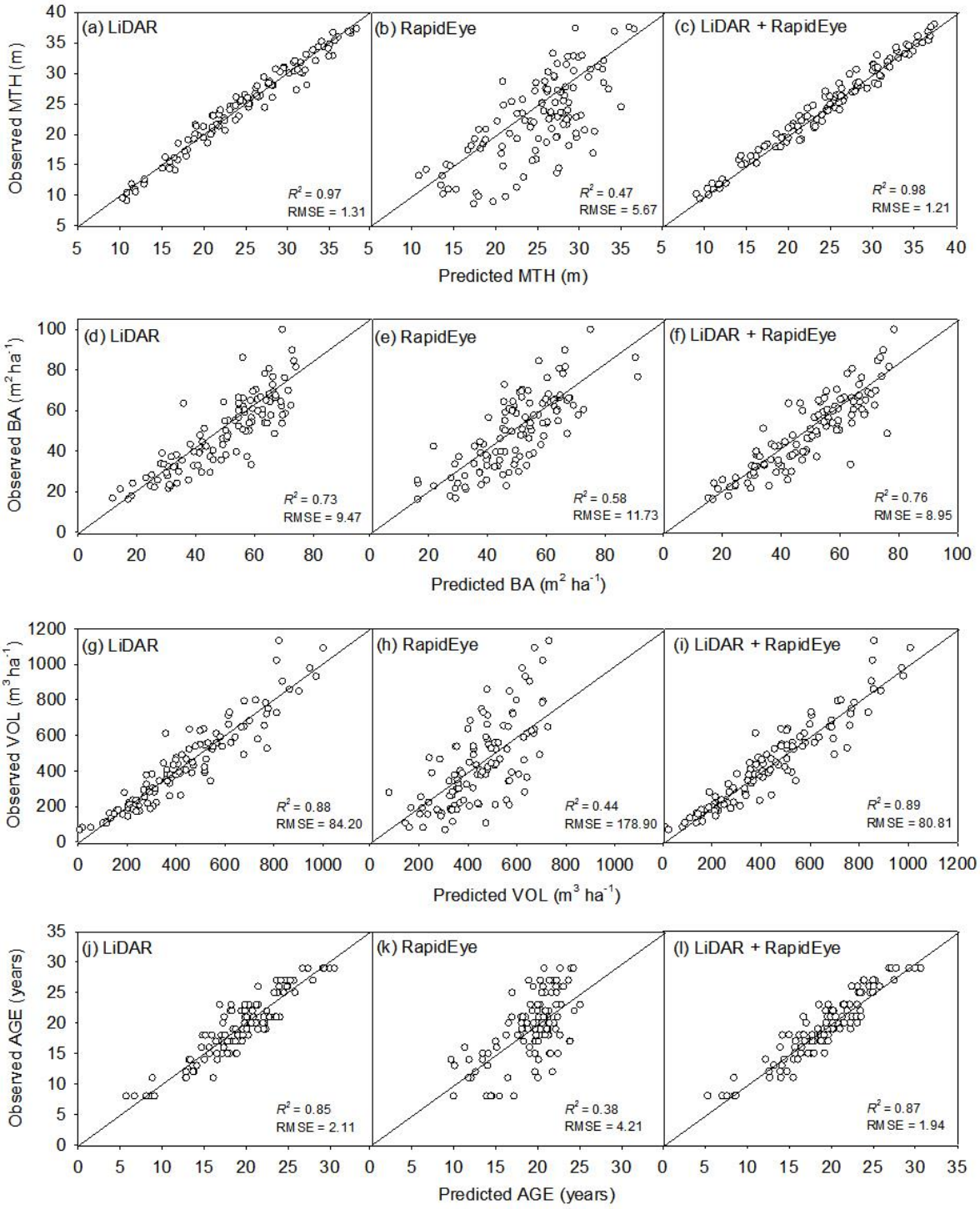

Figure 5-4: Relationship between observed and predicted MTH, BA, VOL and age using the best multiple linear regression. The diagonal line shows the 1:1 line. R^2 shown are adjusted R^2.

5.7.2 Seemingly Unrelated Regression

Figure 5-5 shows the correlation between predicted and observed MTH, BA, VOL and age using seemingly unrelated regression models. SUR models used the same set of predictors that were selected for MLR models, which also excluded the correlated predictors. They additionally take the correlation among response variables into consideration. Similar to MLR models, LiDAR metrics alone proved useful in estimating MTH, BA, VOL and age. The R^2 and RMSE produced by SUR models using only LiDAR metrics were very similar to using MLR models, with only marginal decreases in R^2 and increases in RMSE. However, SUR models using RapidEye only metrics performed worse than MLR models for estimating all variables, especially for VOL with an RMSE of 44% of the predicted mean VOL (RMSE = 191.60m^3 ha^{-1}). Combining LiDAR and RapidEye metrics hardly improved the estimation of MTH, VOL and age, with R^2 only improving by 1% compared with using LiDAR metrics only (R^2 = 0.98, 0.88 and 0.85 respectively for MTH, VOL and age). The R^2 of BA improved slightly by 2% and RMSE reduced by 0.5% (RMSE = 9.20 m^2 ha^{-1}, $RMSE_{\%}$ = 19%).

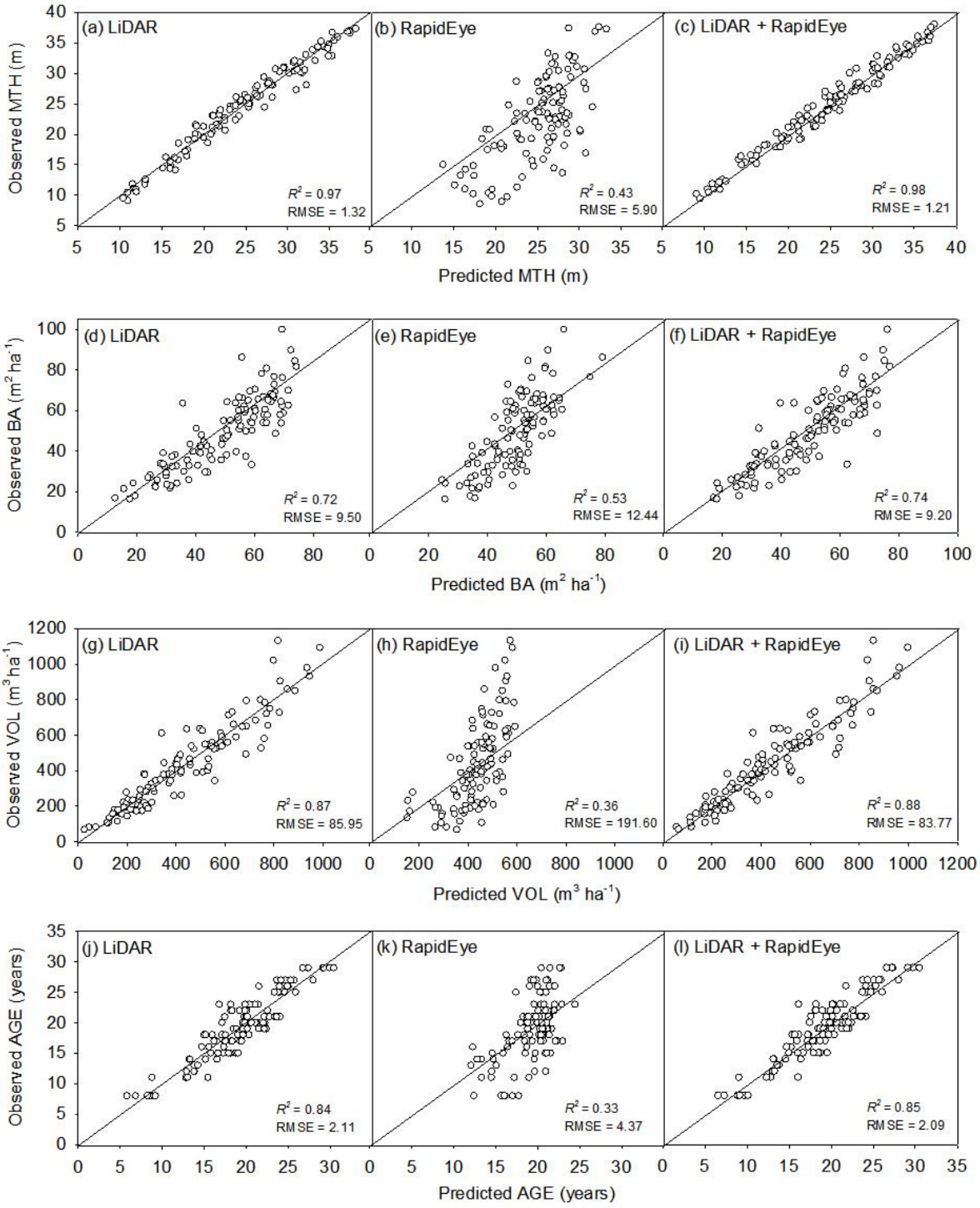

Figure 5-5: Relationship between observed and predicted stand variables using the best seemingly unrelated regression for estimating MTH, BA, VOL and age. The diagonal line shows the 1:1 line. R^2 shown are adjusted R^2.

5.7.3 K-Nearest Neighbour

The simulated annealing approach selected a large number of useful predictors (between 23 and 68 predictors) for k-NN models. Some of the most useful predictors identified for estimating MTH, BA, VOL and age were:

- MTH: LiDAR metrics – H_max, H95, H90, Hqav; and RapidEye metrics – grey-level co-occurrence matrix (GLCM) correlation, GLCM contrast and Green Ratio;
- BA: LiDAR metrics – percentage of 1st return above 3 m, percentage of all returns above 3 m, H_mean, I_L1; and RapidEye metrics – GLCM entropy, GLCM correlation, red ratio and GLCM mean;
- VOL: LiDAR metrics – H_mean, percentage of all returns above mean over total 1st returns , b50, I_min; and RapidEye metrics – NDVI, red ratio, GLCM contrast, and GLCM StdDev;
- Age: LiDAR metrics – percentage of all returns above 3 m over total first returns, I_L3, percentage of of 1st returns above 3 m, I_kurt; and RapidEye metrics – skewness of blue band, NDVI, RENDVI and standard deviation of NIR.

The number of neighbours (k value) used for k-nearest neighbour modelling significantly affects the accuracy of model prediction for forest stand variables. K values ranging from 1- 20 were tested in k-NN models to estimate MTH, BA, VOL and age using all plot data. As shown in Table 5-3, RMSE of models varied considerably at different k values. Of the 20 k values tested, the difference between the largest and smallest RMSEs for MTH estimation ranged from 0.57 to 2.01 m, for BA ranged from 1.31 to 3.39 m^2 ha^{-1}, for VOL ranged from 23.02 to 45.71 m^3 ha^{-1} and for age ranged from 0.99 to 1.31 years with different sensors. Smaller k values (i.e. using fewer neighbours) tended to produce lower RMSE than using larger k values. The k values that produced minimum RMSE were selected for use in k-NN models for estimating each stand variable from the calibration dataset.

Table 5-3: RMSE summary of MTH, BA and VOL estimation using k-NN model at various k values. The minimum RMSE for each model is shown bold. For calibration data, the k value used in models ranged from 1 to 6.

	MTH			BA			VOL			AGE		
k	LiDAR	RE	RE+LiDAR	LiDAR	RE	RE+LiDAR	LiDAR	RE	RE+LiDAR	LiDAR	RE	RE+LiDAR
1	1.52	3.55	1.6	8.81	8.06	9.55	83.56	103.01	77.68	1.36	**1.39**	**0.54**
2	**1.31**	2.76	1.46	7.65	**7.8**	8.08	70.42	91.28	62.48	**1.21**	1.71	0.55
3	1.33	**2.55**	**1.45**	7.56	8.36	7.6	67.77	96.21	**51.18**	1.26	1.75	0.64
4	1.4	2.67	1.46	**7.49**	8.97	**7.33**	68.24	**89.64**	54.66	1.3	1.48	0.78
5	1.38	2.97	1.46	7.56	9.14	7.6	67.8	95.61	56.33	1.38	1.42	0.85
6	1.41	3.07	1.51	7.76	9.18	7.49	**65.36**	104.57	59.53	1.3	1.51	0.81
7	1.46	3.28	1.54	8.06	9.56	7.49	66.93	106.82	59.42	1.35	1.73	0.87
8	1.51	3.35	1.57	8.07	9.55	7.46	66.26	107.63	60.41	1.37	1.82	0.96
9	1.57	3.44	1.57	7.95	9.76	7.37	67.04	113.07	62.05	1.43	2.02	0.98
10	1.59	3.64	1.62	7.85	9.67	7.4	69.53	114.69	61.31	1.52	2.2	1.07
11	1.63	3.72	1.64	7.97	9.84	7.46	70.1	116.01	62.47	1.58	2.31	1.18
12	1.66	3.74	1.68	8.12	10.17	7.69	71.84	120.13	64.91	1.66	2.42	1.31
13	1.69	3.84	1.71	8.29	10.35	7.82	73.87	123.27	67.75	1.76	2.56	1.43
14	1.73	3.99	1.75	8.31	10.52	7.86	76.4	125.59	70.27	1.8	2.6	1.49
15	1.74	4.03	1.79	8.38	10.61	7.76	78.97	126.74	72.84	1.87	2.69	1.56
16	1.77	4.22	1.84	8.53	10.6	7.99	81.15	128.94	73.4	1.92	2.74	1.61
17	1.85	4.3	1.88	8.49	10.78	8.11	83.42	130.35	73.48	2	2.87	1.68
18	1.9	4.36	1.95	8.44	10.87	8.22	85.16	132.73	74.33	2.07	2.94	1.73
19	1.97	4.48	1.99	8.57	11.11	8.32	85.55	134.59	76.2	2.13	3	1.79
20	2.02	4.56	2.03	8.57	11.19	8.33	88.38	135.36	77.77	2.21	3.06	1.85

Figure 5-6 shows the correlation between predicted and observed MTH, BA, VOL and age using k-NN models with k values that produced minimum RMSE (shown bold inTable 5-3). All k-NN models accurately estimated the four stand variables and achieved higher R^2 (ranging from 0.82 to 0.98) and lower RMSE than either parametric model described previously. Similar to parametric models, using LiDAR metrics alone estimated MTH, BA, VOL and age well. Although models using RapidEye metrics produced lower R^2 and higher RMSE than using LiDAR metrics, they obtained significant improvements over previously described parametric models. This was especially true for the estimation of BA, where RapidEye metrics and LiDAR metrics produced similar accuracy (RMSE = 7.49 m^2 ha^{-1} using LiDAR metrics and RMSE = 7.80 m^2 ha^{-1} using RapidEye metrics). Combining LiDAR and RapidEye metrics generally did not improve the performance of MTH and BA relative to using LiDAR metrics, with the exception of VOL and especially age where the RMSE of VOL decreased by 14.21 m^3 ha^{-1} (RMSE = 51.18 m^3 ha^{-1}, $RMSE_{\%}$ = 12%) and RMSE of age decreased by 0.67 years (RMSE = 0.54, $RMSE_{\%}$ = 3%).

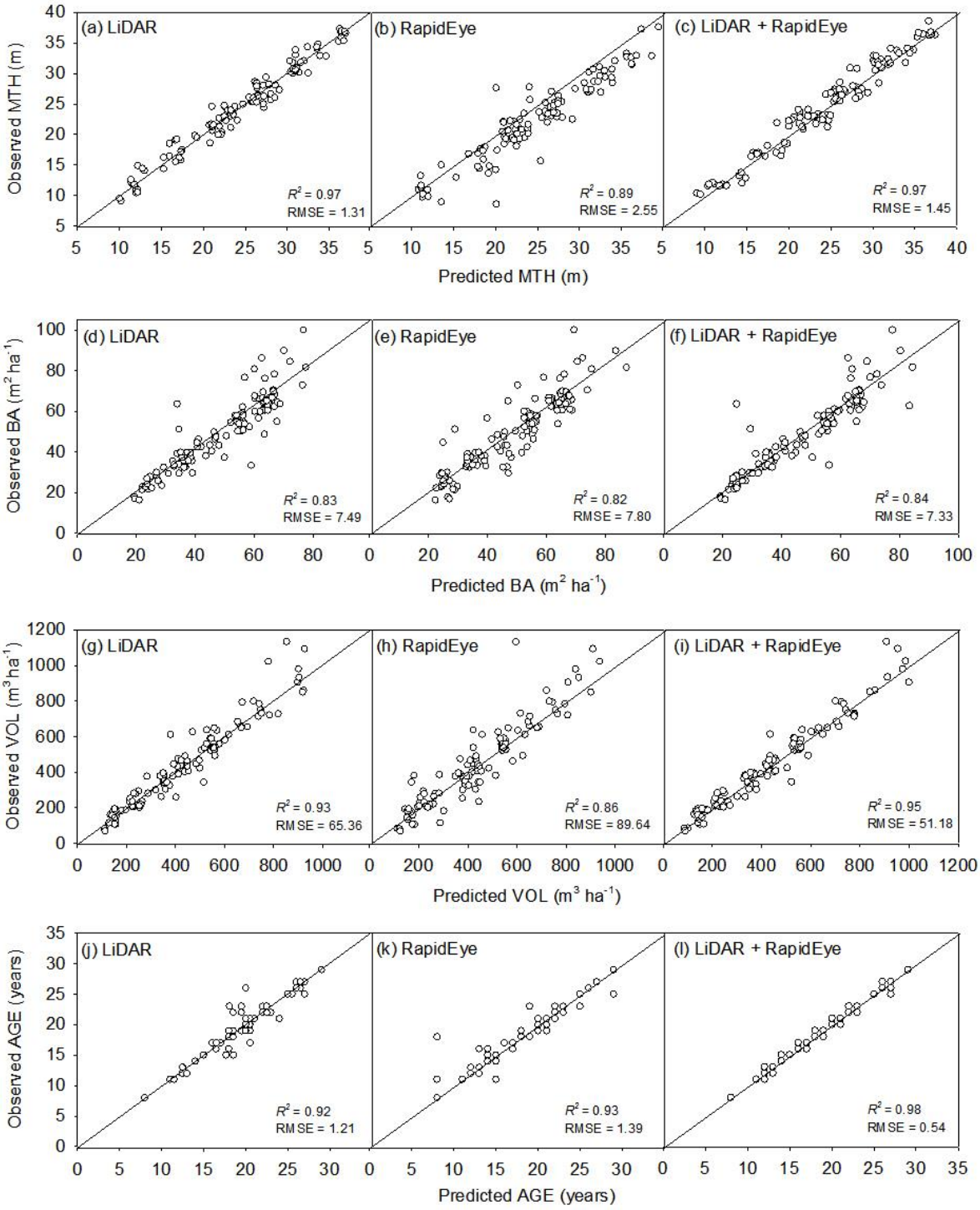

Figure 5-6: Relationship between observed and predicted MTH, BA, VOL and age using k-NN models with the k values selected from Table 3. The diagonal line shows the 1:1 line. R^2 shown are adjusted R^2.

5.7.4 Random forest

Although random forest models are considered as a "black box", the useful predictors used in the models can be identified through the "importance ()" function in the randomForest package in R (Liaw & Wiener, 2002). The package computes the increment in mean square error if one of the predictors is removed from imputation; the larger the increment is, the more important the predictor is in estimating a response variable. The important predictors identified include:

- MTH: LiDAR metrics – H90, H95, H99 , H_max; and RapidEye metrics – NDVI, red ratio, RENDVI, skewness of blue band and GLCM mean;
- BA: LiDAR metrics – Percentage of 1st returns above 3 m, Percentage of all returns above 3 m, percentage of all returns above 3 m over total 1st returns, H10; and RapidEye metrics – red ratio, NDVI, mean red, standard deviation of red band, GLCM mean;
- VOL: LiDAR metrics – H30, H_mean, H_L1, percentage of all returns above 3 m over total 1st returns; and RapidEye metrics – red ratio, NDVI, RENDVI and GLCM dissimilarity ;
- Age: LiDAR metrics – percentage of all returns above 3 m over total 1st returns, percentage of all returns above 3 m, H99, H95, H_mean; and RapidEye metrics – red ratio, NDVI, NIR ratio, RENDVI and EVI.

The relationship between predicted and observed MTH, BA, VOL and age using RF models is shown in Figure 5-7. RF models using LiDAR metrics generally estimated MTH, VOL and age well, with R^2 of 0.97, 0.83 and 0.70 respectively. However, the estimation of BA using LiDAR metrics appeared less accurate (R^2 = 0.66. RMSE of 10.42 $m^2 ha^{-1}$, $RMSE_{\%}$= 21%). Using RapidEye metrics performed poorly in estimating all forest stand variables, all obtained higher RMSE and lower R^2 than models using LiDAR metrics. Combining LiDAR and RapidEye metrics achieved only marginal improvement (R^2 increased by up to 1%) for estimating BA (RMSE= 10.33 $m^2 ha^{-1}$, $RMSE_{\%}$= 21%), VOL (RMSE = 94.79 $m^3 ha^{-1}$, $RMSE_{\%}$= 22%) and age (RMSE= 2.20, $RMSE_{\%}$= 11%) compared with using LiDAR metrics. On the other hand, using combined metrics produced slightly poorer estimation of MTH (RMSE= 1.45 m, $RMSE_{\%}$= 6%) than using LiDAR metrics alone.

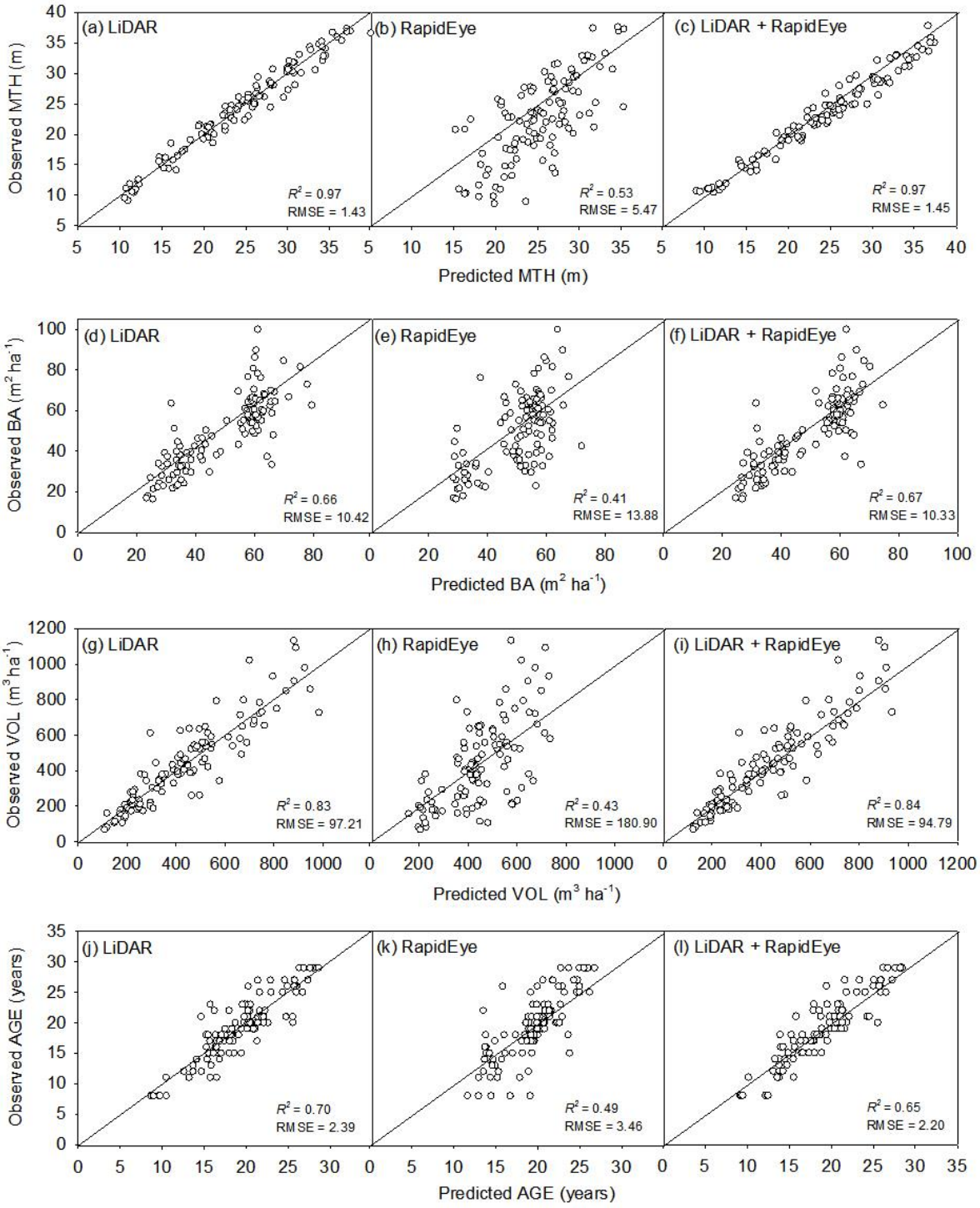

Figure 5-7: Relationship between observed and predicted MTH, BA, VOL and age using random forest models. The diagonal line shows the 1:1 line. R^2 shown are adjusted R^2.

5.8 Model Comparison based on cross validation

The performance of different modelling approaches was evaluated by comparing RMSE and mean deviation (MD) obtained from 10-fold cross validation. The RMSEs and MDs are expressed as percentage of predicted means for all models are shown in Figure 5-8 with additional details shown in Table 5-4. In terms of estimating forest stand variables using all four types of models, the prediction error of MTH was the smallest (mean RMSE% of 12.2%), followed by age (mean RMSE% of 17.3%) and BA (mean RMSE% of 24.4%) and then VOL (mean RMSE% of 30.3%). The RMSE percentage for all plots ranged from 5.4% to 26.2% for MTH, 18.5% to 30.7% for BA, 19.7% to 49.0% for VOL and 10.5% to 45.1% for age depending on the modelling approach. The MD percentage was also the highest for VOL estimation, followed by BA, age and MTH. This indicates that the prediction of MTH was the least biased (mean MD% of -0.1%), whereas VOL prediction was most biased (mean MD% of 2.21%). The mean MD% for age was -0.3% and for BA was 1.5%. The models tend to slightly overestimate MTH and age, and underestimate BA and VOL.

The cross-validation showed different results for different sensors. All cross-validated models using RapidEye metrics produced considerably higher RMSEs than LiDAR metrics and combined metrics, especially for MTH and VOL. The RMSE percentage using RE metrics was up to 20.3% higher than using LiDAR metrics for MTH prediction, up to 10.1% higher for BA prediction, up to 25.0% higher for VOL prediction and up to 22.8% for age estimation. Overall, there was hardly any difference in RMSE for models using LiDAR metrics or combined metrics irrespective of modelling approach. For MTH estimation, using LiDAR metrics alone produced a slightly lower RMSE than using combined metrics for all types of models. The combination of LiDAR and RapidEye metrics only reduced RMSE percentage by up to 1% for BA and VOL estimation compared with using LiDAR metrics for all models except SUR models. However, compared with using LiDAR only metrics, using combined metrics to estimate age reduced the RMSE for all four modelling approaches, especially for SUR, where the RMSE for age decreased by 1.2 years (5.8 %) compared with using LiDAR metrics alone. The MD of models using different metrics did not show a clear trend. Estimation using RapidEye metrics generally had higher bias than using LiDAR metrics, yet there was no clear difference in the MD% between estimation using LiDAR and combined metrics.

When comparing the performance of MLR, SUR, k-NN and Random Forest models using the cross-validation datasets, all the models performed similarly except SUR which produced noticeably higher RMSE for estimating BA, VOL and age. The RF model estimating MTH using LiDAR metrics produced the lowest RMSE (1.4 m) compared with all other models; MLR models using combined metrics produced the lowest RMSE for estimating BA (9.4 m^2 ha^{-1}) and estimating VOL (91.2 m^3 ha^{-1}); Both MLR and k-NN models using combined metrics produced the lowest RMSE for estimating age, at RMSE 2.06 and 2.05 years respectively.

There was no clear trend in the MD among different models but generally speaking MLR and RF models appeared to produce lower MD for all estimated variables. When estimating MTH, the lowest MD (0.003 m) was achieved using k-NN models with LiDAR metrics alone. RF models using RapidEye metrics resulted in the lowest MD for estimating BA (-0.2 m^2ha^{-1}) and also age (0.0005 years). Volume estimates with lowest MD (1.7 m^3 ha^{-1}) were achieved by MLR models using combined LiDAR and RapidEye metrics.

Based on the 10-fold cross-validation analysis, all models with LiDAR metrics alone produced satisfactory results. Conversely models using RapidEye metrics did not perform well. Using LiDAR metrics alone was the most useful in estimating MTH with all four different models, RapidEye metrics did not contribute to the estimation of MTH, they even reduced the model accuracy once combined with LiDAR metrics. For BA and VOL estimation, combined metrics achieved a marginally lower RMSE compared with using only LiDAR metrics with MLR and RF models. In contrast, RMSE was the lowest with LiDAR metrics alone and k-NN modelling or SUR modelling and did not improve for BA estimation. Age was the only variable that benefited slightly from combined metrics, where using combined metrics consistently resulted in lower RMSE for all four models.

Ultimately, on the basis of producing the lowest RMSE in the cross-validation analyses, the best model for predicting MTH is RF model with LiDAR metrics; the best model for predicting BA is MLR using combined metrics; the best model for predicting VOL is MLR using combined metrics; and the best model for predicting age is either MLR or k-NN with combined metrics.

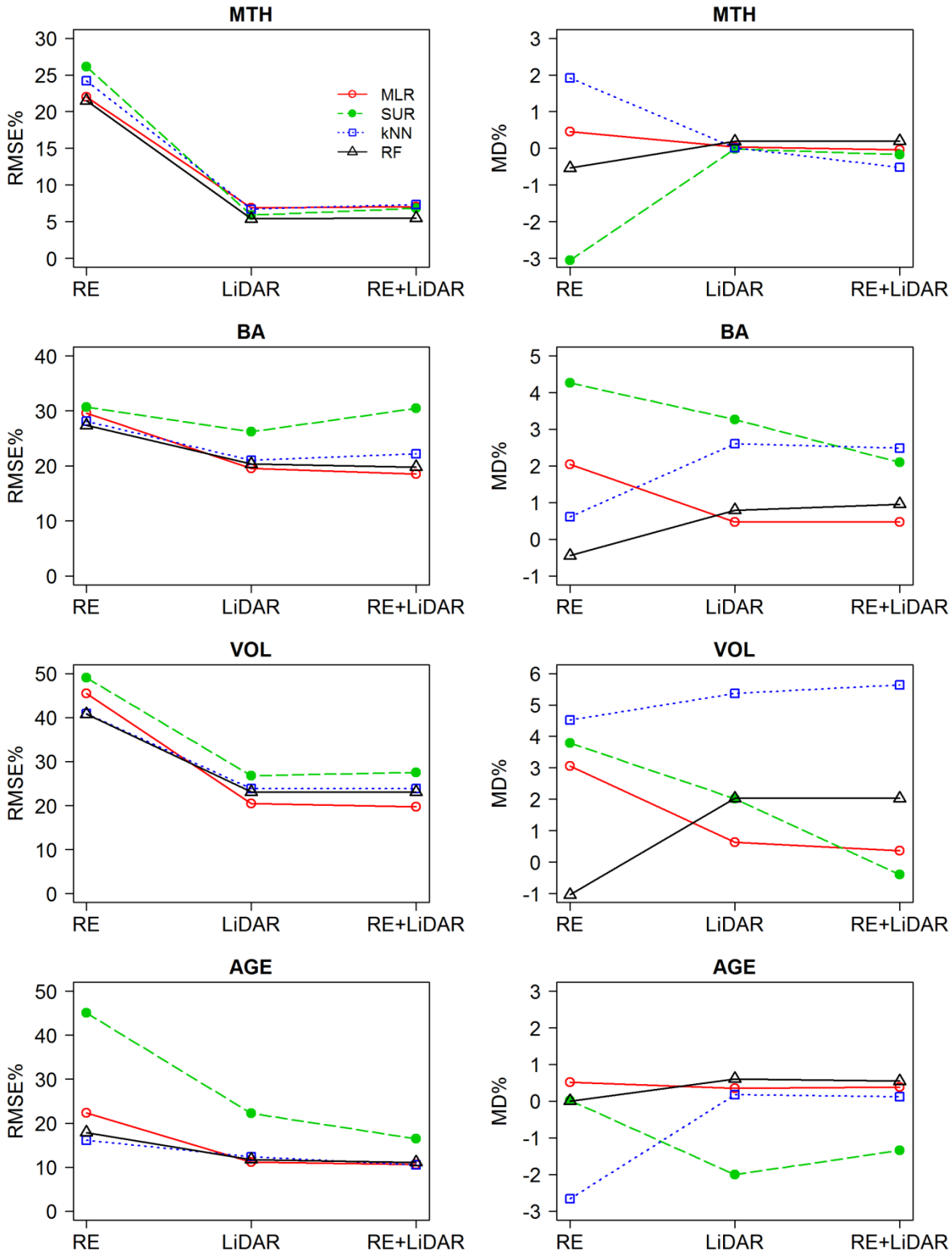

Figure 5-8: Comparison of Root Mean Square Error as a percentage of predicted mean (RMSE%) and Mean Deviation as a percentage of predicted mean (MD%) for MTH, BA, VOL and age estimated by MLR, SUR, k-NN and RF models.

Table 5-4: Summary of model prediction RMSE and Mean Deviation from 10-fold cross validation for estimating MTH, BA, VOL and age.

Model	Stand Variable	Input Data	RMSE	RMSE%	MD (bias)	MD%
MLR	MTH	LiDAR	1.81	6.90%	0.01	0.04%
		RE	5.76	22.01%	0.12	0.46%
		LiDAR+RE	1.86	7.08%	-0.01	-0.04%
	BA	LiDAR	9.92	19.54%	0.24	0.47%
		RE	14.81	29.61%	1.02	2.05%
		LiDAR+RE	9.42	18.54%	0.24	0.47%
	VOL	LiDAR	94.38	20.46%	2.95	0.64%
		RE	204.80	45.47%	13.77	3.06%
		LiDAR+RE	91.18	19.71%	1.67	0.36%
	AGE	LiDAR	2.17	11.17%	0.07	0.35%
		RE	4.33	22.31%	0.10	0.51%
		LiDAR+RE	2.06	10.61%	0.07	0.38%
SUR	MTH	LiDAR	1.49	5.92%	0.00	-0.02%
		RE	6.57	26.15%	-0.77	-3.05%
		LiDAR+RE	1.72	6.84%	-0.04	-0.17%
	BA	LiDAR	12.64	26.24%	1.57	3.27%
		RE	15.25	30.68%	2.12	4.26%
		LiDAR+RE	14.86	30.50%	1.02	2.10%
	VOL	LiDAR	114.88	26.79%	8.64	2.02%
		RE	214.10	49.03%	16.57	3.79%
		LiDAR+RE	120.30	27.55%	-1.70	-0.39%
	AGE	LiDAR	4.40	22.28%	-0.40	-2.00%
		RE	8.73	45.08%	0.00	0.02%
		LiDAR+RE	3.23	16.46%	-0.26	-1.34%
kNN	MTH	LiDAR	1.70	6.70%	0.00	0.01%
		RE	6.01	24.20%	0.48	1.92%
		LiDAR+RE	1.87	7.33%	-0.13	-0.52%
	BA	LiDAR	10.26	21.00%	1.27	2.60%
		RE	14.00	28.11%	0.31	0.61%
		LiDAR+RE	10.86	22.20%	1.21	2.48%
	VOL	LiDAR	100.56	23.86%	22.61	5.36%
		RE	173.66	40.87%	19.20	4.52%
		LiDAR+RE	100.24	23.85%	23.70	5.64%
	AGE	LiDAR	2.41	12.39%	0.03	0.18%
		RE	3.23	16.11%	-0.53	-2.66%
		LiDAR+RE	2.05	10.53%	0.02	0.12%
RF	MTH	LiDAR	1.37	5.40%	0.05	0.19%
		RE	5.46	21.50%	-0.14	-0.54%
		LiDAR+RE	1.39	5.50%	0.05	0.20%
	BA	LiDAR	10.11	20.36%	0.39	0.79%
		RE	13.81	27.39%	-0.22	-0.44%
		LiDAR+RE	9.82	19.80%	0.48	0.96%
	VOL	LiDAR	100.65	23.10%	8.82	2.03%
		RE	182.24	40.80%	-4.61	-1.03%
		LiDAR+RE	100.50	23.07%	8.85	2.03%
	AGE	LiDAR	2.28	11.75%	0.12	0.61%
		RE	3.49	17.87%	0.00	0.00%
		LiDAR+RE	2.15	11.09%	0.11	0.55%

The model prediction errors and bias from all datasets and cross-validation datasets are summarised in Table 5-5. The summary only included the models with the most useful metrics that produced the lowest RMSE. The comparison shows the difference in RMSE and $RMSE_{\%}$ from both calibration and cross-validation datasets for each model. This summary indicates the applicability of each model. Ideally there should be a small difference in the model performance when the model is applied to different datasets, yet a large difference indicates that the model may have limited general applicability. Random Forest models were the least accurate models for the calibration data, but there was hardly any difference compared to the RMSEs produced from validation dataset. The RMSEs were even lower for cross-validation datasets for estimation of all variables except VOL. Additionally, the differences between RMSE for calibration and cross-validation data for MLR models were also very small (2% for MTH, 1% for BA, VOL and age), which suggests MLR and RF models developed using this dataset can be applied more broadly with similar performance expected.

One the other hand, k-NN and SUR models applied to cross-validation datasets produced much higher RMSEs than those using the calibration data. The RMSE percentage of cross-validated MTH, BA, VOL and age prediction increased by 2%, 7%, 12% and 8% respectively for k-NN models, and increased by 1%, 7%, 8% and 5% respectively for SUR models. This suggests that k-NN and SUR models can estimate forest variables accurately for the existing data collected, yet they cannot perform equally well for predicting "new" datasets. This is supported by the fact the RMSEs were the lowest among all models when estimating variables with the calibration dataset, but were the highest for the cross-validation dataset. It can be inferred that k-NN and SUR models may not be suitable for estimating forest stand variables over different datasets.

Table 5-5: Comparison of RMSEs and RMSE expressed as a percentage of mean (shown in brackets) of the best models for estimating MTH, BA and VOL from fitting all plot data and 10-fold cross-validation analysis.

Model	Stand Variable	All Data	10-fold Cross Validation
MLR	MTH	1.31 (0.05)	1.81 (0.07)
	BA	8.95 (0.18)	9.42 (0.19)
	VOL	80.81 (0.19)	91.18 (0.20)
	AGE	1.94 (0.10)	2.06 (0.11)
SUR	MTH	1.21 (0.05)	1.49 (0.06)
	BA	9.20 (0.19)	12.64 (0.26)
	VOL	83.77 (0.19)	114.88 (0.27)
	AGE	2.09 (0.11)	3.23 (0.16)
kNN	MTH	1.31 (0.05)	1.70 (0.07)
	BA	7.33 (0.15)	10.26 (0.21)
	VOL	51.18 (0.12)	100.24 (0.24)
	AGE	0.54 (0.03)	2.05 (0.11)
RF	MTH	1.43 (0.06)	1.37 (0.06)
	BA	10.33 (0.21)	9.82 (0.20)
	VOL	94.79 (0.22)	100.50 (0.23)
	AGE	2.20 (0.11)	2.15 (0.11)

5.9 Discussion

One of the objectives of this study was to compare the influence of using LiDAR metrics, RapidEye metrics and combined LiDAR and RapidEye metrics in estimating mean top height, basal area, volume and stand age of radiata pine plantations. It was found that LiDAR metrics alone were very useful in predicting forest stand variables, whereas combined LiDAR and RapidEye metrics led to marginal improvement in estimating forest stand variables. Over the last two decades, the effectiveness of LiDAR metrics in predicting forest structural variables has been supported by many studies and the technique has been widely accepted in the forestry industry (Carson et al., 2004; Lefsky et al., 2002; Pirotti et al., 2012; van Leeuwen & Nieuwenhuis, 2010). In this study, RapidEye was found to be much less accurate in estimating forest stand variables than LiDAR, producing RMSE increases between 10 and 25%. Similar studies on plantation forests also revealed that RapidEye metrics were not well suited to estimating forest stand variables (Dash et al., 2016; Wallner et al., 2014). It was found that image saturation after canopy closure limits the utility of optical data for estimating stand variables especially for productive plantation forests, where the spectral and textural differences become less apparent (Tomppo et al., 1999).

Combining LiDAR metrics with satellite-derived metrics has also been widely used due to improvements found in forest variable estimation compared to using LiDAR alone (Estornell et al., 2012; St-Onge et al., 2008; Tonolli et al., 2011; Xu et al., 2015). Generally, combined sensors have improved height estimation by 1-7% and volume estimation by 2 to 29% compared to using LiDAR metrics alone. However, these studies were generally for mixed species forests or natural forests, where LiDAR metrics may not be sufficient to capture the full structural characteristics of heterogeneous mixed-species forests. Therefore, additional spectral or textural information collected from optical sensors may provide more dimensions for estimating forest stand variables. Studies in forests similar to those in our study found negligible improvement in combining LiDAR and RapidEye metrics in estimating forest structural variables and productivity (Watt et al., 2015; Watt et al., 2016).Given the additional costs of RapidEye, it is not recommended to acquire optical data to predict forest stand variables in managed plantation forests.

This study also compared the performance of four modelling approaches: parametric multiple linear regression and seemingly unrelated regression, and non-parametric k-Nearest Neighbour and Random Forest models. Based on cross-validation results of these models, there was not much difference in the prediction results for MTH, BA, VOL and age among all four models. There was no single model that achieved the highest accuracy for estimating all four stand variables. According to the RMSE and MD comparison from cross-validation on all four stand variables, MLR was the most accurate parametric model and RF was the most accurate non-parametric model. SUR and k-NN worked well for the calibration dataset, but did not perform very well for the cross-validation dataset, limiting their

general applicability. The RF model was found to be the least biased model, followed by MLR. The most biased model was the k-NN model. The k-NN model picked the one nearest neighbour for estimating stand age using only RapidEye metrics and also combined metrics, but despite this, obtained extremely accurate estimation. This is because the target plot and its nearest neighbour generally belong to the same forest stand; hence the target is likely to be estimated as the same forest age. This can limit the application of the k-NN model as the forest stand age of neighbouring plots may not be always known. Based on the lowest RMSE values, the RF model was the most accurate model for predicting MTH, while MLR was the most accurate model for predicting BA, VOL and age.

The cross-validated results were compared with results from calibration data, and the RF approach was found the most consistent model given that the RMSE hardly changed when predicting stand variables for different datasets. This is likely because the nature of random forest algorithm bootstraps randomly and iteratively sampled data and variables to form a group of decision trees (Breiman, 2001). Only a subset of predicting variables are used to find the best split at each tree node (Brosofske et al., 2014). In a way, the RF algorithm does many "cross-validations" during model development, even when using all the data as calibration data. The MLR model also yielded favourable cross-validation results.

On the other hand, the k-NN model was found to be least consistent due to large difference in RMSE between calibration data and cross-validation data. The value k plays an important role in k-NN model performance. The k-NN models with calibration data were more likely to select the closest neighbours as the optimal k values in the modelling process, and the optimal k values for estimating forest stand variables ranged from 1 to 6, whereas the optimal k values ranged from 3 to 17 for cross validation models. This indicates that k-NN models tend to model forest variables based on the closest neighbours for calibration data and hence produce results with small RMSE. When k-NN models are applied to other datasets during cross-validation, the model required more neighbours to estimate stand variables, as previously selected neighbours were insufficient to characterise new datasets. The inconsistent performance of k-NN models suggest the over-fit of k-NN models for the calibration data, which consequently limits the applicability of k-NN models in estimating forest stand variables.

Unlike other studies where non-parametric models tend to outperform parametric models, this study did not find the superiority of non-parametric models. It is critical for k-NN models to collect ground samples that cover the full range of conditions for the response variable as k-NN cannot be used to predict beyond the range of the reference dataset (Chirici et al., 2016; McRoberts et al., 2015). Similarly, the performance of RF regression is limited by the range of response variables. According to Horning (2010), because of the way the regression trees are constructed, RF cannot predict beyond the range of the response variables in the samples selected. Due to the limited field data from small-scale forests that could be obtained in the region, the field data collected were not likely to cover the

full range of conditions of plantation forests in the region. Therefore, this could be the key factor non-parametric models did not perform as expected.

Parametric multiple linear regression performed very well overall, giving relatively low prediction error for both calibration and validation data. There have not been many studies that compare MLR and SUR performance. One study by Næsset et al. (2005) found only minor discrepancy between MLR and SUR estimated tree height, BA and volume. This study also found marginal difference between the performance of MLR and SUR using calibration data. However, SUR produced higher errors for BA, VOL and age prediction for cross-validation datasets. This suggests that the SUR model was outcompeted by MLR models in this study. Even though there was no single modelling solution for estimating all variables, MLR models appeared to produce most reliable and consistent results for estimating all four stand variables.

5.10 Conclusion

This study compared the performance of two parametric models (multiple linear regression and Seemingly Unrelated regression) and two non-parametric models (k-Nearest Neighbour and Random Forest) models in estimating forest stand variables MTH, BA and VOL with different combinations of remote sensing datasets. LiDAR-derived metrics were found to be more useful in estimating forest stand variables than RapidEye metrics; combining LiDAR metrics with RapidEye metrics did not provide large gains in variable prediction. Non-parametric models and parametric models performed similarly, likely due to the narrow range of structural characteristics in the collected field data. Overall, multiple linear regression was deemed to be the best option for estimating forest variables for less well known forests as the approach has provided sound and consistent estimation of stand variables and it is relatively easy to understand and interpret.

Chapter 6 - Obtaining forest description for Wairarapa region using LiDAR and RapidEye

6.1 Introduction

Previously the optimal approach for deriving plantation area and stand variables was investigated by evaluating a number of combinations of mapping and modelling approaches and remote sensing datasets. The optimal approach for mapping net stocked plantation area was using Classification and Regression Tree (CART) with both RapidEye and LiDAR-derived surfaces. Meanwhile multiple linear regression with LiDAR-derived metrics was the best for deriving stand variables. This chapter aims to apply these approaches to the whole Wairarapa region, in order to estimate the stocked plantation area and forest stand variables – mean top height (MTH), basal area (BA), volume (VOL) and stand age. The area mapped will be compared with records from existing National Exotic Forest Description (NEFD) and Land cover database (LCDB). The yield information derived will be benchmarked against the yield tables developed for the Wood Availability Forecast (WAF) report for Southern North Island. The latest WAF report was prepared by Indufor Asia Pacific for the Ministry of Primary Industries (MPI) for the period from 2014 to 2050 (MPI, 2016b), and forecasts the regional wood supply for nine regions and for New Zealand and serves as a planning tool for the forest industry, government and infrastructure and service providers.

6.2 Methodology

6.2.1 Plantation area

The optimal approach selected from Chapter 4 was using object-based CART classification approach with combined RapidEye and LiDAR derived layers. The derivation of plantation areas followed the same approach described in Chapter 4 but was applied to a larger extent. In total 21 RapidEye images each covering a 25 by 25 km extent were acquired to cover the Wairarapa region, four of the scenes did not cover any plantation areas hence only 17 images were used to map net stocked plantation areas in Wairarapa region. Plantation mapping was done on a scene-by-scene basis. In Chapter 4 the finest scale factor used to capture small-scale forests was 100; hence the same setting was used in the image segmentation process in order to capture small polygons. Additional training sample points representing each land cover class were purposely selected to cover the wide range of land covers in the Wairarapa region. There was no prerequisite for the number of training samples prior to selection, the training samples were selected objectively based on their representativeness for each land cover class, with a focus mainly on the plantation class. The selection covering all images ended with 1612

training sample points including 432 for plantations selected as representative training samples for automated classification.

Automated CART classification was applied to all RapidEye images in eCognition (Trimble, 2013). Further classification refinements which involved building a decision tree that adjusted the thresholds of object features of misclassified plantation polygons were applied scene-by-scene to cater for any spectral inconsistency. Generally, the refinements were similar among the 17 scenes, though the thresholds used in the classification were not identical across all scenes. The main focus was to extract plantation areas; hence the refinements were mainly applied to planted areas to make sure plantation areas were adequately mapped. The details of operator refinements were described in Chapter 4 - section 4.3.1. Rededge ration (REratio), Rededge and Green Normalised Difference Vegetation Index (REGNDVI), and canopy height model (CHM) were the key metrics used to further differentiate plantation from other land cover classes in the manual refinement process.

The plantation areas mapped in individual scenes were aggregated into a single layer. All isolated plantation patches that were less than 0.1 ha were removed according to the mapping standard set previously. Furthermore, due to limited capability of capturing young plantations using the mapping approach with 5 m resolution RapidEye imagery, young plantings were further manually digitised using both aerial photography and RapidEye imagery. The plantation areas extracted by the mapping approach together with digitised young plantations were compared with NEFD and LCDB plantation areas. The NEFD used for comparison was the 2014 data (MPI, 2014), which is within the same timeframe as the remote sensing data acquisition. LCDB was the latest version 4.1 retrieved from Landcare research (Landcare Research, 2016), and the satellite imagery used was acquired in summer 2012 and 2013. All plantation areas refer to the net stocked forests, and exclude areas that have been harvested or are awaiting replanting.

6.2.2 Plantation stand variables

Results from Chapter 5 suggested a multiple linear regression model with only LiDAR metrics was the optimal approach for estimating forest stand variables MTH, BA, VOL and age. Table 6-1 lists the multiple linear models with parameters used for extracting forest stand variables. The LiDAR metrics were derived in raster format for all of the Wairarapa region, using "GridMetrics" function with LTK processor in Fusion (McGaughey, 2016a). LTK processor is designed to process large area LiDAR acquisition and extract seamless LiDAR metric surfaces. All the metric surfaces were derived as five metre resolution grids. After all the LiDAR surfaces were derived, the layers used to model forest stand variables were loaded in ArcMap (ESRI, 2017) and "raster calculator" was used to calculate the stand variables based on the model parameters listed in Table 6-1.

Table 6-1: Multiple linear models selected for estimating forest stand variables

Stand Variable	Multiple linear regression model
MTH	MTH = 3.269 + 1.043 * H90
BA	BA = -29.842 - 2.500 * 4th_return_above_0.5 + 0.036 * qav + 0.600 * I99 + 0.701 * %1st_return_above_3
VOL	VOL = -214.787 - 21.758 * 4th_return_above_0.5 + 0.995 * qav + 264.325 * I_L4 + 3.278 * (all_return_above_3) / (total_1st_returns) * 100
Age	Age = -0.425 - 4.724 * I_skewness +0.643 * I10 + 0.751 * H95

The stand variables were calculated for each five metre cell within the output raster. Because the stand variables were modelled based on the plot data collected and only reflect the range of plot data, there are likely to be extreme values in the estimated stand variable raster where the input data are beyond the plot data range. There were some pixels with negative values in the stand variable raster derived, which could affect the stand variables derived within each plantation polygon. Therefore, all pixels with negative values were replaced by the mean value of their surrounding five by five pixel neighbourhood. Then, using the "zonal statistics" function in ArcMap, a mean MTH, BA, VOL and age was obtained for each mapped plantation polygon. It was assumed that the stand characteristics were the same within each individual polygon.

The estimated MTH, BA and VOL variables were plotted against estimated stand age to investigate the relationship between stand age and the three structural variables. The coefficient of determination (r^2) was used to describe the fit of the relationship.

The recoverable volume is the standing volume less the waste generated by cutting logs. On average, the recoverable volume is 85% of the total standing volume for radiata pine (Maclaren, 2000). Therefore, a 15% waste factor was applied to the standing volume to calculate the recoverable volume.

The correlation between age and the modelled recoverable volume was used to develop a yield table which was then contrasted against the latest post-1989 WAF yield tables for Southern North Island-East. Since this study does not separate silvicultural regimes, the WAF yield tables which were provided as pruned and unpruned tables were averaged by weighting the pruned and unpruned areas in the Southern North Island-East. Furthermore, the volume of each polygon was calculated by the Beekhuis equation (Beekhuis, 1966) based on modelled BA and MTH in order to compare with modelled VOL:

$$VOL = BA *(0.9 +0.3*MTH) \quad (7)$$

6.3 Results and Discussion

6.3.1 Plantation area

In total 4379 individual polygons were mapped by the mapping approach developed, and another 134 polygons were manually detected and digitised as young plantation (Table 6-2). Overall the plantation area extracted for Wairarapa region was 50 124 ha, including 47 168 ha of automatically mapped and 2 956 ha of young plantations that were manually digitised. The young plantation area missed by the mapping approach was 5.9% of all the plantation area reported. The mean area for individual plantation patches was 11.45 ha.

For mapped plantations, over 90% of polygons were less than 10 ha, which accounts for 12.6% of the area of mapped plantations. In Chapter 4 it was found that the mapping approach was less accurate for forest patches that are less than 10 ha, so it is possible that the small forest plantation patches mapped here were mapped less accurately than the larger patches. Although there were fewer polygons for patches exceeding 100 ha, the area of larger forest patches accounted for 77% of the area of all plantations mapped.

Table 6-2: Plantation area summary by patch size

Patch size class	Digitised young plantation		Mapped plantation	
	Area (ha)	No. of polygons	Area (ha)	No. of polygons
< 10 ha	288	82	5 931	4 013
10 - 39 ha	666	36	4 829	261
40 - 99 ha	567	9	2 701	45
100 - 499 ha	888	6	10 301	44
500 - 999 ha	548	1	6 619	9
> 1000 ha	0	0	16 787	7
Total	**2 956**	**134**	**47 168**	**4 379**

The total mapped plantation area comprised 1747 fewer hectares (3.4%) than the NEFD reported plantation area for Wairarapa region and 5914 fewer hectares (11.4%) than the plantation area reported in the LCDB (Table 6-3). When breaking down the plantation area by territorial authorities, Masterton district had the largest plantation area, followed by Carterton and South Wairarapa. This is also consistent with NEFD and LCDB plantation area. The plantation area derived in this study was generally lower than both NEFD and LCDB, except in Masterton where the mapped plantation exceeded the NEFD area by 943 ha. Furthermore, the mapped plantation area using the automated approach found 4703 (9.1%) fewer hectares than the NEFD reported plantation area for Wairarapa region and 8871 (15.8%) fewer hectares than the plantation area reported in the LCDB.

Table 6-3: Summary and comparison of plantation areas: Mapped plantation area was estimated from the automated mapping approach, young plantation area was manually identified and digitised, adding them together form the total plantation area.

Wairarapa	Mapped plantation (ha)	Digitised young plantation (ha)	Total plantation (ha)	NEFD plantation (ha)	LCDB plantation (ha)
Carterton district	8 743	917	9 660	10 532	10 742
Masterton district	31 942	1 798	33 740	32 797	37 659
South Wairarapa district	6 483	241	6 723	8 542	7 637
Total	**47 168**	**2 956**	**50 124**	**51 871**	**56 038**

Overall the mapping approach proves to be applicable for a wider extent in delineating forest plantation at different patch scales. This approach captured less plantation area compared with both the NEFD and LCDB record, yet the results from Chapter 4 indicated the approach developed overestimated the plantation area by 3% compared with the manually digitised area. However, it is important to recognise that the NEFD area for the small-scale forests may not be accurate as the area of over half of the small-scale forests was not from surveys of individual owners but was imputed based on the number of seedlings sold to nurseries (MPI, 2014). Currently there is no measurement of error in the NEFD area information; hence the area summary stated may not be accurate especially for small-scale forests. Furthermore, currently there is no spatial representation of NEFD plantation area, making it impossible to infer other reasons for the differences between the mapped plantation area and the NEFD. LCDB plantation area was 11% higher than the mapped plantation mainly because LCDB used 10 m SPOT and 30 m Landsat imagery, which tends to overestimate the forest area by delineating coarser boundaries of small-scale forest patches and missing out internal gaps within forest patches. Unfortunately, so far there is no record of the accuracy measurement for the latest LCDB v4.1. The utility of LCDB-derived plantation area in commercial forest management and reporting is currently limited due to its coarser resolution.

A recent case study using manual digitisation to derive plantation areas based on aerial photography was carried out by the fourth-year students at the New Zealand School of Forestry, University of

Canterbury (Fourth Year Students, 2017). The preliminary results indicated there were 8 670 ha, 35 547 ha and 5 620 ha of plantations for Carterton, Masterton and South Wairarapa respectively. In spite of the variations in the plantation areas derived in this study and the case study within individual districts, the total plantation area for Wairarapa region derived from this study was only 287 (0.6%) ha more than the case study-derived area.this finding has further confirmed the applicability of using remote sensing technique to derive plantation areas which can produce comparable results to manually digitised plantation areas using high resolution aerial photography, yet takes less time.

One limitation with this approach is that it is unable to detect young plantings due to the resolution of remote sensing datasets; hence manual digitisation is required to map the young plantations. Although the young plantations require manual detection and digitisation using the approach developed in this research, the young plantations mapped was just 5.9% of total plantations mapped, which means that 94% of the plantation areas can be derived automatically. The automated mapping process of young trees could be further explored in a future study, such as finding higher resolution remote sensing sources or metrics that could differentiate young trees from other land cover types. For example, a study carried by Zhou et al. (2013) used 0.5 m resolution Worldview images and successfully mapped the density of young eucalyptus plantations at 6, 9 and 13 months.

6.3.2 Plantation stand variables

For each of the mapped geographically isolated polygons, a mean MTH, BA, VOL and stand age was extracted. Table 6-4 summarises the modelled MTH, BA, VOL and stand age for all plantation polygons mapped in the Wairarapa region.

Table 6-4: Summary of modelled stand variables for each mapped plantation polygon in the Wairarapa region.

Stand Variable	Minimum	Maximum	Mean	Standard deviation
MTH (m)	3.86	43.63	21.51	6.85
BA ($m^2 ha^{-1}$)	1.41	89.68	49.51	12.56
VOL ($m^3 ha^{-1}$)	6.09	1175.51	358.03	158.57
Age (years)	5.55	33.33	19.56	4.51

The relationships between modelled age and other stand variables MTH, BA and VOL are presented in Figure 6-1, Figure 6-2 and Figure 6-3 respectively. A linear correlation was observed for age with both MTH and BA. MTH and age were closely correlated, a positive linear relationship was observed with r^2 =0.63. However, stand age and basal area appeared to be less closely correlated, with a weaker positive correlation (r^2 = 0.42). Additionally, a quadratic relationship was derived between stand age and volume, giving an r^2 of 0.57. The modelled volume was compared with the calculated Beekhuis volume (Figure 6-4). Overall the two sets of volumes were similar, the modelled volume ranged from

6 to 1176 m^3 ha^{-1} and the calculated volume ranged from 3 to 1207 m^3 ha-1. The mean modelled volume was 28 m^3 ha^{-1} less than the calculated volume.

Using the multiple linear regression approach developed with LiDAR metrics proved successful in estimating forest stand variables for the whole Wairarapa region as these modelled values were all in a realistic range. The mean top height, basal area, volume and age can be estimated for every single plantation in Wairarapa using remote sensing data. However, a single average value for stand variable per plantation polygon may not be realistic especially for large-scale plantations where multiple stands with different silvicultural regimes and age classes could exist in a single mapped plantation polygon. Although delineating forest stands within each plantation polygon is out of scope for this study, it is believed that the derivation of stand variables could be further improved with finer delineation of forest stand boundaries. Haywood and Stone (2009) have proved that it is possible to delineate forest stands using a combination of LiDAR and aerial photography. For future studies, the spatial representation of stand boundaries could be acquired from large-scale forest owners so that an average stand variable could be extracted for each stand. It may not be as critical for small-scale forests especially for under 100 ha plantations, as the owners generally plant the forests under the same silvicultural regime at the same age.

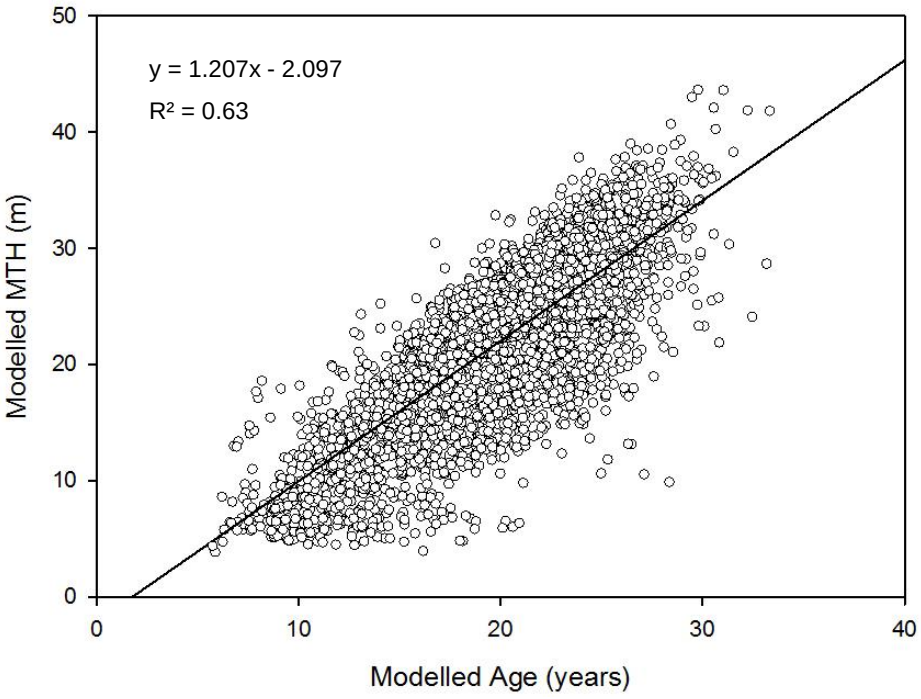

Figure 6-1: Modelled mean top height against modelled age for all plantations in the Wairarapa region. The line shown is the line of the best fit.

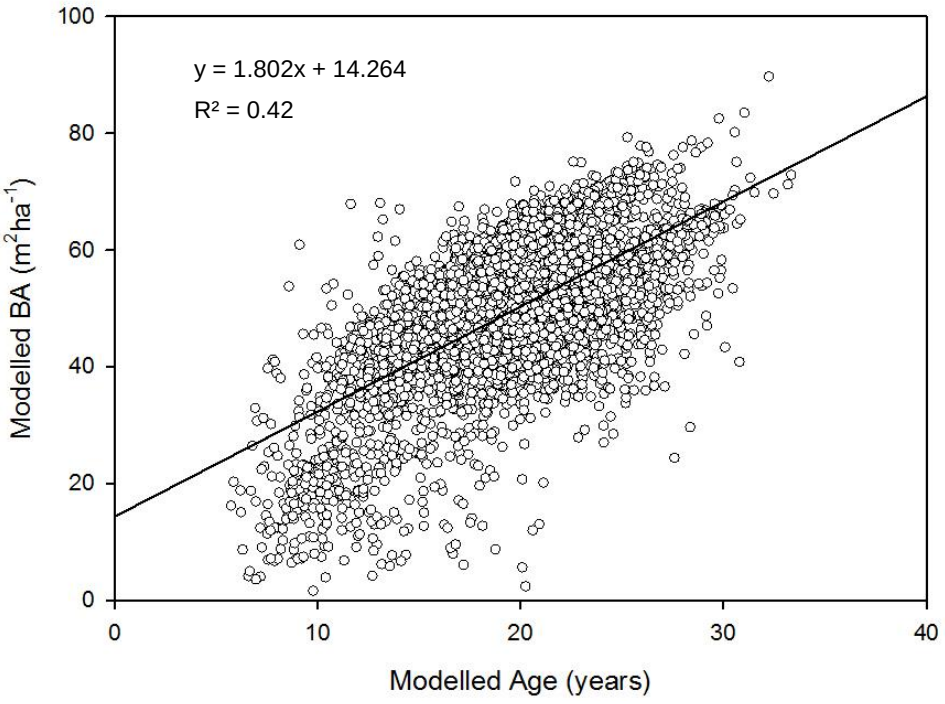

Figure 6-2: Modelled basal area against modelled age for all plantations in the Wairarapa region. The line shown is the line of the best fit.

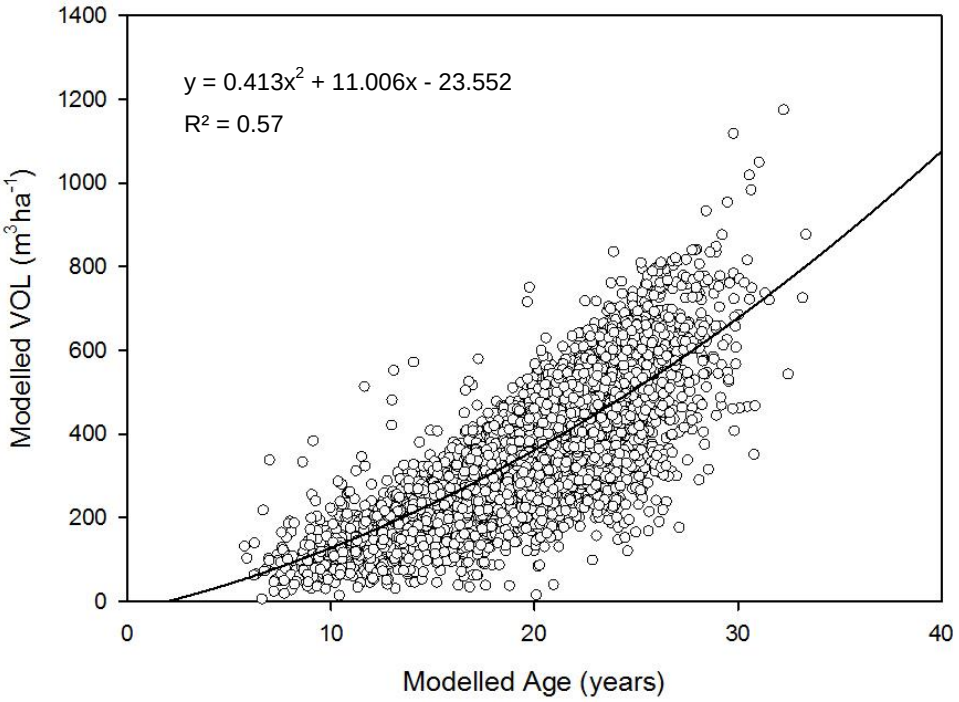

Figure 6-3: Modelled standing volume against modelled age for all plantations in the Wairarapa region. The line shown is the line of the best fit.

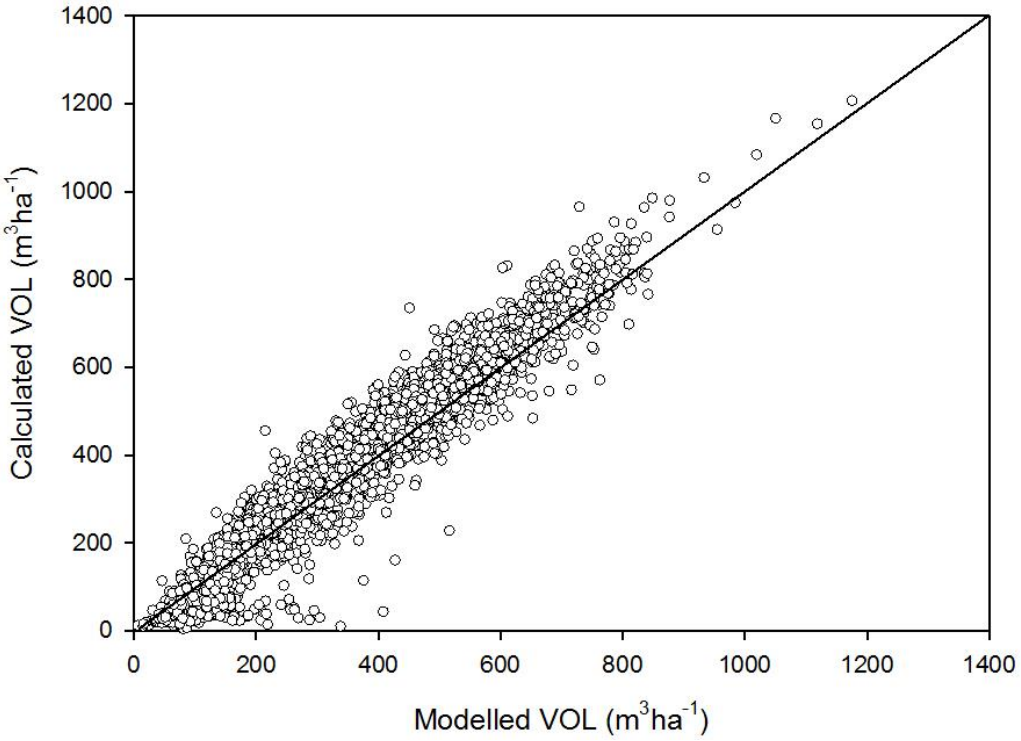

Figure 6-4: Modelled volume and calculated volume based on Beekhuis equation using modelled MTH and BA. The diagonal line shows the 1:1 line.

The relationship between the recoverable volume and age was compared with the WAF yield table (Figure 6-5). For simplicity, only the post-1989 yield tables from WAF were used for comparison as most of the plot data collected were from post-1989 forests. There were two sets of yield tables derived: one was the "modelled VOL" derived based on the quadratic model shown in Figure 6-3, the other one was calculated as the average yield for each stand age. Both sets of yields derived in this study were very similar, with a mean difference of 1 m^3 ha^{-1}. The yield table derived in this study was not split into pruned and unpruned regimes due to limited information collected. The derived yield table was compared with the area-weighted total recoverable volume against age from the WAF yield. Overall, the modelled yield table produced consistently higher yield than the unpruned WAF yield from age 11 to 16, giving on average 21 m^3 ha^{-1} higher yields than the WAF yield table; After age 16, the modelled yield was lower than the WAF yield right through to age 30, with an average of 40 m^3 ha^{-1} lower volume. Overall the mean difference between the modelled yield and WAF yield was 25 m^3 ha^{-1}, which suggests that the modelled yield was lower than the WAF yield.

The yield tables used in the wood availability forecast report were based on yield tables provided by several large-scale forest owners in the region, which were then averaged on an area-weighted basis to derive the regional yield tables for different regimes. The area-weighted average regional yield tables developed for the large-scale forests were also applied to the small-scale forests in the WAF report for

Southern North Island (MPI, 2016c). It was assumed that the yield tables from large-scale owners who undertake regular yield assessment and well-designed silvicultural operations in their estate were the same as the small-scale owners whose forests may not have the optimal management practices implemented in reality. The yield table derived based on plot data collected mainly from the small-scale forests and corresponding LiDAR metrics produced lower yield than the WAF yield, which could potentially be a result of different yields between large and small-scale forests.

Overall, the yield table developed from remote sensing data generally agrees with the WAF yield table, which further indicates the utility of this approach in extracting forest yield information for Wairarapa. It provides a means for estimating area and yield information for previously less well understood small-scale plantations. With the availability of area and yield information, the potential future wood flow coming from this region could be estimated using a forest estate modelling system.

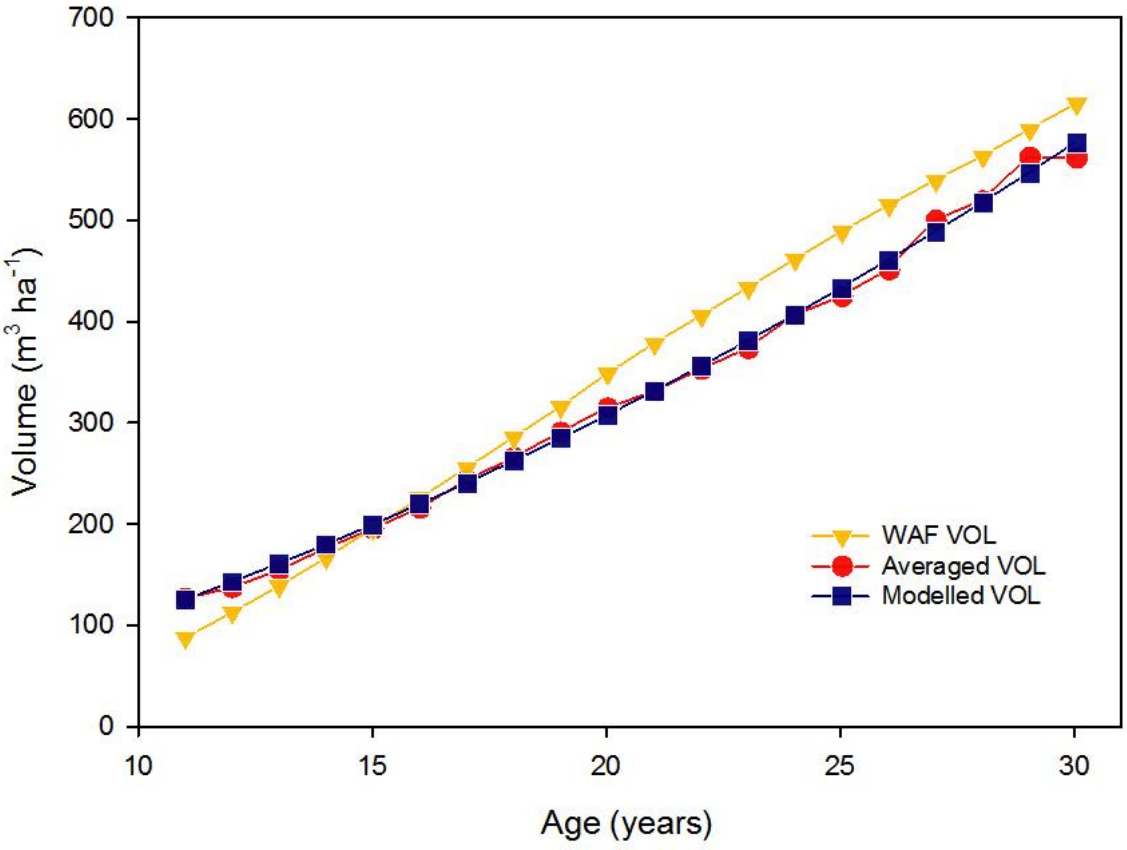

Figure 6-5: Comparison of modelled yield tables with WAF yield tables.

With the availability of mapped plantation area and modelled age for the whole Wairarapa region, the area by age class could be derived and compared with the NEFD area description. The comparison of area by age class is shown in Figure 6-6. Overall the area distribution by age class from modelled data showed a similar pattern as the NEFD information. However, the range of ages estimated in this study

was much narrower than the NEFD data. The NEFD recorded forest stand ages ranging from age 1-50, whereas modelled age ranged from age 6- 33. Therefore, the area distribution from modelled data were mainly concentrated between age 16 and 25. This is likely due to the limited field data collected which did not cover a wide range of plantation ages. Future research could acquire spatial stand age information from large-scale plantation owners from the same region. This would cover a wider range of stand ages, and use the known age and corresponding metrics derived from remote sensing data as training samples for modelling a wider range of stand ages.

Alternatively, different modelling approaches for estimating stand age could be further investigated to see if the estimation could extend to a wider range. An initial attempt was made by excluding the int.skewness predictor from the linear model described in Table 6-1 and the estimated age ranged from 2-39 years, which extended the age estimation.

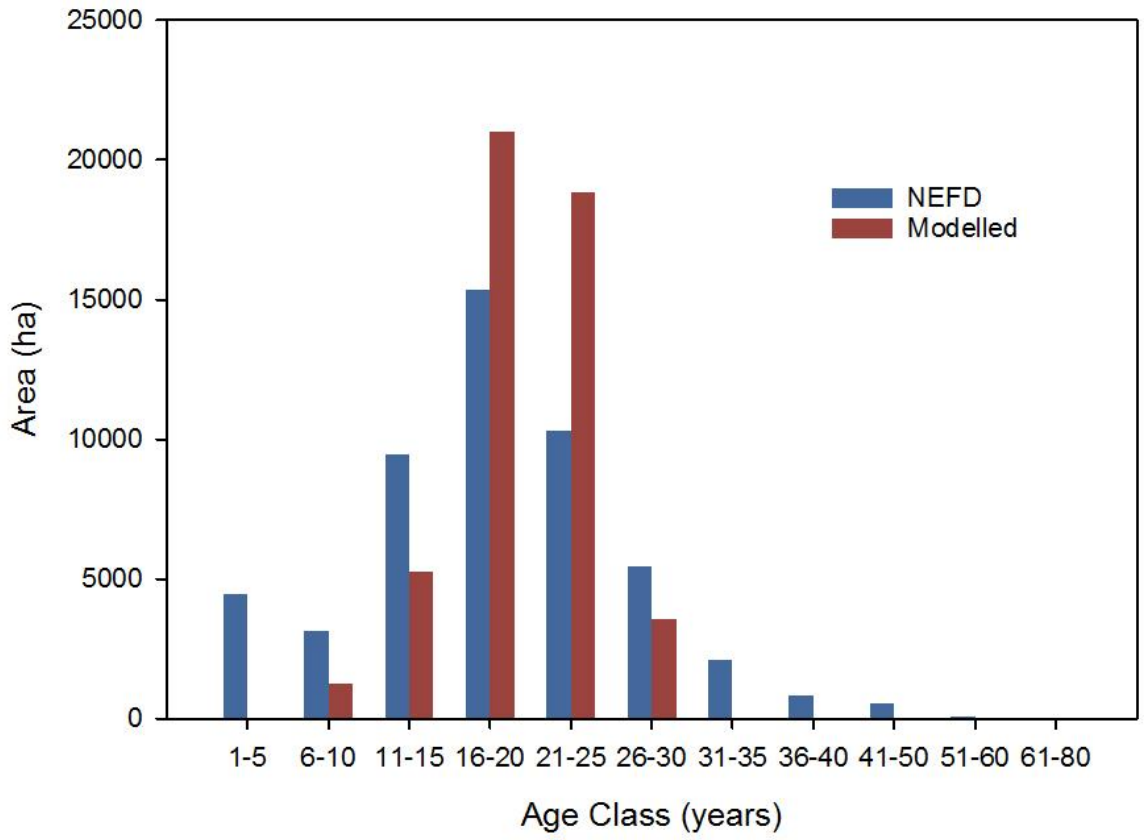

Figure 6-6: Area by age class derived from modelled age and mapped plantation for Wairarapa, compared with NEFD area by age class.

6.4 Conclusion

The optimal mapping and modelling approach using remote sensing datasets was applied to the Wairarapa region to investigate the implications of the designed approach. The automated mapped plantation area derived from combined RapidEye and LiDAR surfaces using Classification and Regression Tree was 9.1% less than the NEFD plantation area. Together with manually digitised young plantations, the overall plantation area derived was 3.4% lower than the NEFD area. There is no assurance of accuracy in current NEFD data especially for the small-scale forests. In a recent manual digitisation exercise by the University of Canterbury, the plantation area digitised was almost the same as the area derived in this study. This suggests the approach developed here can produce comparable results as manually digitised plantation area, and further confirms the applicability of this approach. However, one limitation with this approach is that it is unable to detect young plantings due to the resolution of remote sensing datasets; hence manual digitisation is required to map the young plantations. The automated mapping process of young trees could be further explored in a future study, such as finding higher resolution image sources or metrics that could differentiate young trees from other land cover types.

Forest stand variables mean top height, basal area, volume and age were modelled for the region using multiple linear regression with LiDAR-derived metrics. Based on the modelled stand variables, recoverable volume at different ages (yield) could be generated. The yield tables developed using modelled information were all within a realistic range and were similar to NEFD yield tables. This implies that the approach could describe forest yield information. However, in this study the approach fails to predict any plantations that were younger than five years or older than 33 years. The estimation of plantation age could be further improved by including plot data with a wider range of stand age or investigating different models for age.

Overall, the mapping and modelling approaches developed in this study provide a proof of concept for estimating plantation area and stand variables using remotely sensed data in the Wairarapa region, and they are especially important for small-scale forests where the forest area and stand variables are poorly understood. However, the approach could be further improved by incorporating a wider range of field validation data to better capture different ranges of silvicultural regimes, plantation species and age classes. With the area and yield information derived, the potential wood flow coming from the region including small-scale forests could be estimated.

Chapter 7 - Thesis Conclusion

7.1 Summary of main findings

The total forest plantation area in New Zealand is approximately 1.70 million ha, 70% of which are owned by large-scale owners with over 1000 ha. These forests are under regular monitoring and assessment. On the other hand, the other 30% of plantations are small-scale and generally less likely to have regular area and yield assessment (MPI, 2014). Therefore, the knowledge of these small-scale forests, especially those under 100 ha remains very limited. Conducting a comprehensive survey and field assessment of these patchy forests is impractical. Additionally, these small-scale forests, which were mostly planted as post-1989 forests, will play an important role in providing the wood supply in the next couple of decades. By 2020, the small-scale forests will have the capacity to provide around 15 million m^3 of radiata pine logs per annum, which will be over 40% of the total radiata pine supply (MPI, 2016b). Therefore, it is critical to better understand these small-scale forests in order to plan effectively for the marketing, harvesting, logistics and transport capacity that will be required for this additional wood availability.

In recent years, remote sensing technologies have proven to be useful in providing information on forest area (Machala & Zejdova, 2014; Nordkvist et al., 2012), classifying species mix (Dalponte et al., 2012; Sasaki et al., 2012), and extracting forest structural variables (Mora et al., 2013; Popescu et al., 2004). Therefore, with the advanced development of these technologies and low-cost availability of satellite imagery and LiDAR datasets, the description of plantation forests, especially small-scale forests, could be potentially enhanced. This research focused on developing the optimal approaches for deriving area and yield information using LiDAR and RapidEye for the Wairarapa region.

7.1.1 Literature Review

Firstly, this research provided a comprehensive review on the applications of integrated LiDAR and other optical sensors in forestry. A review of the literature shows that fusion of different sensors has resulted in superior performance relative to individual sensors for classifying and delineating forest areas (up to 20% accuracy improvement), identifying species (up to 21% accuracy improvement), and estimating forest volume and biomass (up to 55% accuracy improvement). In contrast, sensor fusion achieved only minor improvements for tree or forest height estimation (1-7% accuracy improvement); this is likely because LiDAR alone is already so effective. This review was unable to draw conclusions on the performance of sensor fusion for forest age and productivity assessment due to the limited number of studies. The lack of results in these areas presents an opportunity for future research. The literature clearly demonstrated the utility of integrating LiDAR and satellite data for many aspects of forest description. Perhaps the greatest challenge moving forward will be

operationalising the research such that forestry companies and governments can take advantage of the benefits of data fusion.

7.1.2 Area Assessment

This research also compared a factorial combination of two classification approaches and two remote sensing datasets for their ability to accurately classify land cover, specifically plantation forest area. The approaches included nearest neighbour with RapidEye only, nearest neighbour with RapidEye and LiDAR, CART with RapidEye and CART with RapidEye and LiDAR. In an initial classification of nine training grids, CART with both RapidEye and LiDAR outperformed the other three approaches producing the highest overall accuracy and plantation accuracy. The addition of LiDAR data to RapidEye has improved the overall classification accuracy by 8% using the CART approach, and the producer's accuracy of planted forest improved by 7% compared to using RapidEye images alone. Therefore, the CART approach with both RapidEye and LiDAR was chosen to be used for land cover mapping in the remaining 60 validation grids.

Overall using the selected mapping approach gave good classification results, producing 89% overall accuracy; the producer's accuracy for plantations was 79% and user's accuracy was 91%. After excluding the harvesting and new plantings due to temporal difference in satellite and aerial photography, the producer's accuracy of plantation increased to 89%. The mapping approach used here has produced classification results comparable to previous studies (Haywood & Stone, 2009; Hellesen & Matikainen, 2013; Machala & Zejdova, 2014; Nordkvist et al., 2012; Sasaki et al., 2012).

The efficiency of the method was further examined by comparing the mapped plantations with manual digitisation of plantations. For all sample grids, the mapping approach overestimated the plantation area by 3%, which is a significant improvement on the 24% overestimation by the LCDB. Patch size proved to have an impact on mapping accuracy. Mapping of smaller patches (less than 10 ha) appears more variable and less accurate compared to "true" representation, whereas larger patches (over 10 ha) are generally more accurately mapped (less than 20% error).

7.1.3 Modelling approach

This study further determined the optimal modelling approach for deriving forest stand variables-mean top height, basal area, volume and stand age by comparing the performance of two parametric models (multiple linear regression and seemingly unrelated regression) and two non-parametric models (k-Nearest Neighbour and Random Forest) combined with the three remote sensing datasets (LiDAR only, RapidEye only and LiDAR + RapidEye). In total 48 models were finalised as the best models (based on highest R^2 and lowest RMSE values), using all 112 sets of plot data and corresponding remote sensing data.

The results from 10-fold cross-validation of all 48 models indicated that LiDAR-derived metrics alone were useful in estimating all four forest stand variables ($RMSE_{\%}$ ranged from 5% to 27%), whereas RapidEye metrics alone produced high prediction error ($RMSE_{\%}$ ranged from 16% to 49%). Combining LiDAR and RapidEye metrics did not provide significant gains in variable prediction compared with using LiDAR metrics alone, with an average reduction of 0.2% RMSE. Non-parametric models and parametric models performed similarly, likely due to the narrow range of structural characteristics in the collected field data.

The study further compared the prediction errors from models using all input calibration data and cross-validation data to investigate the model consistency and applicability. It was found that the difference in RMSEs produced by multiple linear regression and random forest models were the smallest, which suggests that these models could be applied to different datasets with similar performance expected. Overall, multiple linear regression was deemed to be the best option for estimating forest variables as the approach has provided sound and consistent estimation of stand variables and it is relatively easy to understand and interpret.

7.1.4 Application to Wairarapa

Finally, the optimal mapping and modelling approach using remote sensing datasets was applied to the Wairarapa region to investigate the implications of the designed approach. The automated mapped plantation area derived from combined RapidEye and LiDAR surfaces using Classification and Regression Tree was 9.1% lower than the National Exotic Forest Description (NEFD) plantation area. Together with manually digitised young plantations, the overall plantation area derived was 3.4% lower than the NEFD area. There is no assurance of accuracy in current NEFD data especially for the small-scale forests, and there is no current spatial representation of the plantation area in NEFD. In a recent manual digitisation exercise carried out by the University of Canterbury, the plantation digitised based on aerial photography was 287 ha (0.6%) lower than the area derived in this study. This suggests the approach developed here can produce results comparable to manually digitised plantation area, and further confirms the applicability of this approach.

Forest stand variables mean top height, basal area, volume and stand age were modelled for the region using multiple linear regression with LiDAR-derived metrics. Based on the modelled stand variables, recoverable volume at different ages (yield) could be generated. The yield tables developed using modelled information were all within a realistic range and were slightly lower than wood availability forecast (WAF) yield tables. This implies that using this approach could describe forest yield information.

7.2 Implications of research

The combination of multispectral RapidEye features and relatively low point density LiDAR-derived surfaces proved to be sufficient to detect land cover features, even for small plantation patches. The CART approach has superior ability for testing a large number of object features in a timely manner and selecting useful features to be used in a classification tree. Moreover, the results of classification tree analysis can be easily interpreted and implemented (Hellesen & Matikainen, 2013). The CART approach with both RapidEye and LiDAR has proven to be an effective way of detecting and delineating planted forests, especially for forest patches larger than 10 ha. This approach was further proved by application to the Wairarapa region, producing a spatial representation of the net stocked plantation areas that in total was 3% lower than the NEFD reported area. Given the fact that the approach is mostly automated and easy to apply, it is potentially applicable for assessing plantation area and monitoring temporal changes for other parts of New Zealand.

A multiple linear regression model with LiDAR-derived metrics was applied to the Wairarapa region and successfully estimated the forest stand variables – MTH, BA, VOL and age within each mapped plantation polygon. This indicates that using LiDAR metrics with limited field plot data can provide yield information for less-well-known small-scale forests, and it can be applied to other regions in New Zealand to obtain an enhanced understanding of small-scale plantations. With the information generated using remotely sensed data, the forest description of area and yield could be obtained using the approach tested in this research. The wood availability coming from these small-scale forests could be accurately described, thereby allowing the forest industry to plan more effectively for the marketing, harvesting, logistics and transport capacity required for additional wood availability.

To apply the developed mapping and modelling approach over all regions in New Zealand, the key requirement is the availability of remote sensing data and corresponding plot data. Cloud-free RapidEye images (or other satellite imagery with similar spatial and spectral resolution) and simultaneously collected LiDAR data covering the whole country are needed for mapping of plantations in New Zealand. Ideally RapidEye images should be collected on the same date within the same region to avoid spectral inconsistency on images acquired on different dates, alternatively more complex image correction and matching processing will be required prior to mapping processes. Plot

measurements covering a wide range of growth conditions in different regions are required as field validation data, and thus need to be collected at the same time as LiDAR acquisition. The key challenge of applying this approach is to obtain RapidEye, LiDAR and plot data simultaneously to minimise the errors caused by temporal difference among data sources. In addition to data sources, a computer workstation with strong processing capacity will be required to process large amount of remote sensing data and modelling.

7.3 Limitations and future research

One limitation with the mapping approach is that it is unable to detect young plantings due to the resolution of remote sensing datasets; hence manual digitisation is required to map the young plantations. In this study, the young plantations mapped accounted for 6% of total plantations in the Wairarapa, which means that 94% of the plantation areas can be derived automatically. This still saves a substantial amount of time and reduces the inconsistency in operators' performance. Furthermore, an automated mapping process for newly planted areas could be explored in a future study; higher spatial or spectral resolution remote sensing sources or metrics that could differentiate young trees from other land cover types may be useful. For example, a study carried by (Zhou et al., 2013) used 0.5 m resolution Worldview images and successfully mapped the density of young eucalyptus plantations aged at 6, 9 and 13 months.

Two non-parametric classifiers NN and CART were examined in this study, whereas other non-parametric classifiers such as Random Forest (RF) and Support Vector Machine (SVM) have not been evaluated due to limited processing resources. These machine learning algorithms could be tested in the future with CART to see which classifier produces the most accurate forest mapping accuracy for the New Zealand small-scale plantation estate. Recent studies have found alternative classification algorithms SVM and RF have also worked successfully in deriving forest areas (Müller et al., 2015; Pham et al., 2016).

In the application of the methods, the approach fails to predict any plantations that were younger than five years and older than 33 years. This was mainly because the range of forest stand ages from field data was limited. The estimation of plantation age could be further improved by including plot data with a wider range of stand ages or exploring alternative modelling approaches for estimating stand age. It is also noticeable that all plot data was collected for radiata pine forests, hence the estimation of stand variables was only applicable to radiata pine. In the Wairarapa region, radiata pine occupies 98% of all plantation area, whereas there are only 2% of plantations are planted with other species including Douglas fir, eucalyptus and cypress species (MPI, 2014). The forest yield of the minor species was not investigated in this study. Generally speaking, the estimation of stand variables could

be enhanced by incorporating a wider range of field validation data to better capture different ranges of silvicultural regimes, plantation species and age classes.

In conclusion, the mapping and modelling approaches developed in this study provide proof of concept for estimating plantation area and stand variables using remotely sensed data in the Wairarapa region, and they are especially important for small-scale forests where the forest area and stand variables are poorly understood.

Chapter 8 - References

Ackermann, F. (1999). Airborne laser scanning: Present status and future expectations. *Isprs Journal of Photogrammetry and Remote Sensing, 54*(2-3), 64-67. doi: 10.1016/s0924-2716(99)00009-x

Aertsen, W., Kint, V., van Orshoven, J., Özkan, K., & Muys, B. (2010). Comparison and ranking of different modelling techniques for prediction of site index in Mediterranean mountain forests. *Ecological Modelling, 221*(8), 1119-1130. doi: 10.1016/j.ecolmodel.2010.01.007

Avery, T. E., & Berlin, G. L. (1992). *Fundamentals of remote sensing and airphoto interpretation* (5 ed.). Prentice Hall: Englewood Cliffs, NJ.

Avery, T. E., & Burkhart, H. E. (1983). *Forest measurements*. Dubuque, IA: McGraw-Hill.

Baatz, M., & Schäpe, A. (2000). Multiresolution segmentation: an optimization approach for high quality multi-scale image segmentation. *Angewandte Geographische Informationsverarbeitung XII*, 12-23.

Balthazar, V., Vanacker, V., & Lambin, E. F. (2012). Evaluation and parameterization of ATCOR3 topographic correction method for forest cover mapping in mountain areas. *International Journal of Applied Earth Observation and Geoinformation, 18*(0), 436-450. doi: 10.1016/j.jag.2012.03.010

Beekhuis, J. (1966). Prediction of yield and increment in Pinus radiata stands in New Zealand. *Forest Research InstituteTechnical paper No. 49*, 41.

Benko, M., & Balenovic, I. (2011). Past, present and future of application of remote sensing methods in Croatian forest inventory *Sumarski List, 135*, 272-281.

Berk, A., Anderson, G. P., Acharya, P. K., & Shettle, E. P. (2008). *MODTRAN®5.2.0.0 User's Manual*. Burlington MA, Air Force Research Laboratory Spectral Sciences Inc.

Berk, A., Bernstein, L. S., Anderson, G. P., Acharya, P. K., Robertson, D. C., Chetwynd, J. H., & Adler-Golden, S. M. (1998). MODTRAN Cloud and Multiple Scattering Upgrades with Application to AVIRIS. *Remote Sensing of Environment, 65*(3), 367-375. doi: 10.1016/S0034-4257(98)00045-5

Berterretche, M., Hudak, A. T., Cohen, W. B., Maiersperger, T. K., Gower, S. T., & Dungan, J. (2005). Comparison of regression and geostatistical methods for mapping Leaf Area Index (LAI) with Landsat ETM+ data over a boreal forest. *Remote Sensing of Environment, 96*(1), 49-61. doi: 10.1016/j.rse.2005.01.014

Bi, H., Fox, J. C., Li, Y., Lei, Y., & Pang, Y. (2012). Evaluation of nonlinear equations for predicting diameter from tree height. *Canadian Journal of Forest Research-Revue Canadienne De Recherche Forestiere, 42*(4), 789-806. doi: 10.1139/x2012-019

BlackBridge. (2013). Satellite Imagery Product Specifications. from http://blackbridge.com/rapideye/upload/RE_Product_Specifications_ENG.pdf

Blanchard, S. D., Jakubowski, M. K., & Kelly, M. (2011). Object-Based Image Analysis of Downed Logs in Disturbed Forested Landscapes Using Lidar. *Remote Sensing, 3*(11), 2420-2439. doi: 10.3390/rs3112420

Blaschke, T. (2010). Object based image analysis for remote sensing. *Isprs Journal of Photogrammetry and Remote Sensing, 65*(1), 2-16. doi: 10.1016/j.isprsjprs.2009.06.004

Bontemps, J.-D., & Bouriaud, O. (2014). Predictive approaches to forest site productivity: recent trends, challenges and future perspectives. *Forestry, 87*(1), 109-128. doi: 10.1093/forestry/cpt034

Bork, E. W., & Su, J. G. (2007). Integrating LiDAR data and multispectral imagery for enhanced classification of rangeland vegetation: A meta analysis. *Remote Sensing of Environment, 111*(1), 11-24. doi: 10.1016/j.rse.2007.03.011

Boyd, D. S., & Danson, F. M. (2005). Satellite remote sensing of forest resources: Three decades of research development. *Progress in Physical Geography, 29*(1), 1-26. doi: 10.1191/0309133305pp432ra

Breidenbach, J., Nothdurft, A., & Kandler, G. (2010). Comparison of nearest neighbour approaches for small area estimation of tree species-specific forest inventory attributes in central Europe using airborne laser scanner data. *European Journal of Forest Research, 129*(5), 833-846. doi: 10.1007/s10342-010-0384-1

Breiman, L. (2001). Random forests. *Machine Learning, 45*(1), 5-32. doi: 10.1023/a:1010933404324

Breiman, L., Friedman, J., Stone, C. J., & Olshen, R. A. (1984). *Classification and regression trees*. Wadsworth International Group: Belmont, CA, USA.

Brosofske, K. D., Froese, R. E., Falkowski, M. J., & Banskota, A. (2014). A review of methods for mapping and prediction of inventory attributes for operational forest management. *Forest Science, 60*(4), 733-756. doi: 10.5849/forsci.12-134

Campbell, J. B., & Wynne , R. H. (2011). *Introduction to remote sensing*. New York, NY: The Guilford Press.

Carson, W. W., Andersen, H. E., Reutebuch, S. E., & McGaughey, R. J. (2004). *Lidar applications in forestry: An overview.* Paper presented at the ASPRS Annual Conference Denver, Colorado.

Cartus, O., Kellndorfer, J., Rombach, M., & Walker, W. (2012). Mapping Canopy Height and Growing Stock Volume Using Airborne Lidar, ALOS PALSAR and Landsat ETM. *Remote Sensing, 4*(11), 3320-3345. doi: 10.3390/rs4113320

Chen, G., & Hay, G. J. (2011). A support vector regression approach to estimate forest biophysical parameters at the object level using airborne LiDAR transects and Quickbird data. *Photogrammetric Engineering and Remote Sensing, 77*(7), 733-741. doi: 10.14358/PERS.77.7.733

Chen, Y., & Zhu, X. (2012). Site quality assessment of a Pinus radiata plantation in Victoria, Australia, using LiDAR technology. *Southern Forests: a Journal of Forest Science, 74*(4), 217-227. doi: 10.2989/20702620.2012.741767

Chirici, G., Barbati, A., Corona, P., Marchetti, M., Travaglini, D., Maselli, F., & Bertini, R. (2008). Non-parametric and parametric methods using satellite images for estimating growing stock volume in alpine and Mediterranean forest ecosystems. *Remote Sensing of Environment, 112*(5), 2686-2700. doi: 10.1016/j.rse.2008.01.002

Chirici, G., Mura, M., McInerney, D., Py, N., Tomppo, E. O., Waser, L. T., . . . McRoberts, R. E. (2016). A meta-analysis and review of the literature on the k-Nearest Neighbors technique for forestry applications that use remotely sensed data. *Remote Sensing of Environment, 176*, 282-294. doi: 10.1016/j.rse.2016.02.001

Chubey, M. S., Franklin, S. E., & Wulder, M. A. (2006). Object-based analysis of Ikonos-2 imagery for extraction of forest inventory parameters. *Photogrammetric Engineering & Remote Sensing, 72*(4), 383-394. doi: 10.14358/PERS.72.4.383

Clark, A., Daniels, R. F., & Borders, B. E. (2006). *Effect of rotation age and physiographic region on weight per cubic foot of planted loblolly pine.* Paper presented at the Proceedings of the 13th Biennial Southern Silvicultural Research Conference. USDS, Forest Service, Southern Research Station, Asheville, NC.

Cohen, W. B., Maiersperger, T. K., Gower, S. T., & Turner, D. P. (2003). An improved strategy for regression of biophysical variables and Landsat ETM+ data. *Remote Sensing of Environment, 84*(4), 561-571. doi: 10.1016/S0034-4257(02)00173-6

Cohen, W. B., Spies, T. A., & Fiorella, M. (1995). Estimating the age and structure of forests in a multi-ownership landscape of Western Oregon, USA. *International Journal of Remote Sensing, 16*(4), 721-746.

Congalton, R. G. (1991). A review of assessing the accuracy of classifications of remotely sensed data. *Remote Sensing of Environment, 37*(1), 35-46. doi: 10.1016/0034-4257(91)90048-B

Crookston, N. L., & Finley, A. O. (2008). yaImpute: An R Package for kNN Imputation. *Journal of Statistical Software, 23*(10), 1-16.

d'Oliveira, M. V. N., Reutebuch, S. E., McGaughey, R. J., & Andersen, H. E. (2012). Estimating forest biomass and identifying low-intensity logging areas using airborne scanning LiDAR in Antimary State Forest, Acre State, Western Brazilian Amazon. *Remote Sensing of Environment, 124*, 479-491. doi: 10.1016/j.rse.2012.05.014

Dalponte, M., Bruzzone, L., & Gianelle, D. (2008). Fusion of hyperspectral and LiDAR remote sensing data for classification of complex forest areas. *Geoscience and Remote Sensing, IEEE Transactions on, 46*(5), 1416-1427. doi: 10.1109/TGRS.2008.916480

Dalponte, M., Bruzzone, L., & Gianelle, D. (2012). Tree species classification in the Southern Alps based on the fusion of very high geometrical resolution multispectral/hyperspectral images and LiDAR data. *Remote Sensing of Environment, 123*, 258-270. doi: 10.1016/j.rse.2012.03.013

Dandois, J. P., & Ellis, E. C. (2013). High spatial resolution three-dimensional mapping of vegetation spectral dynamics using computer vision. *Remote Sensing of Environment, 136*(0), 259-276. doi: 10.1016/j.rse.2013.04.005

Dash, J. P., Marshall, H. M., & Rawley, B. (2015). Methods for estimating multivariate stand yields and errors using k-NN and aerial laser scanning. *Forestry, 88*(2), 237-247. doi: 10.1093/forestry/cpu054

Dash, J. P., Watt, M. S., Bhandari, S., & Watt, P. (2016). Characterising forest structure using combinations of airborne laser scanning data, RapidEye satellite imagery and environmental variables. *Forestry, 89*(2), 159-169. doi: 10.1093/forestry/cpv048

Donoghue, D. N. M., & Watt, P. J. (2006). Using LiDAR to compare forest height estimates from IKONOS and Landsat ETM+ data in Sitka spruce plantation forests. *International Journal of Remote Sensing, 27*(11), 2161-2175. doi: 10.1080/01431160500396493

Drăguţ, L., Csillik, O., Eisank, C., & Tiede, D. (2014). Automated parameterisation for multi-scale image segmentation on multiple layers. *Isprs Journal of Photogrammetry and Remote Sensing, 88*, 119-127. doi: 10.1016/j.isprsjprs.2013.11.018

Drăguţ, L., Tiede, D., & Levick, S. R. (2010). ESP: a tool to estimate scale parameter for multiresolution image segmentation of remotely sensed data. *International Journal of Geographical Information Science, 24*(6), 859-871. doi: 10.1080/13658810903174803

Dubayah, R. O., & Drake, J. B. (2000). Lidar remote sensing for forestry. *Journal of Forestry, 98*(6), 44-46.

Dupuy, S., Laine, G., Tassin, J., & Sarrailh, J. M. (2013). Characterization of the horizontal structure of the tropical forest canopy using object-based LiDAR and multispectral image analysis. *International Journal of Applied Earth Observation and Geoinformation, 25*, 76-86. doi: 10.1016/j.jag.2013.04.001

Eid, T., Gobakken, T., & Naesset, E. (2004). Comparing stand inventories for large areas based on photo-interpretation and laser scanning by means of cost-plus-loss analyses. *Scandinavian Journal of Forest Research, 19*(6), 512-523. doi: 10.1080/02827580410019463

Eklundh, L., Harrie, L., & Kuusk, A. (2001). Investigating relationships between Landsat ETM+ sensor data and leaf area index in a boreal conifer forest. *Remote Sensing of Environment, 78*(3), 239-251. doi: 10.1016/S0034-4257(01)00222-X

Erdody, T. L., & Moskal, L. M. (2010). Fusion of LiDAR and imagery for estimating forest canopy fuels. *Remote Sensing of Environment, 114*(4), 725-737. doi: 10.1016/j.rse.2009.11.002

Eskelson, B. N. I., Temesgen, H., Lemay, V., Barrett, T. M., Crookston, N. L., & Hudak, A. T. (2009). The roles of nearest neighbor methods in imputing missing data in forest inventory and monitoring databases. *Scandinavian Journal of Forest Research, 24*(3), 235-246. doi: 10.1080/02827580902870490

ESRI. (2017). ArcGIS destop (Version 10.3). Califonia, USA: Environmental Systems Research

Estornell, J., Ruiz, L. A., Velazquez-Marti, B., & Hermosilla, T. (2012). Estimation of biomass and volume of shrub vegetation using LiDAR and spectral data in a Mediterranean environment. *Biomass & Bioenergy, 46*, 710-721. doi: 10.1016/j.biombioe.2012.06.023

Eysn, L., Hollaus, M., Schadauer, K., & Pfeifer, N. (2012). Forest delineation based on airborne LiDAR data. *Remote Sensing, 4*(3), 762-783. doi: 10.3390/rs4030762

Falkowski, M. J., Evans, J. S., Martinuzzi, S., Gessler, P. E., & Hudak, A. T. (2009). Characterizing forest succession with lidar data: An evaluation for the Inland Northwest, USA. *Remote Sensing of Environment, 113*(5), 946-956. doi: 10.1016/j.rse.2009.01.003

Fehrmann, L., Lehtonen, A., Kleinn, C., & Tomppo, E. (2008). Comparison of linear and mixed-effect regression models and a k-nearest neighbour approach for estimation of single-tree biomass. *Canadian Journal of Forest Research-Revue Canadienne De Recherche Forestiere, 38*(1), 1-9. doi: 10.1139/x07-119

Food and Agriculture Organization. (2014). *State of the world's forests 2014.* Retrieved from http://www.fao.org/3/a-i3710e/i3710e00.pdf

Foody, G. M. (2002). Status of land cover classification accuracy assessment. *Remote Sensing of Environment, 80*(1), 185-201. doi: 10.1016/S0034-4257(01)00295-4

Fourth Year Students. (2017). *Mapping of plantation areas for Southern North Island (unpublished)*. New Zealand School of Forestry, University of Canterbury.

Franco-Lopez, H., Ek, A. R., & Bauer, M. E. (2001). Estimation and mapping of forest stand density, volume, and cover type using the k-nearest neighbors method. *Remote Sensing of Environment, 77*(3), 251-274. doi: 10.1016/s0034-4257(01)00209-7

Gao, J. (2009). Classification accuracy assessment. *Digital analysis of remotely sensed imagery*. New York: McGraw Hill.

Gatziolis, D. (2007). LIDAR-derived site index in the US pacific northwest–challenges and opportunities. *The International Archives of the Photogrammetry, Remote Sensing and Spatial Information Sciences, Espoo, Finland, 36*(Part 3/W52), pp.136-143.

Gemmell, F. M. (1995). Effects of forest cover, terrain, and scale on timber volume estimation with thematic mapper data in a rocky-mountain site. *Remote Sensing of Environment, 51*(2), 291-305. doi: 10.1016/0034-4257(94)00056-s

Gill, S. J., Biging, G. S., & Murphy, E. C. (2000). Modeling conifer tree crown radius and estimating canopy cover. *Forest Ecology and Management, 126*(3), 405-416. doi: 10.1016/S0378-1127(99)00113-9

Gleason, C. J., & Im, J. (2011). A review of remote sensing of forest biomass and biofuel: Options for small-area applications. *Giscience & Remote Sensing, 48*(2), 141-170. doi: 10.2747/1548-1603.48.2.141

Gobakken, T., & Naesset, E. (2009). Assessing effects of positioning errors and sample plot size on biophysical stand properties derived from airborne laser scanner data. *Canadian Journal of Forest Research-Revue Canadienne De Recherche Forestiere, 39*(5), 1036-1052. doi: 10.1139/x09-025

Graham, M. H. (2003). CONFRONTING MULTICOLLINEARITY IN ECOLOGICAL MULTIPLE REGRESSION. *Ecology, 84*(11), 2809-2815. doi: 10.1890/02-3114

Haapanen, R., Ek, A. R., Bauer, M. E., & Finley, A. O. (2004). Delineation of forest/nonforest land use classes using nearest neighbor methods. *Remote Sensing of Environment, 89*(3), 265-271. doi: 10.1016/j.rse.2003.10.002

Haara, A., & Haarala, M. (2002). Tree species classification using semi-automatic delineation of trees on aerial images. *Scandinavian Journal of Forest Research, 17*(6), 556-565. doi: 10.1080/02827580260417215

Hall, R. J., Skakun, R. S., Arsenault, E. J., & Case, B. S. (2006). Modeling forest stand structure attributes using Landsat ETM+ data: Application to mapping of aboveground biomass and stand volume. *Forest Ecology and Management, 225*(1-3), 378-390. doi: 10.1016/j.foreco.2006.01.014

Hall, S. A., Burke, I. C., Box, D. O., Kaufmann, M. R., & Stoker, J. M. (2005). Estimating stand structure using discrete-return LiDAR: An example from low density, fire prone ponderosa pine forests. *Forest Ecology and Management, 208*(1-3), 189-209. doi: 10.1016/j.foreco.2004.12.001

Hantson, S., & Chuvieco, E. (2011). Evaluation of different topographic correction methods for Landsat imagery. *International Journal of Applied Earth Observation and Geoinformation, 13*(5), 691-700. doi: 10.1016/j.jag.2011.05.001

Haywood, A., & Stone, C. (2009). Semi-automating the stand delineation process in mapping natural eucalpt forest. *Australian Foestry, 74*(1), 13-22.

Hellesen, T., & Matikainen, L. (2013). An Object-Based Approach for Mapping Shrub and Tree Cover on Grassland Habitats by Use of LiDAR and CIR Orthoimages. *Remote Sensing, 5*(2), 558-583. doi: 10.3390/rs5020558

Henningsen, A., & Hamann, J. D. (2007). systemfit: A Package to estimate simultaneous equation systems in R. *Journal of Statistical Software, 23*, 1-40.

Hirata, Y., Furuya, N., Suzuki, M., & Yamamoto, H. (2009). Airborne laser scanning in forest management: Individual tree identification and laser pulse penetration in a stand with different levels of thinning. *Forest Ecology and Management, 258*(5), 752-760. doi: 10.1016/j.foreco.2009.05.017

Holmgren, J., Persson, A., & Soderman, U. (2008). Species identification of individual trees by combining high resolution LiDAR data with multi-spectral images. *International Journal of Remote Sensing, 29*(5), 1537-1552. doi: 10.1080/01431160701736471

Holmgren, P., Thuresson, T., & Holm, S. (1997). Estimating forest characteristics in scanned aerial photographs with respect to requirements for economic forest management planning. *Scandinavian Journal of Forest Research, 12*(2), 189-199. doi: 10.1080/02827589709355400

Holopainen, M., Vastaranta, M., Haapanen, R., Yu, X., Hyyppä, J., Kaartinen, H., . . . Hyyppä, H. (2010). Site-type estimation using airborne laser scanning and stand register data. *Photogramm. J. Fin, 22*, 16-32.

Horning, N. (2010). *Random Forests: An algorithm for image classification and generation of continuous fields data sets.* Paper presented at the International Conference on Geoinformatics for Spatial Infrastructure Development in Earth and Allied Sciences 2010, Bangkok, Thailand.

Huang, H., Gong, P., Clinton, N., & Hui, F. (2008). Reduction of atmospheric and topographic effect on Landsat TM data for forest classification. *International Journal of Remote Sensing, 29*(19), 5623-5642. doi: 10.1080/01431160802082148

Hubert-Moy, L., Cotonnec, A., Le Du, L., Chardin, A., & Perez, P. (2001). A Comparison of Parametric Classification Procedures of Remotely Sensed Data Applied on Different Landscape Units. *Remote Sensing of Environment, 75*(2), 174-187. doi: 10.1016/S0034-4257(00)00165-6

Hudak, A. T., Crookston, N. L., Evans, J. S., Hall, D. E., & Falkowski, M. J. (2008). Nearest neighbor imputation of species-level, plot-scale forest structure attributes from LiDAR data. *Remote Sensing of Environment, 112*(5), 2232-2245. doi: 10.1016/j.rse.2007.10.009

Hudak, A. T., Evans, J. S., & Smith, A. M. S. (2009). LiDAR utility for natural resource managers. *Remote Sensing, 1*(4), 934-951. doi: 10.3390/rs1040934

Hudak, A. T., Lefsky, M. A., Cohen, W. B., & Berterretche, M. (2002). Integration of LiDAR and Landsat ETM plus data for estimating and mapping forest canopy height. *Remote Sensing of Environment, 82*(2-3), 397-416. doi: 10.1016/s0034-4257(02)00056-1

Hyde, P., Dubayah, R., Walker, W., Blair, J. B., Hofton, M., & Hunsaker, C. (2006). Mapping forest structure for wildlife habitat analysis using multi-sensor (LiDAR, SAR/InSAR, ETM plus , Quickbird) synergy. *Remote Sensing of Environment, 102*(1-2), 63-73. doi: 10.1016/j.rse.2006.01.021

Hyyppa, J., Hyyppa, H., Leckie, D., Gougeon, F., Yu, X., & Maltamo, M. (2008). Review of methods of small-footprint airborne laser scanning for extracting forest inventory data in boreal forests. *International Journal of Remote Sensing, 29*(5), 1339-1366. doi: 10.1080/01431160701736489

Immitzer, M., Atzberger, C., & Koukal, T. (2012). Tree species classification with random forest using very high spatial resolution 8-band Worldview-2 satellite data. *Remote Sensing, 4*(9), 2661-2693. doi: 10.3390/rs4092661

Ingram, J. C., Dawson, T. P., & Whittaker, R. J. (2005). Mapping tropical forest structure in southeastern Madagascar using remote sensing and artificial neural networks. *Remote Sensing of Environment, 94*(4), 491-507. doi: 10.1016/j.rse.2004.12.001

Jensen, J. L. R., Humes, K. S., Vierling, L. A., & Hudak, A. T. (2008). Discrete return LiDAR-based prediction of leaf area index in two conifer forests. *Remote Sensing of Environment, 112*(10), 3947-3957. doi: 10.1016/j.rse.2008.07.001

Jensen, J. R., Qiu, F., & Ji, M. H. (1999). Predictive modelling of coniferous forest age using statistical and artificial neural network approaches applied to remote sensor data. *International Journal of Remote Sensing, 20*(14), 2805-2822.

Jensen, R. R., & Binford, M. W. (2004). Measurement and comparison of Leaf Area Index estimators derived from satellite remote sensing techniques. *International Journal of Remote Sensing, 25*(20), 4251-4265. doi: 10.1080/01431160410001680400

Jochem, A., Hollaus, M., Rutzinger, M., & Höfle, B. (2010). Estimation of Aboveground Biomass in Alpine Forests: A Semi-Empirical Approach Considering Canopy Transparency Derived from Airborne LiDAR Data. *Sensors, 11*(1), 278-295. doi: 10.3390/s110100278

Johnson, B., & Xie, Z. (2011). Unsupervised image segmentation evaluation and refinement using a multi-scale approach. *Isprs Journal of Photogrammetry and Remote Sensing, 66*(4), 473-483. doi: 10.1016/j.isprsjprs.2011.02.006

Jones, T. G., Coops, N. C., & Sharma, T. (2010). Assessing the utility of airborne hyperspectral and LiDAR data for species distribution mapping in the coastal Pacific Northwest, Canada. *Remote Sensing of Environment, 114*(12), 2841-2852. doi: 10.1016/j.rse.2010.07.002

Kaasalainen, S., Pyysalo, U., Krooks, A., Vain, A., Kukko, A., Hyyppä, J., & Kaasalainen, M. (2011). Absolute Radiometric Calibration of ALS Intensity Data: Effects on Accuracy and Target Classification. *Sensors (Basel, Switzerland), 11*(11), 10586-10602. doi: 10.3390/s111110586

Kadmon, R. (2001). Remote sensing and image processing. *Encyclopedia of Biodiversity, 5*, 121-143.

Katila, M., & Tomppo, E. (2001). Selecting estimation parameters for the Finnish multisource National Forest Inventory. *Remote Sensing of Environment, 76*(1), 16-32. doi: 10.1016/s0034-4257(00)00188-7

Katz, A., Dunningham, A. G., & Gordon, A. (1984). A Compatible Volume and Taper Equation for New Zealand Pinus Radiata D. Don Grown Under the Direct Sawlog Regime. *New Zealand Forest Research Institute Bulletin No. 67* (pp. 12): Forest Research Institute.

Kayitakire, F., Hamel, C., & Defourny, P. (2006). Retrieving forest structure variables based on image texture analysis and IKONOS-2 imagery. *Remote Sensing of Environment, 102*(3-4), 390-401. doi: 10.1016/j.rse.2006.02.022

Ke, Y. H., Quackenbush, L. J., & Im, J. (2010). Synergistic use of QuickBird multispectral imagery and LiDAR data for object-based forest species classification. *Remote Sensing of Environment, 114*(6), 1141-1154. doi: 10.1016/j.rse.2010.01.002

Kellndorfer, J. M., Walker, W. S., LaPoint, E., Kirsch, K., Bishop, J., & Fiske, G. (2010). Statistical fusion of lidar, InSAR, and optical remote sensing data for forest stand height characterization: A regional-scale method based on LVIS, SRTM, Landsat ETM plus , and ancillary data sets. *Journal of Geophysical Research-Biogeosciences, 115*. doi: 10.1029/2009jg000997

Kirkpatrick, S., Gelatt, C. D., & Vecchi, M. P. (1983). Optimization by Simulated Annealing. *Science, 220*, 671-680.

Kohavi, R. (1995). *A study of cross-validation and bootstrap for accuracy estimation and model selection.* Paper presented at the Proceedings of the 14th international joint conference on Artificial intelligence-Volume 2.

Kovats, M. (1997). A large-scale aerial photographic technique for measuring tree heights on long-term forest installations. *Photogrammetric Engineering and Remote Sensing, 63*(6), 741-747.

Kozak, A., & Kozak, R. (2003). Does cross validation provide additional information in the evaluation of regression models? *Canadian Journal of Forest Research, 33*(6), 976-987. doi: 10.1139/x03-022

Kraus, K., & Pfeifer, N. (1998). Determination of terrain models in wooded areas with airborne laser scanner data. *Isprs Journal of Photogrammetry and Remote Sensing, 53*(4), 193-203. doi: 10.1016/S0924-2716(98)00009-4

Kuhn, M. (2015). A Short Introduction to the caret Package. *R Project website. cran. r-project. org/web/packages/caret/vignettes/caret. pdf. Published August, 6*.

Landcare Research. (2016). LCDB v4.1—Land Cover Database version 4.1. Retrieved 20 Aug 2016, 2016, from https://lris.scinfo.org.nz/layer/423-lcdb-v41-land-cover-database-version-41-mainland-new-zealand/

Latifi, H., Nothdurft, A., Straub, C., & Koch, B. (2012). Modelling stratified forest attributes using optical/LiDAR features in a central European landscape. *International Journal of Digital Earth, 5*(2), 106-132. doi: 10.1080/17538947.2011.583992

Lefsky, M., Cohen, W., & Spies, T. (2001a). An evaluation of alternate remote sensing products for forest inventory, monitoring, and mapping of Douglas-fir forests in western Oregon. *Canadian Journal of Forest Research, 31*(1), 78-87.

Lefsky, M. A., Cohen, W. B., Parker, G. G., & Harding, D. J. (2002). Lidar remote sensing for ecosystem studies. *Bioscience, 52*(1), 19-30. doi: 10.1641/0006-3568(2002)052[0019:lrsfes]2.0.co;2

Lefsky, M. A., Cohen, W. B., & Spies, T. A. (2001b). An evaluation of alternate remote sensing products for forest inventory, monitoring, and mapping of Douglas-fir forests in western Oregon. *Canadian Journal of Forest Research-Revue Canadienne De Recherche Forestiere, 31*(1), 78-87. doi: 10.1139/cjfr-31-1-78

Lefsky, M. A., Turner, D. P., Guzy, M., & Cohen, W. B. (2005). Combining LiDAR estimates of aboveground biomass and Landsat estimates of stand age for spatially extensive validation of modeled forest productivity. *Remote Sensing of Environment, 95*(4), 549-558. doi: 10.1016/j.rse.2004.12.022

Li, W., Guo, Q., Jakubowski, M. K., & Kelly, M. (2012). A new method for segmenting individual trees from the LiDAR point cloud. *Photogrammetric Engineering and Remote Sensing, 78*(1), 75-84. doi: 10.14358/PERS.78.1.75

Liaw, A., & Wiener, M. (2002). Classification and Regression by randomForest. *R news, 2*(3), 18-22.

Lim, K., Treitz, P., Wulder, M., St-Onge, B., & Flood, M. (2003). LiDAR remote sensing of forest structure. *Progress in Physical Geography, 27*(1), 88-106. doi: 10.1191/0309133303pp360ra

Lu, D., & Weng, Q. (2007). A survey of image classification methods and techniques for improving classification performance. *International Journal of Remote Sensing, 28*(5), 823-870. doi: 10.1080/01431160600746456

Lumley, T., & Miller, A. (2009). leaps: regression subset selection: R package version 2.9. Retrieved from https://CRAN.R-project.org/package=leaps

Machala, M., & Zejdova, L. (2014). Forest mapping through object-based image analysis of multispectral and LiDAR aerial data. *European Journal of Remote Sensing, 47*(1), 117-131. doi: 10.5721/EuJRS20144708

Maclaren, J. P. (2000). Conversion to volume. *How much wood haws your woodlot got? A practical guide to estimating the volume and value of planted trees*: Forest Research Bulletin No. 217.

Mallinis, G., Koutsias, N., Tsakiri-Strati, M., & Karteris, M. (2008). Object-based classification using Quickbird imagery for delineating forest vegetation polygons in a Mediterranean test site. *Isprs Journal of Photogrammetry and Remote Sensing, 63*(2), 237-250. doi: 10.1016/j.isprsjprs.2007.08.007

Mallows, C. L. (1973). Some Comments on C_P. *Technometrics, 15*(4), 661-675. doi: 10.2307/1267380

Maltamo, M., Packalén, P., Suvanto, A., Korhonen, K. T., Mehtätalo, L., & Hyvönen, P. (2009). Combining ALS and NFI training data for forest management planning: a case study in Kuortane, Western Finland. *European Journal of Forest Research, 128*(3), 305-317. doi: 10.1007/s10342-009-0266-6

Manley, B., Somerville, O., Turbitt, M., & Lane, P. (2003). Review of new forest planting estimates. *New Zealand Journal of Forestry, 48*(3), 34-37.

Marshall, H., Dash, J., Rawley, B., & Adams, T. (2012). Using LiDAR based regression estimation in New Zealand Forestry Inventory: Future Forests Research Report R070.

Maselli, F., Chirici, G., Bottai, L., Corona, P., & Marchetti, M. (2005). Estimation of Mediterranean forest attributes by the application of kNN procedures to multitemporal Landsat ETM+ images. *International Journal of Remote Sensing, 26*(17), 3781-3796. doi: 10.1080/01431160500166433

McCombs, J. W., Roberts, S. D., & Evans, D. L. (2003). Influence of fusing LiDAR and multispectral imagery on remotely sensed estimates of stand density and mean tree height in a managed loblolly pine plantation. *Forest Science, 49*(3), 457-466.

McGaughey, R. J. (2016a). Fusion (Version 3.42). Pacific Northwest Research Station

McGaughey, R. J. (2016b). FUSION/LDV: Software for LIDAR Data Analysis and Visualization-user guide: USDA Forest Service.

McInerney, D. O., & Nieuwenhuis, M. (2009). A comparative analysis of kNN and decision tree methods for the Irish National Forest Inventory. *International Journal of Remote Sensing, 30*(19), 4937-4955. doi: 10.1080/01431160903022936

McInerney, D. O., Suarez-Minguez, J., Valbuena, R., & Nieuwenhuis, M. (2010). Forest canopy height retrieval using LiDAR data, medium-resolution satellite imagery and kNN estimation in Aberfoyle, Scotland. *Forestry, 83*(2), 195-206. doi: 10.1093/forestry/cpq001

McIntosh, A. C. S., Gray, A. N., & Garman, S. L. (2012). Estimating Canopy Cover from Standard Forest Inventory Measurements in Western Oregon. *Forest Science, 58*(2), 154-167. doi: 10.5849/forsci.09-127

McRoberts, R. E. (2012). Estimating forest attribute parameters for small areas using nearest neighbors techniques. *Forest Ecology and Management, 272*, 3-12. doi: 10.1016/j.foreco.2011.06.039

McRoberts, R. E., Næsset, E., & Gobakken, T. (2015). Optimizing the k-Nearest Neighbors technique for estimating forest aboveground biomass using airborne laser scanning data. *Remote Sensing of Environment, 163*, 13-22. doi: 10.1016/j.rse.2015.02.026

MfE. (2004). New Zealand Land Cover Database 2 User Guide: Ministry for the Environment.

Ministry of Agriculture and Forestry. (2009). A guide to mapping forest land for the Emissions Trading Scheme. from http://www.mpi.govt.nz

Mora, B., Wulder, M. A., White, J. C., & Hobart, G. (2013). Modeling stand height, volume, and biomass from very high spatial resolution satellite imagery and samples of airborne LiDAR. *Remote Sensing, 5*(5), 2308-2326. doi: 10.3390/rs5052308

Morgenroth, J., & Visser, R. (2013). Uptake and barriers to the use of geospatial technologies in forest management. *New Zealand Journal of Forestry Science, 43*(1), 16. doi: 10.1186/1179-5395-43-16

Mountrakis, G., Im, J., & Ogole, C. (2011). Support vector machines in remote sensing: A review. *Isprs Journal of Photogrammetry and Remote Sensing, 66*(3), 247-259. doi: 10.1016/j.isprsjprs.2010.11.001

MPI. (2014). 2014 National Exotic Forest Description. Wellington: Ministry of Primary Industries.

MPI. (2016a). 2016 National Exotic Forest Description. Wellington: Ministry of Primary Industries.

MPI. (2016b). Wood Availability Forecasts – New Zealand 2014–2050. Wellington: Ministry of Primary Industries.

MPI. (2016c). Wood Availability Forecasts – Western & Eastern Southern North Island 2014. Wellington: Ministry of Primary Industries.

Müller, M. U., Shepherd, J. D., & Dymond, J. R. (2015). Support vector machine classification of woody patches in New Zealand from synthetic aperture radar and optical data, with LiDAR training. *Journal of Applied Remote Sensing, 9*(1), 095984-095984. doi: 10.1117/1.JRS.9.095984

Mustonen, J., Packalén, P., & Kangas, A. (2008). Automatic segmentation of forest stands using a canopy height model and aerial photography. *Scandinavian Journal of Forest Research, 23*(6), 534-545. doi: 10.1080/02827580802552446

Myint, S. W., Gober, P., Brazel, A., Grossman-Clarke, S., & Weng, Q. (2011). Per-pixel vs. object-based classification of urban land cover extraction using high spatial resolution imagery. *Remote Sensing of Environment, 115*(5), 1145-1161. doi: 10.1016/j.rse.2010.12.017

Naesset, E. (2002). Predicting forest stand characteristics with airborne scanning laser using a practical two-stage procedure and field data. *Remote Sensing of Environment, 80*(1), 88-99. doi: 10.1016/S0034-4257(01)00290-5

Naesset, E. (2007). Airborne laser scanning as a method in operational forest inventory: Status of accuracy assessments accomplished in Scandinavia. *Scandinavian Journal of Forest Research, 22*(5), 433-442. doi: 10.1080/02827580701672147

Naesset, E., & Bjerknes, K. (2001). Estimating tree heights and number of stems in young forest stands using airborne laser scanner data. *Remote Sensing of Environment, 78*(3), 328 - 340. doi: 10.1016/S0034-4257(01)00228-0

Næsset, E., Bollandsås, O. M., & Gobakken, T. (2005). Comparing regression methods in estimation of biophysical properties of forest stands from two different inventories using laser scanner data. *Remote Sensing of Environment, 94*(4), 541-553. doi: 10.1016/j.rse.2004.11.010

Naesset, E., Gobakken, T., Holmgren, J., Hyyppa, H., Hyyppa, J., Maltamo, M., . . . Soderman, U. (2004). Laser scanning of forest resources: The Nordic experience. *Scandinavian Journal of Forest Research, 19*(6), 482-499. doi: 10.1080/02827580410019553

Nordkvist, K., Granholm, A. H., Holmgren, J., Olsson, H., & Nilsson, M. (2012). Combining optical satellite data and airborne laser scanner data for vegetation classification. *Remote Sensing Letters, 3*(5), 393-401. doi: 10.1080/01431161.2011.606240

NZFOA. (2016). Facts and Figures 2015/16 New Zealand Plantation Forest Industry: New Zealand Forest Owners Association.

O'Brien, R. M. (2007). A Caution Regarding Rules of Thumb for Variance Inflation Factors. *Quality & Quantity, 41*(5), 673-690. doi: 10.1007/s11135-006-9018-6

Ohmann, J. L., & Gregory, M. J. (2002). Predictive mapping of forest composition and structure with direct gradient analysis and nearest- neighbor imputation in coastal Oregon, U.S.A. *Canadian Journal of Forest Research, 32*(4), 725-741. doi: 10.1139/x02-011

Orka, H. O., Dalponte, M., Gobakken, T., Naesset, E., & Ene, L. T. (2013). Characterizing forest species composition using multiple remote sensing data sources and inventory approaches. *Scandinavian Journal of Forest Research, 28*(7), 677-688. doi: 10.1080/02827581.2013.793386

Packalen, P., & Maltamo, M. (2007). The k-MSN method for the prediction of species-specific stand attributes using airborne laser scanning and aerial photographs. *Remote Sensing of Environment, 109*(3), 328-341. doi: 10.1016/j.rse.2007.01.005

Packalen, P., & Maltamo, M. (2008). Estimation of species-specific diameter distributions using airborne laser scanning and aerial photographs. *Canadian Journal of Forest Research-Revue Canadienne De Recherche Forestiere, 38*(7), 1750-1760. doi: 10.1139/x08-037

Packalén, P., Mehtätalo, L., & Maltamo, M. (2011). ALS-based estimation of plot volume and site index in a eucalyptus plantation with a nonlinear mixed-effect model that accounts for the clone effect. *Annals of Forest Science, 68*(6), 1085-1092. doi: 10.1007/s13595-011-0124-9

Packalén, P., Temesgen, H., & Maltamo, M. (2012). Variable selection strategies for nearest neighbor imputation methods used in remote sensing based forest inventory. *Canadian Journal of Remote Sensing, 38*(5), 557-569. doi: 10.5589/m12-046

Pascual, C., Garcia-Abril, A., Cohen, W. B., & Martin-Fernandez, S. (2010). Relationship between LiDAR-derived forest canopy height and Landsat images. *International Journal of Remote Sensing, 31*(5), 1261-1280. doi: 10.1080/01431160903380656

Peper, P. J., McPherson, E. G., & Mori, S. M. (2001). Equations for predicting diameter, height, crown width, and leaf area of San Joaquin valley street trees. *Journal of Arboriculture, 27*(6), 306-317.

Petterson, H. (1955). *Yield of coniferous forests*. Medd. Stat Skogsforsoksanct 45 IB, Sweden.

Pham, L. T. H., Brabyn, L., & Ashraf, S. (2016). Combining QuickBird, LiDAR, and GIS topography indices to identify a single native tree species in a complex landscape using an object-based classification approach. *International Journal of Applied Earth Observation and Geoinformation, 50*, 187-197. doi: 10.1016/j.jag.2016.03.015

Pirotti, F., Grigolato, S., Lingua, E., Sitzia, T., & Tarolli, P. (2012). Laser Scanner Applications in Forest and Environmental Sciences. *Italian Journal of Remote Sensing-Rivista Italiana Di Telerilevamento, 44*(1), 109-123. doi: 10.5721/ItJRS20124419

Popescu, S. C., & Wynne, R. H. (2004). Seeing the trees in the forest: Using LiDAR and multispectral data fusion with local filtering and variable window size for estimating tree height. *Photogrammetric Engineering and Remote Sensing, 70*(5), 589-604. doi: 10.14358/PERS.70.5.589

Popescu, S. C., Wynne, R. H., & Scrivani, J. A. (2004). Fusion of small-footprint LiDAR and multispectral data to estimate plot-level volume and biomass in deciduous and pine forests in Virginia, USA. *Forest Science, 50*(4), 551-565.

R Development Core Team. (2016). R: A language and environment for statistical computing R Foundation for Statistical Computing, Vienna, Austria. Retrieved from http://www.R-project.org

Racine, E. B., Coops, N. C., St-Onge, B., & Bégin, J. (2014). Estimating Forest Stand Age from LiDAR-Derived Predictors and Nearest Neighbor Imputation. *Forest Science, 60*(1), 128-136. doi: 10.5849/forsci.12-088

Rana, P., Tokola, T., Korhonen, L., Xu, Q., Kumpula, T., Vihervaara, P., & Mononen, L. (2014). Training Area Concept in a Two-Phase Biomass Inventory Using Airborne Laser Scanning and RapidEye Satellite Data. *Remote Sensing, 6*(1), 285-309. doi: 10.3390/rs6010285

Rapidlasso GmbH. (2016). LAStools. Germany.

Räsänen, A., Kuitunen, M., Tomppo, E., & Lensu, A. (2014). Coupling high-resolution satellite imagery with ALS-based canopy height model and digital elevation model in object-based boreal forest habitat type classification. *Isprs Journal of Photogrammetry and Remote Sensing, 94*(0), 169-182. doi: 10.1016/j.isprsjprs.2014.05.003

Raulier, F., Lambert, M.-C., Pothier, D., & Ung, C.-H. (2003). Impact of dominant tree dynamics on site index curves. *Forest Ecology and Management, 184*(1–3), 65-78. doi: 10.1016/S0378-1127(03)00149-X

Richter, R., Kellenberger, T., & Kaufmann, H. (2009). Comparison of Topographic Correction Methods. *Remote Sensing, 1*(3), 184-196. doi: 10.3390/rs1030184

Richter, R., & Schläpfer, D. (2014). Atmospheric/topographic correction for satellite imagery. *ATCOR 2/3 User Guide. Version 8.3.1*.

Roberts, J. W., Tesfamichael, S., Gebreslasie, M., van Aardt, J., & Ahmed, F. B. (2007). Forest structural assessment using remote sensing technologies: An overview of the current state of the art. *Southern Hemisphere Forestry Journal, 69*(3), 183-203. doi: 10.2989/shfj.2007.69.3.8.358

Rombouts, J., Ferguson, I. S., & Leech, J. W. (2010). Campaign and site effects in LiDAR prediction models for site-quality assessment of radiata pine plantations in South Australia. *International Journal of Remote Sensing, 31*(5), 1155-1173. doi: 10.1080/01431160903380573

Rosenqvist, A., Milne, A., Lucas, R., Imhoff, M., & Dobson, C. (2003). A review of remote sensing technology in support of the Kyoto Protocol. *Environmental Science & Policy, 6*(5), 441-455. doi: 10.1016/s1462-9011(03)00070-4

Rosner, B. (2011). Hypothesis Testing: Categorical Data - Estimation of Sample Size and Power for Comparing Two Binomial Proportions *Fundamentals of biostatistics (7th ed.)*. Boston: Brooks/Cole, Cengage Learning.

Sasaki, T., Imanishi, J., Ioki, K., Morimoto, Y., & Kitada, K. (2012). Object-based classification of land cover and tree species by integrating airborne LiDAR and high spatial resolution imagery data. *Landscape and Ecological Engineering, 8*(2), 157-171. doi: 10.1007/s11355-011-0158-z

Shamsoddini, A., Trinder, J. C., & Turner, R. (2013). Pine plantation structure mapping using WorldView-2 multispectral image. *International Journal of Remote Sensing, 34*(11), 3986-4007. doi: 10.1080/01431161.2013.772308

Sharma, R. P., Brunner, A., & Eid, T. (2012). Site index prediction from site and climate variables for Norway spruce and Scots pine in Norway. *Scandinavian Journal of Forest Research, 27*(7), 619-636. doi: 10.1080/02827581.2012.685749

Shataee, S. (2013). Forest attributes estimation using aerial laser scanner and TM data. *Forest Systems, 22*(3), 484-496. doi: 10.5424/fs/2013223-03874

Skovsgaard, J. P., & Vanclay, J. K. (2008). Forest site productivity: a review of the evolution of dendrometric concepts for even-aged stands. *Forestry, 81*(1), 13-31. doi: 10.1093/forestry/cpm041

Song, C., Woodcock, C. E., Seto, K. C., Lenney, M. P., & Macomber, S. A. (2001). Classification and change detection using Landsat TM data: When and how to correct atmospheric effects? *Remote Sensing of Environment, 75*(2), 230-244. doi: 10.1016/s0034-4257(00)00169-3

St-Onge, B., Hu, Y., & Vega, C. (2008). Mapping the height and above-ground biomass of a mixed forest using LiADR and stereo Ikonos images. *International Journal of Remote Sensing, 29*(5), 1277-1294. doi: 10.1080/01431160701736505

Stephens, P. R., Kimberley, M. O., Beets, P. N., Paul, T. S. H., Searles, N., Bell, A., . . . Broadley, J. (2012). Airborne scanning LiDAR in a double sampling forest carbon inventory. *Remote Sensing of Environment, 117*, 348-357. doi: 10.1016/j.rse.2011.10.009

Stephens, P. R., Watt, P. J., Loubser, D., Haywood, A., & Kimberley, M. O. (2007). *Estimation of carbon stocks in New Zealand planted forests using airborne scanning lidar*. Paper presented at the ISPRS Workshop on Laser Scanning 2007 and SilviLaser 2007, Espoo, September 12-14, 2007, Finland.

Suárez, J. C., Ontiveros, C., Smith, S., & Snape, S. (2005). Use of airborne LiDAR and aerial photography in the estimation of individual tree heights in forestry. *Computers & Geosciences, 31*(2), 253-262. doi: 10.1016/j.cageo.2004.09.015

Tehrany, M. S., Pradhan, B., & Jebuv, M. N. (2014). A comparative assessment between object and pixel-based classification approaches for land use/land cover mapping using SPOT 5 imagery. *Geocarto International, 29*(4), 351-369. doi: 10.1080/10106049.2013.768300

Tomé, J., Tomé, M., Barreiro, S., & Paulo, J. A. (2006). Age-independent difference equations for modelling tree and stand growth. *Canadian Journal of Forest Research, 36*(7), 1621-1630. doi: 10.1139/x06-065

Tomppo, E., Goulding, C., & Katila, M. (1999). Adapting Finnish multi-source forest inventory techniques to the New Zealand preharvest inventory. *Scandinavian Journal of Forest Research, 14*(2), 182-192. doi: 10.1080/02827589950152917

Tomppo, E., Olsson, H., Stahl, G., Nilsson, M., Hagner, O., & Katila, M. (2008). Combining national forest inventory field plots and remote sensing data for forest databases. *Remote Sensing of Environment, 112*(5), 1982-1999. doi: 10.1016/j.rse.2007.03.032

Tonolli, S., Dalponte, M., Neteler, M., Rodeghiero, M., Vescovo, L., & Gianelle, D. (2011). Fusion of airborne LiDAR and satellite multispectral data for the estimation of timber volume in the Southern Alps. *Remote Sensing of Environment, 115*(10), 2486-2498. doi: 10.1016/j.rse.2011.05.009

Trimble. (2013). eCognition Developer 8.9 User Guide.

Tuominen, S., & Pekkarinen, A. (2005). Performance of different spectral and textural aerial photograph features in multi-source forest inventory. *Remote Sensing of Environment, 94*(2), 256-268. doi: 10.1016/j.rse.2004.10.001

Ustin, S. L., & Gamon, J. A. (2010). Remote sensing of plant functional types. *New Phytologist, 186*(4), 795-816. doi: 10.1111/j.1469-8137.2010.03284.x

van Leeuwen, M., & Nieuwenhuis, M. (2010). Retrieval of forest structural parameters using LiDAR remote sensing. *European Journal of Forest Research, 129*(4), 749-770. doi: 10.1007/s10342-010-0381-4

Vega, C., & St-Onge, B. (2009). Mapping site index and age by linking a time series of canopy height models with growth curves. *Forest Ecology and Management, 257*(3), 951-959. doi: 10.1016/j.foreco.2008.10.029

Wallerman, J., & Holmgren, J. (2007). Estimating field-plot data of forest stands using airborne laser scanning and SPOT HRG data. *Remote Sensing of Environment, 110*(4), 501-508. doi: 10.1016/j.rse.2007.02.028

Wallner, A., Elatawneh, A., Schneider, T., & Knoke, T. (2014). Estimation of forest structural information using RapidEye satellite data. *Forestry: An International Journal of Forest Research, 88*(1), 96-107. doi: 10.1093/forestry/cpu032

Wang, K., Franklin, S. E., Guo, X. L., & Cattet, M. (2010). Remote Sensing of Ecology, Biodiversity and Conservation: A Review from the Perspective of Remote Sensing Specialists. *Sensors, 10*(11), 9647-9667. doi: 10.3390/s101109647

Wang, Z., & Boesch, R. (2007). Color- and texture-based image segmentation for improved forest delineation. *Ieee Transactions on Geoscience and Remote Sensing, 45*(10). doi: 10.1109/TGRS.2007.896283

Wang, Z., Boesch, R., & Ginzler, C. (2008). *Integration of high resolution aerial images and airborne LiDAR data for forest delineation.* Paper presented at the The ISPRS XXXVII Congress, Beijing, China.

Watt, M. S., Dash, J. P., Bhandari, S., & Watt, P. (2015). Comparing parametric and non-parametric methods of predicting Site Index for radiata pine using combinations of data derived from environmental surfaces, satellite imagery and airborne laser scanning. *Forest Ecology and Management, 357*, 1-9. doi: 10.1016/j.foreco.2015.08.001

Watt, M. S., Dash, J. P., Watt, P., & Bhandari, S. (2016). Multi-sensor modelling of a forest productivity index for radiata pine plantations. *New Zealand Journal of Forestry Science, 46*. doi: 10.1186/s40490-016-0065-z

Weber, T. C., & Boss, D. E. (2009). Use of LiDAR and supplemental data to estimate forest maturity in Charles County, MD, USA. *Forest Ecology and Management, 258*(9), 2068-2075. doi: 10.1016/j.foreco.2009.08.001

Wehr, A., & Lohr, U. (1999). Airborne laser scanning - An introduction and overview. *Isprs Journal of Photogrammetry and Remote Sensing, 54*(2-3), 68-82. doi: 10.1016/s0924-2716(99)00011-8

Whiteside, T. G., Boggs, G. S., & Maier, S. W. (2011). Comparing object-based and pixel-based classifications for mapping savannas. *International Journal of Applied Earth Observation and Geoinformation, 13*(6), 884-893. doi: 10.1016/j.jag.2011.06.008

Wolter, P. T., Townsend, P. A., & Sturtevant, B. R. (2009). Estimation of forest structural parameters using 5 and 10 meter SPOT-5 satellite data. *Remote Sensing of Environment, 113*(9), 2019-2036. doi: 10.1016/j.rse.2009.05.009

Wulder, M. A., & Seemann, D. (2003). Forest inventory height update through the integration of lidar data with segmented Landsat imagery. *Canadian Journal of Remote Sensing, 29*(5), 536-543. doi: 10.5589/m03-032

Wulder, M. A., White, J. C., Nelson, R. F., Naesset, E., Orka, H. O., Coops, N. C., . . . Gobakken, T. (2012). LiDAR sampling for large-area forest characterization: A review. *Remote Sensing of Environment, 121*, 196-209. doi: 10.1016/j.rse.2012.02.001

Xu, C., Morgenroth, J., & Manley, B. (2015). Integrating Data from Discrete Return Airborne LiDAR and Optical Sensors to Enhance the Accuracy of Forest Description: A Review. *Current Forestry Reports, 1*(3), 206-219. doi: 10.1007/s40725-015-0019-3

Yan, W. Y., Shaker, A., Habib, A., & Kersting, A. P. (2012). Improving classification accuracy of airborne LiDAR intensity data by geometric calibration and radiometric correction. *Isprs Journal of Photogrammetry and Remote Sensing, 67*, 35-44. doi: 10.1016/j.isprsjprs.2011.10.005

Yu, Q., Gong, P., Clinton, N., Biging, G., Kelly, M., & Schirokauer, D. (2006). Object-based Detailed Vegetation Classification with Airborne High Spatial Resolution Remote Sensing Imagery. *Photogrammetric Engineering & Remote Sensing, 72*(7), 799-811. doi: 10.14358/PERS.72.7.799

Yu, X. W., Hyyppa, J., Vastaranta, M., Holopainen, M., & Viitala, R. (2011). Predicting individual tree attributes from airborne laser point clouds based on the random forests technique. *Isprs Journal of Photogrammetry and Remote Sensing, 66*(1), 28-37. doi: 10.1016/j.isprsjprs.2010.08.003

Zellner, A. (1962). An Efficient Method of Estimating Seemingly Unrelated Regressions and Tests for Aggregation Bias. *Journal of the American Statistical Association, 57*(298), 348-368. doi: 10.2307/2281644

Zhang, H., Fritts, J. E., & Goldman, S. A. (2008). Image segmentation evaluation: A survey of unsupervised methods. *Computer Vision and Image Understanding, 110*(2), 260-280. doi: 10.1016/j.cviu.2007.08.003

Zhang, Z., & Liu, X. (2013). WorldView-2 satellite imagery and airborne LiDAR data for object-based forest species classification in a cool temperate rainforest environment. *Developments*

in Multidimensional Spatial Data Models (pp. 103-122). Berlin, Germany: Springer Berlin Heidelberg.

Zheng, D., Rademacher, J., Chen, J., Crow, T., Bresee, M., & le Moine, J. (2004). Estimating aboveground biomass using Landsat 7 ETM+ data across a managed landscape in northern Wisconsin, USA. *Remote Sensing of Environment, 93*(3), 402 - 411. doi: 10.1016/j.rse.2004.08.008

Zhou, J., Proisy, C., Descombes, X., le Maire, G., Nouvellon, Y., Stape, J.-L., . . . Couteron, P. (2013). Mapping local density of young Eucalyptus plantations by individual tree detection in high spatial resolution satellite images. *Forest Ecology and Management, 301*, 129-141. doi: 10.1016/j.foreco.2012.10.007

Zianis, D., & Seura, S. M. (2005). *Biomass and stem volume equations for tree species in Europe* (Vol. 4): Finnish Society of Forest Science, Finnish Forest Research Institute.

Appendix A: The process of selecting LiDAR ground point classification parameters

Run#	Fusion Codes	Changes	Results	Comments
0	groundfilter E:\LiDAR\project\Products\ground\gpts_test.lda 1 E:\LiDAR\project\point\sample\tranche_c_row04col21_2013_nztm_raw.las	Initial attempt	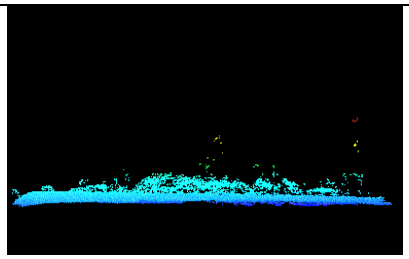	Not working
1	groundfilter E:\LiDAR\project\Products\ground\gpts_test1.lda E:\LiDAR\project\point\sample\tranche_c_row04col21_2013_nztm_raw.las	Change the cell size to 5	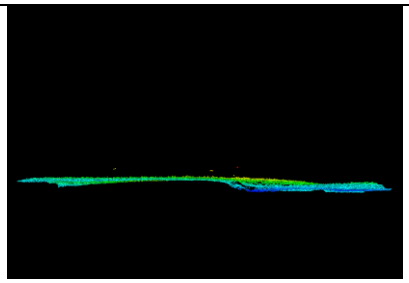	Start to get a surface but too coarse cell size
2	groundfilter /gparam:0 /wparam:0.5 /iterations:10 E:\LiDAR\project\Products\ground\gpts_test1.lda 2 E:\LiDAR\project\point\sample\tranche_c_row04col21_2013_nztm_raw.las	Cell size to 2, add g and w weight parameters	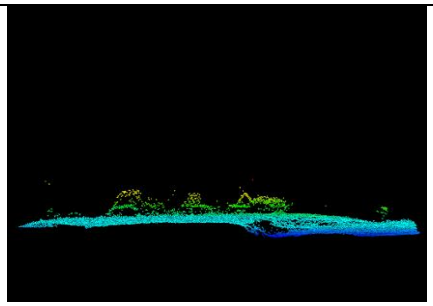	Still contain above ground points
3	groundfilter /gparam:-1 /wparam:2 /iterations:10 E:\LiDAR\project\Products\ground\gpts_test3.lda 2 E:\LiDAR\project\point\sample\tranche_c_row04col21_2013_nztm_raw.las	Change g and w parameters	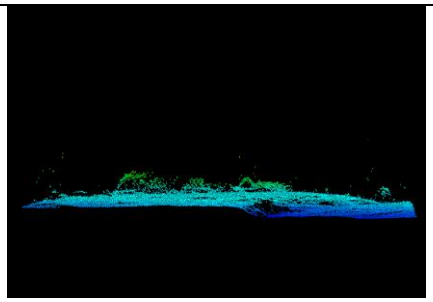	Still contain above ground points
4	groundfilter /gparam:-2 /wparam:2 /tolerance:0.1 /iterations:10 E:\LiDAR\project\Products\ground\gpts_test4.lda 2 E:\LiDAR\project\point\sample\tranche_c_row04col21_2013_nztm_raw.las	Change g and w parameters	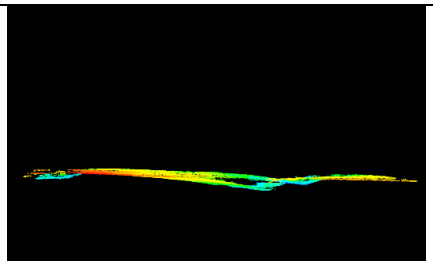	Ground points but miss too many points

Run#	Fusion Codes	Changes	Results	Comments
5	groundfilter /gparam:-1.5 /wparam:2 /tolerance:0.1 /iterations:10 E:\LiDAR\project\Products\ground\gpts_test5.lda 2 E:\LiDAR\project\point\sample\tranche_c_row04col21_2013_nztm_raw.las	Change g and w parameters	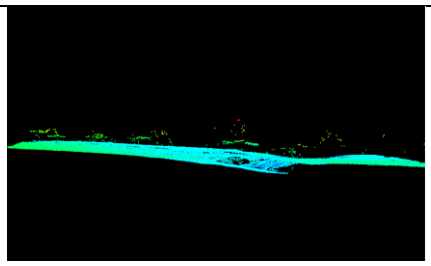	Still contain above ground points, ground points reduced
6	groundfilter /gparam:-1.5 /wparam:1.8 /tolerance:0.1 /iterations:10 E:\LiDAR\project\Products\ground\gpts_test6.lda 2 E:\LiDAR\project\point\sample\tranche_c_row04col21_2013_nztm_raw.las	Change g and w parameters	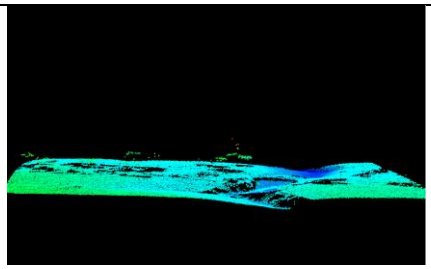	Still contain above ground points, ground points further reduced
7	groundfilter /gparam:-1.7 /wparam:1.8 /tolerance:0.1 /iterations:10 E:\LiDAR\project\Products\ground\gpts_test7.lda 2 E:\LiDAR\project\point\sample\tranche_c_row04col21_2013_nztm_raw.las	Change g and w parameters	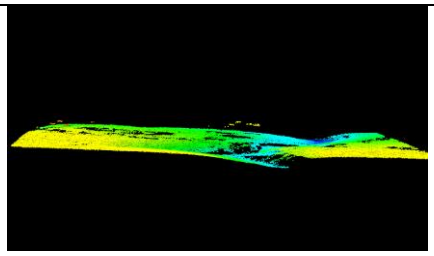	Only few above ground points
8	groundfilter /smooth:3 /gparam:-1.7 /wparam:1.8 /tolerance:0.1 /iterations:10 E:\LiDAR\project\Products\ground\gpts_test8.lda 2 E:\LiDAR\project\point\sample\tranche_c_row04col21_2013_nztm_raw.las	Apply smooth filter at 3x3 window size	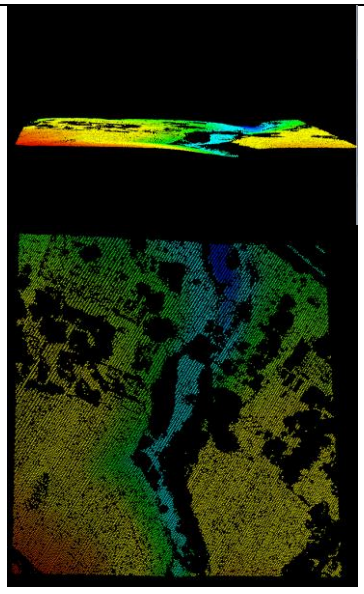	It seems to be working but many points are filtered out

Run#	Fusion Codes	Changes	Results	Comments
9	groundfilter /smooth:3 /gparam:-1.5 /wparam:2 /tolerance:0.1 /iterations:10 E:\LiDAR\project\Products\ground\gpts_test9.lda 2 E:\LiDAR\project\point\sample\tranche_c_row04col21_2013_nztm_raw.las	Change g and w parameters	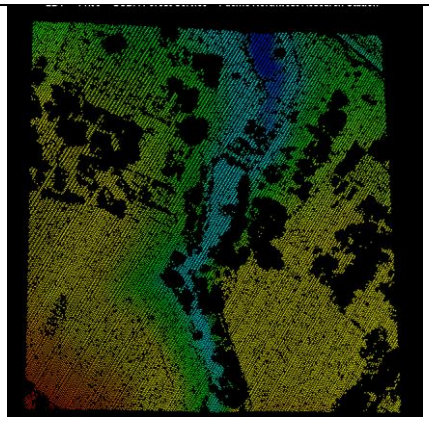	Better, more points left
10	groundfilter /smooth:3 /gparam:0 /wparam:0.5 /tolerance:0.1 /iterations:10 E:\LiDAR\project\Products\ground\gpts_test10.lda 2 E:\LiDAR\project\point\sample\tranche_c_row04col21_2013_nztm_raw.las	Change to original g and w, to see if there is difference	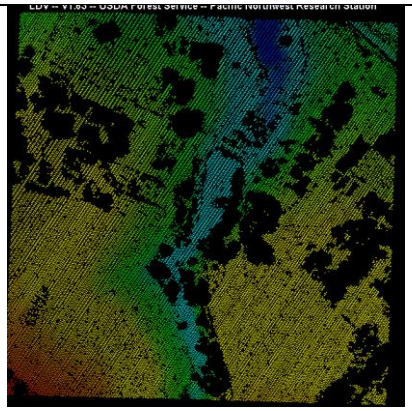	Very similar result as run#9

Appendix B: Atmospheric and Topographic Correction Process

Inputs required:

- Raw RapidEye scenes
- DEM

Derive terrain files required for topographic correction.

15m DEM was retrieved from LINZ. To cover the study area, three individual DEMs were downloaded. The three DEMs were then mosaicked to cover the whole study area. In order to reduce processing time, the mosaic was then clipped to cover the study area only.

The clipped 15m DEM is then used to generate slope, aspect, skyview and shadow files. The zenith and azimuth used are 30 and 43 respectively. Since the study area is large, the zenith and azimuth were calculated based on the centroid coordinates of the study area.

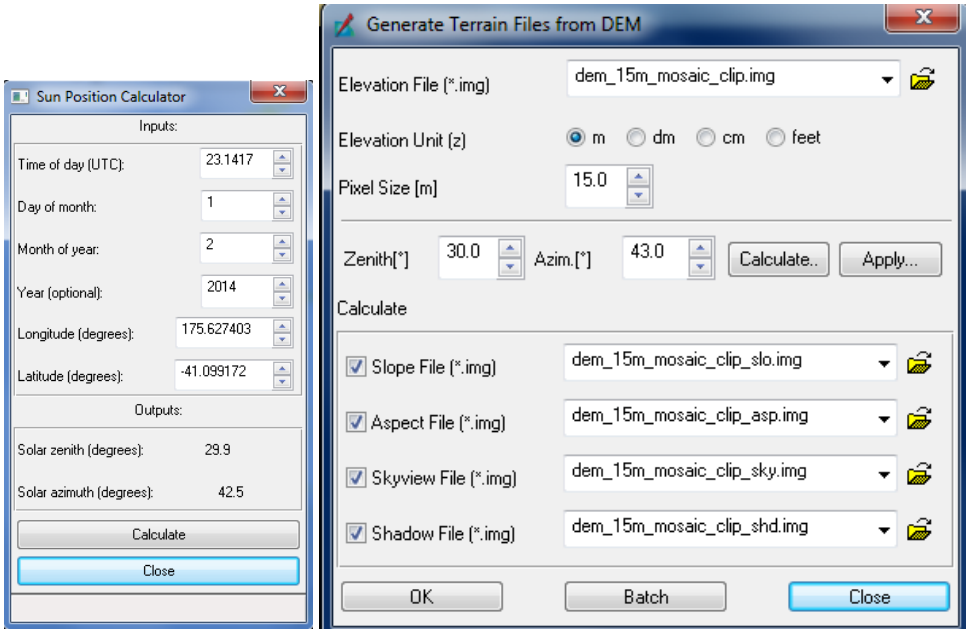

Strong artefacts in the DEM files will immediately be visible in the atmospherically / topographically corrected surface reflectance image. This problem frequently occurs for resampled DEMs (15m to 5 m pixel size). It is important to ensure DEM is in float data instead of integer. Generate slope, aspect and skyview from DEM with original resolution before resampling them down to 5m (use cubic convolution for resampling method).

Check if there is any artefact, if so use low pass convolution filter with 3x3 r 5x5 pixels to smooth the images.

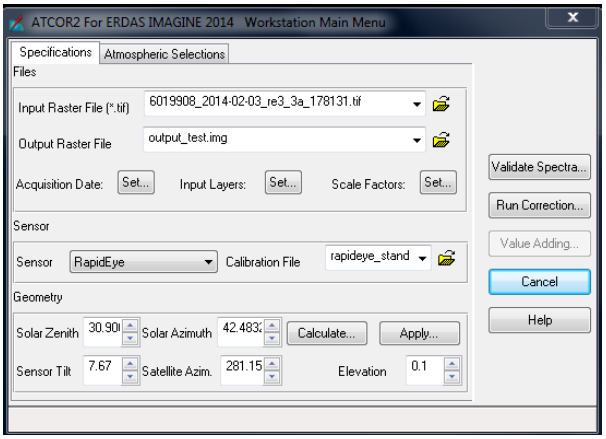

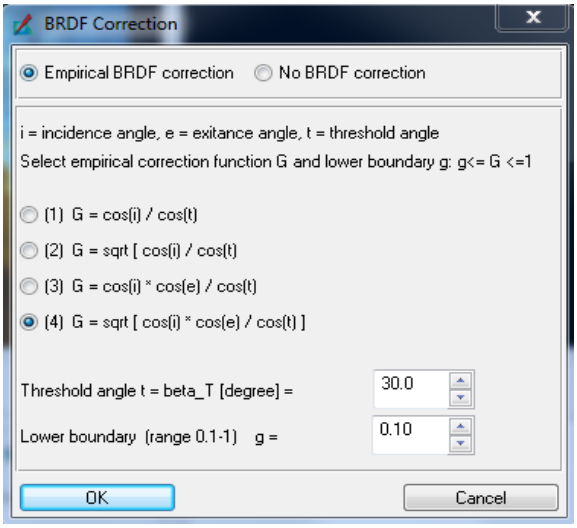

Appendix C: Scale Factor Selection using ESP tool

RapidEye Only

Image Grid	Forest Class	Optimal Segmentation	No. of objects (ESP output)	Reference	Segmentation created
20131201_BQ32_0708	1	60,**92**,106,110,	1297	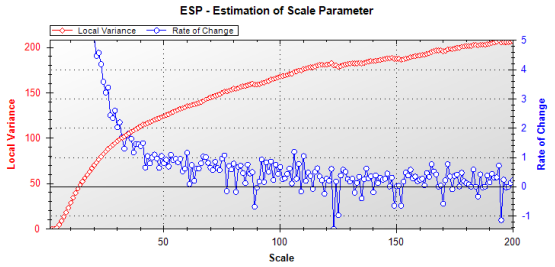	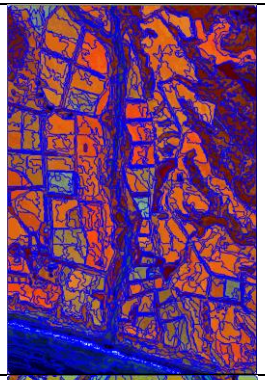
20140203_BP33_0908	1	100,**106**,112,116	636	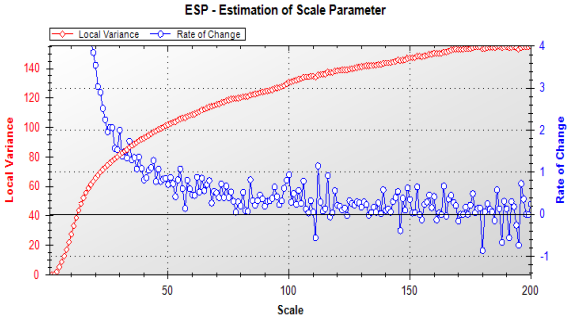	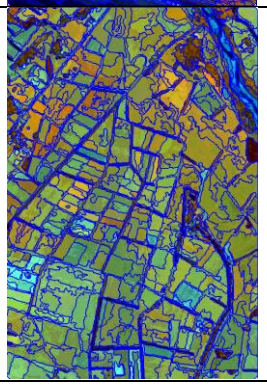

20140220_BP36_0503	1	78, 91,102, 116, **133**,138	588	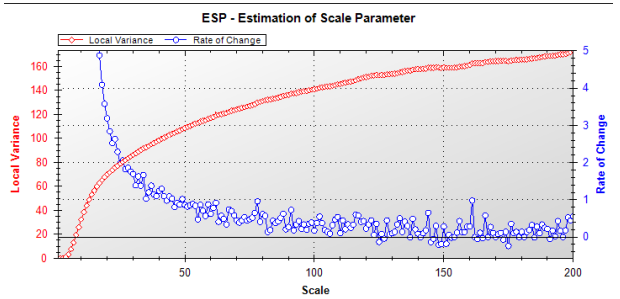	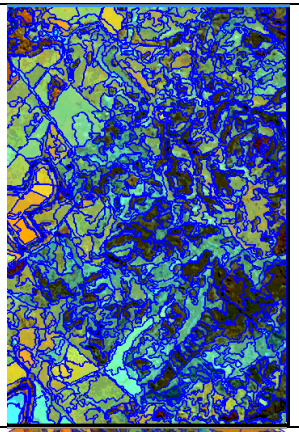
20131201_BP35_1003	2	84,92,103,**118,** 132,143	765	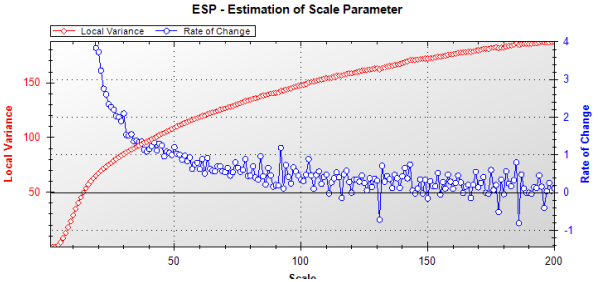	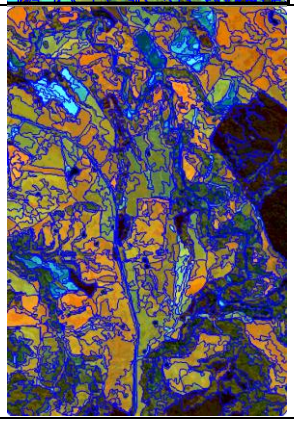

20140203_BQ34_0703	2	120,**130**,141, 152,172,174	494	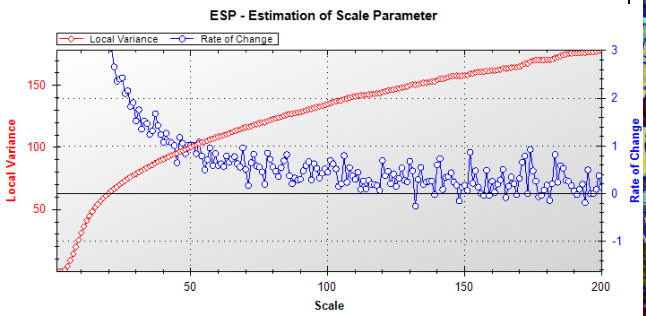	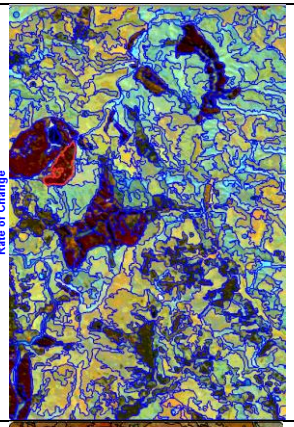
20140220_BP36_0209	2	81, **103**,108,119,14 7	825	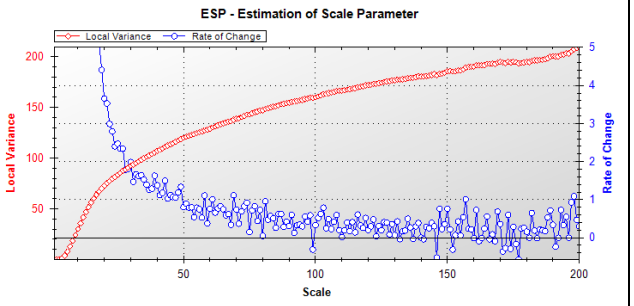	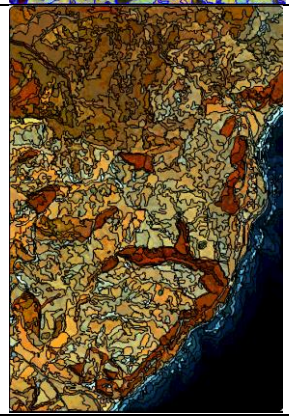

20131201_BN35_1004	3	**148**	808	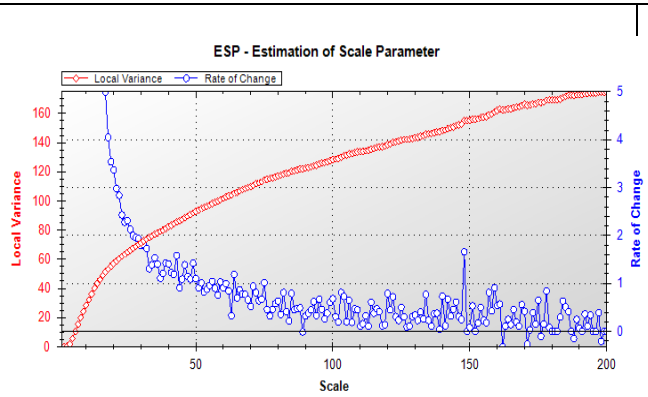	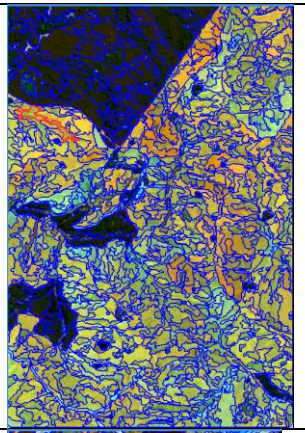
20140203_BQ33_0904	3	**140**,165,170,	592	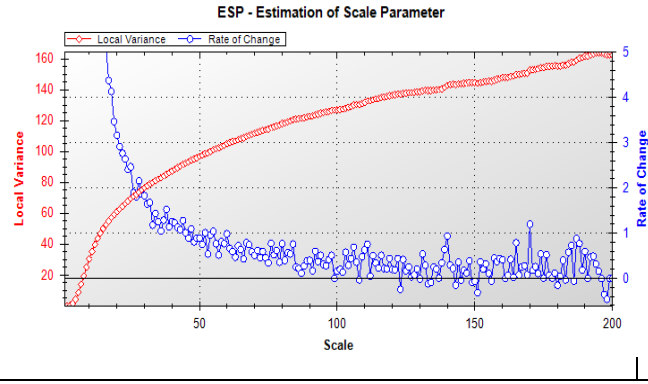	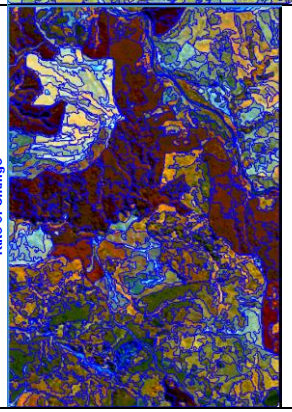

20140220_BQ35_0908	3	133,**148,** 152,161,181	361	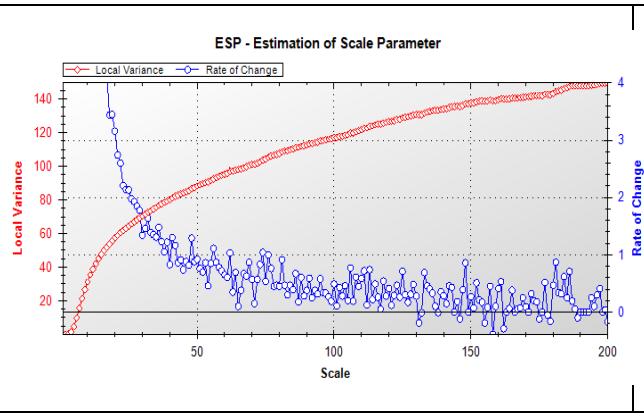	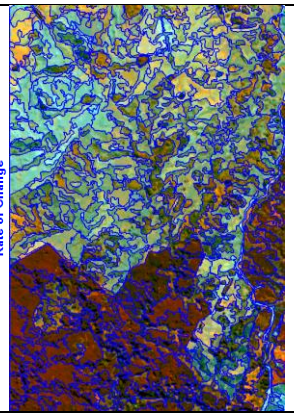

RapidEye and LiDAR

Image Grid	Forest Class	Optimal Segmentation	No. of objects (ESP output)	Reference	Segmentation created
20131201_BQ32_0708	1	**101**,113,140	619	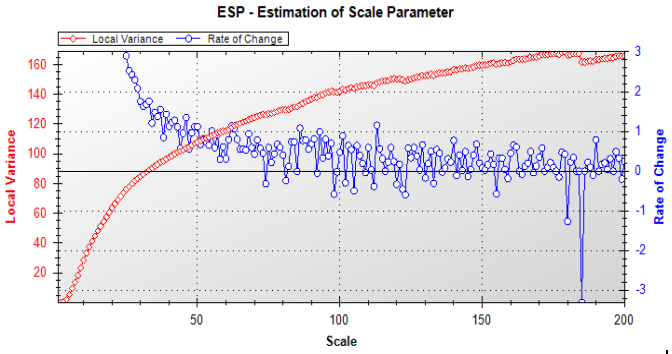	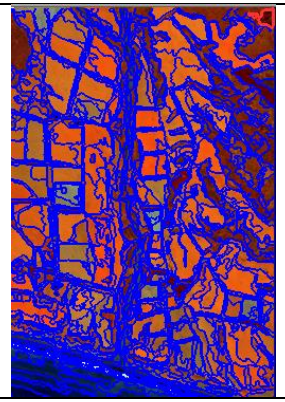

20140203_BP33_0908	1	40,65,80,**97**,113,119	629	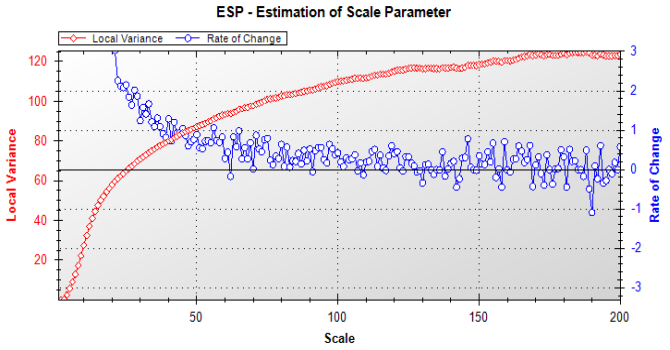	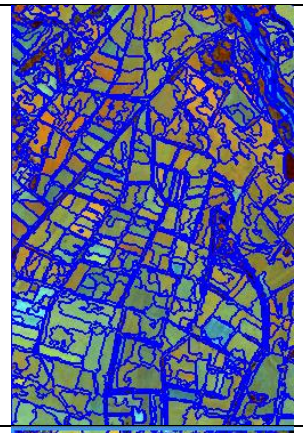
20140220_BP36_0503	1	100, **106**, 110,131,134	583	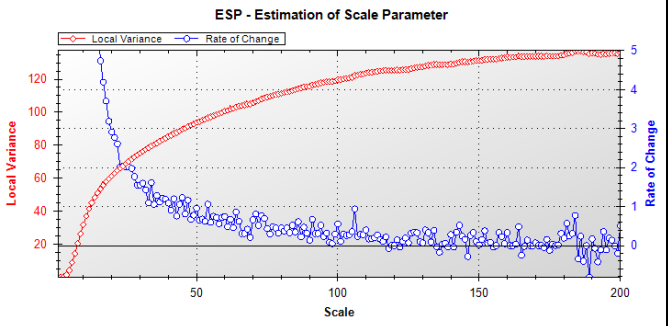	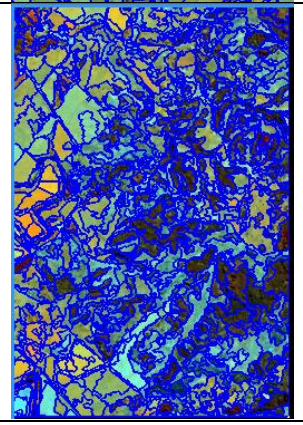

20131201_BP35_1003	2	80,88,98,104, **117,** 139,145,151,155,160,163	548	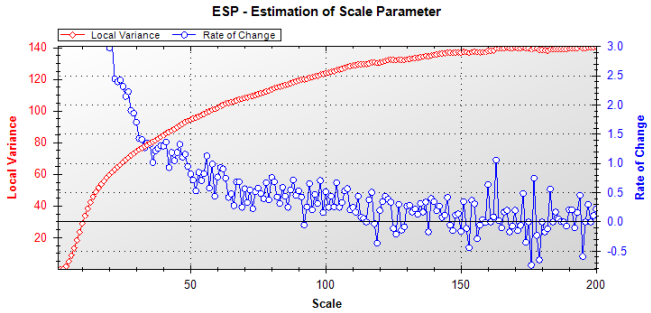	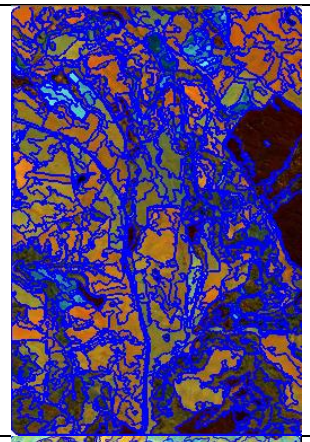
20140203_BQ34_0703	2	**117,**129,139	507	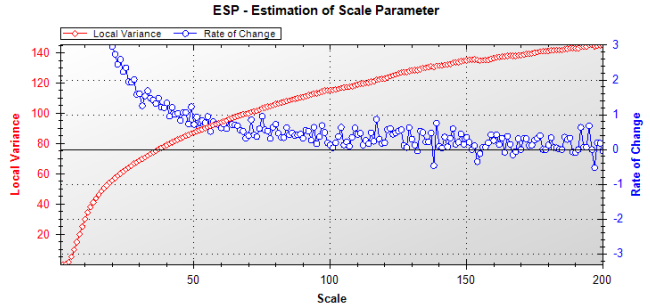	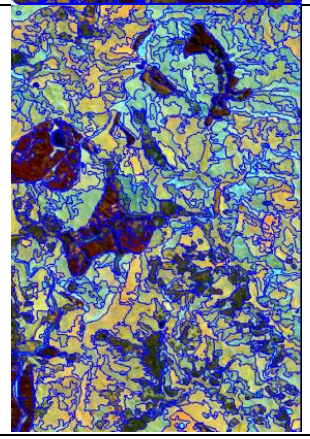

20140220_BP36_0209	2	123, 134, 143, **148**, 165	293	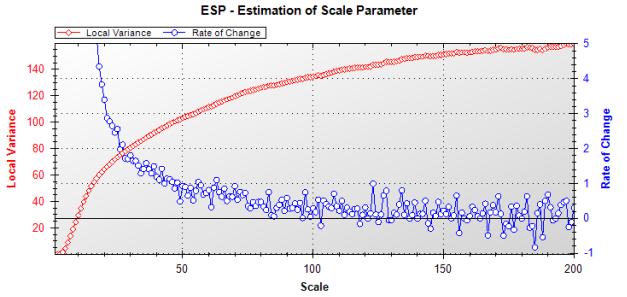	
20131201_BN35_1004	3	81, 109,122,138, **153**	232	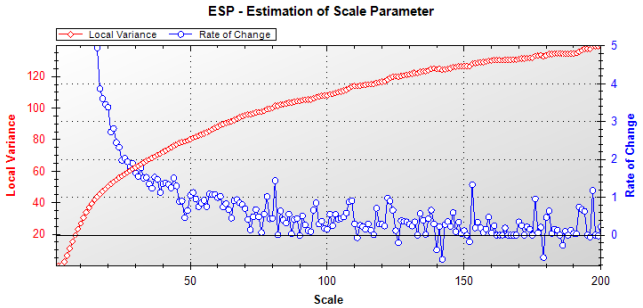	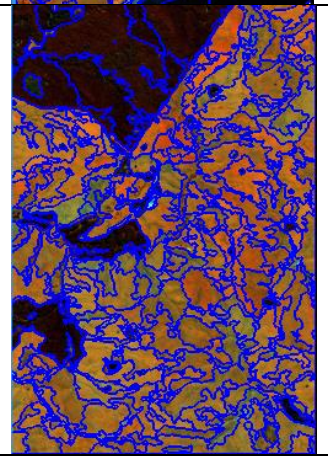

20140203_BQ33_0904	3	138,146,150,159	381	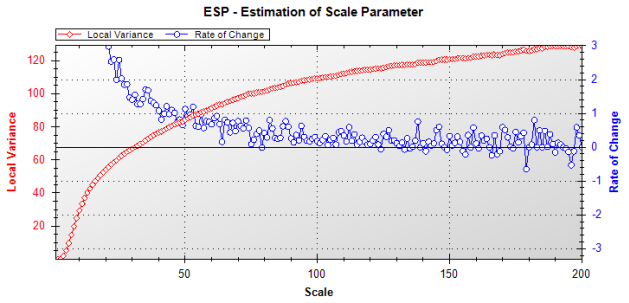	
20140220_BQ35_0908	3	90, 153,193	206	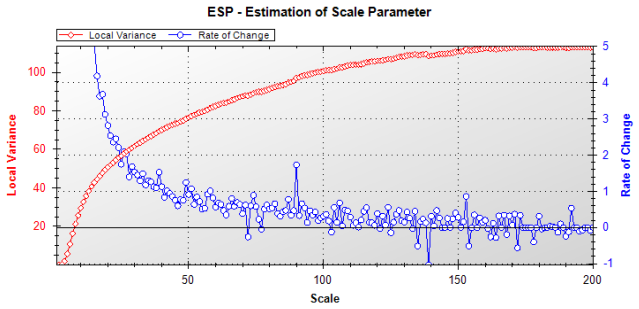	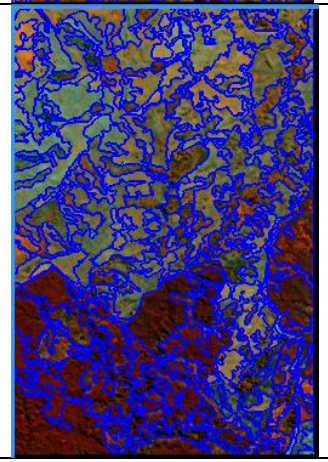

Appendix D: Patch-level comparison by individual grids

Grids	Digitised Plantation (ha)	Mapped Plantation (ha)	Error (ha)	Error (%)	LCDB Plantation (ha)
BN34_1007	11.5	14.5	3.1	27%	27.9
BN35_0905	16.4	20.4	4.0	25%	24.0
BN35_1004	170.2	181.3	11.0	6%	177.6
BN36_0704	12.8	16.4	3.6	28%	11.5
BN36_0805	0.0	3.5	3.5	0%	190.3
BN36_0808	60.1	64.4	4.3	7%	77.6
BN36_0901	235.5	248.4	12.9	5%	397.5
BN36_0903	73.0	78.4	5.5	8%	83.8
BN36_0909	145.2	151.9	6.6	5%	263.5
BN36_1009	151.9	166.0	14.1	9%	156.2
BP33_0908	9.1	11.9	2.8	31%	27.6
BP33_1005	3.3	8.3	5.0	149%	7.9
BP34_0104	0.0	0.0	0.0	0%	0.0
BP34_0305	13.1	13.1	0.0	0%	35.9
BP34_0306	5.8	5.1	-0.8	-13%	16.2
BP34_0809	10.8	12.7	1.9	18%	12.4
BP34_0901	2.1	3.2	1.1	51%	1.1
BP34_1006	13.0	15.6	2.6	20%	17.6
BP35_0209	629.8	635.5	5.7	1%	678.9
BP35_0307	50.0	53.1	3.1	6%	51.5
BP35_0407	150.1	141.9	-8.2	-5%	170.2
BP35_0409	178.1	194.4	16.3	9%	212.2
BP35_0501	1.3	1.3	0.0	0%	0.0
BP35_0604	21.3	24.1	2.7	13%	21.4
BP35_0904	60.0	77.3	17.2	29%	84.3
BP35_0908	214.4	256.0	41.7	19%	250.5
BP35_1003	62.0	61.5	-0.5	-1%	79.5
BP36_0208	204.2	216.4	12.2	6%	234.9
BP36_0209	62.9	73.3	10.4	17%	75.0
BP36_0305	131.5	138.9	7.4	6%	174.1
BP36_0403	8.7	9.5	0.8	9%	16.2
BP36_0503	4.3	0.0	-4.3	-100%	11.0
BP36_0604	88.1	87.8	-0.3	0%	112.2
BP36_0605	48.2	50.1	1.9	4%	54.3
BP36_0703	56.3	61.6	5.4	10%	76.5
BP36_0804	20.8	21.5	0.7	4%	23.3
BP36_1001	12.2	13.7	1.5	12%	10.6
BQ32_0610	7.8	12.6	4.8	62%	18.8
BQ32_0708	11.4	14.3	3.0	26%	15.5
BQ32_0809	0.0	0.0	0.0	0%	0.0

Grids	Digitised Plantation (ha)	Mapped Plantation (ha)	Error (ha)	Error (%)	LCDB Plantation (ha)
BQ33_0104	9.3	14.8	5.5	59%	7.8
BQ33_0502	5.2	7.6	2.3	45%	7.7
BQ33_0504	1.0	3.3	2.3	229%	4.0
BQ33_0510	25.1	24.3	-0.7	-3%	26.9
BQ33_0601	4.6	7.4	2.8	61%	10.2
BQ33_0609	5.7	9.9	4.2	74%	4.9
BQ33_0610	23.3	27.9	4.6	20%	28.2
BQ33_0701	11.5	11.6	0.1	1%	20.2
BQ33_0709	210.5	220.4	9.9	5%	229.8
BQ33_0904	230.2	232.4	2.2	1%	251.3
BQ34_0107	15.1	13.7	-1.4	-9%	16.0
BQ34_0204	11.0	10.8	-0.2	-2%	11.9
BQ34_0303	30.1	28.3	-1.8	-6%	44.1
BQ34_0501	11.7	12.3	0.6	6%	20.3
BQ34_0502	9.8	10.2	0.4	4%	28.6
BQ34_0603	14.1	12.5	-1.6	-12%	19.2
BQ34_0604	0.5	0.9	0.4	84%	1.3
BQ34_0703	56.8	64.2	7.4	13%	76.7
BQ34_0805	165.0	126.0	-39.0	-24%	176.8
BQ34_0808	0.0	0.3	0.3	0%	0.0
BQ34_0902	208.8	194.7	-14.1	-7%	222.7
BQ35_0305	451.3	454.9	3.5	1%	641.8
BQ35_0306	6.0	15.3	9.3	157%	14.1
BQ35_0402	476.3	485.3	8.9	2%	509.5
BQ35_0502	50.0	36.2	-13.8	-28%	49.8
BQ35_0504	337.0	330.8	-6.2	-2%	352.2
BQ35_0703	264.0	243.3	-20.7	-8%	266.0
BR33_0108	0.0	0.2	0.2	0%	0.0
BR33_0504	0.0	0.0	0.0	0%	0.0
Total	**5590.8**	**5759.2**	**168.5**	**3%**	**6941.6**

Appendix E: LiDAR, RapidEye and combined metrics selected as explanatory variables for MLR and SUR models

Stand Variables	LiDAR Metrics	RapidEye Metrics	LiDAR + RapidEye Metrics
MTH	H90	GreenRatio BlueRatio Brightness Rededge_skewness GLCM_ang.2nd_moment 45°	H90 GreenRatio BlueRatio
BA	4th_return_above_0.5m qav I99 %1st_return_above_3	GreenRatio MaxDifference GLCM_correlation 90° GLCM_ang.2nd_moment 135° GLCM_entropy 135° GLCM_mean 45°	4th_return_above_0.5m qav %1st_return_above_3 GLCM_entropy 90° GLCM_ang.2nd_moment 135° GLCM_mean_all direction
VOL	4th_return_above_0.5m qav I_L4 (all_return_above_3m)/(total_1st_return)*100	GreenRatio BlueRatio GLCM_mean 90° GLCM_entropy 135° GLCM_ang.2nd_moment 135°	4th_return_above_0.5m qav I_L4 (all_return_above_3m)/(total_1st_return)*100 GLCM_entropy 135° GLCM_mean 90°
Age	I_skewness I10 H95	GreenRatio Blue_mean NIR_standard deviation GLCM_ang.2nd_moment 45° GLCM_mean 90° GLCM_correlation_all direction	I_skewness I10 H95 GLCM_entropy_all direction